Vom Fachbereich Mathematik der Technischen Universität Kaiserslautern
zur Verleihung des akademischen Grades
Doktor der Naturwissenschaften (Doctor rerum naturalium, Dr. rer. nat.)
genehmigte

Dissertation

Stochastic Modeling and Approximation of Turbulent Spinning Processes

Florian Hübsch

1. Gutachter: Prof. Dr. Klaus Ritter
2. Gutachter: Prof. Dr. Nicole Marheineke

Tag der Disputation: 05.12.2014

D 386

Contents

CHAPTER 1

Introduction

The main topic of this thesis is the efficient simulation of turbulent air flows, which find its application in many fields of science and industry, e.g., in the aerodynamics of aircrafts or the weather prediction in the field of meteorology. We are especially interested in turbulent spinning processes like melt-blowing and spunbond, which are processes for producing textured fibrous webs by spinning hundreds of polymer fibers due to high-velocity air streams. One of the main characteristics of the meltblown process are the huge fiber elongations due to the high velocities, which results in fibers with diameters in micrometer range. Because of these small diameters of the meltblown fibers the resulting webs have a very fine structure. Examples for products are oil adsorbents (quick adsorption of oil dirt) and industrial filters. Because the importance of such products increases and to improve the quality of the resulting webs, simulation methods for turbulent spinning processes are called for. Therefore we need a model that describes the fiber dynamics in a turbulent air flow and a model for the turbulent air flow itself.

In [53] Marheineke and Wegener have developed a random partial differential algebraic equation (PDAE) model for the motion of a fiber immersed in a turbulent air flow. Here, the air velocity of a turbulent flow is described by a random

field

$$\mathbf{U} : \mathbb{R}^3 \times \mathbb{R}_+ \times \Omega \to \mathbb{R}^3$$

on a probability space $(\Omega, \mathcal{A}, P)$. For a fixed $\omega \in \Omega$, $\mathbf{U}(\mathbf{x}, \mathrm{t}, \omega) \in \mathbb{R}^3$ describes the velocity components of a single air flow realization at the spatial position $\mathbf{x} \in \mathbb{R}^3$ and time instance $\mathrm{t} \geq 0$. Assuming integrability, the random field $\mathbf{U}$ may be decomposed as

$$\mathbf{U} = \overline{\mathbf{U}} + \mathbf{U}'$$

where $\overline{\mathbf{U}}$ is the determinstic mean of $\mathbf{U}$ and $\mathbf{U}'$ a centered random field. In this thesis $\mathbf{U}'$ will be of central importance.

In Chapter 2 we will give an introduction to vector-valued random fields, especially to Gaussian random fields, which are completely described by their means and covariance functions. We also will study important structural properties, in particular homogenity, isotropy, and incompressibility. Furthermore we will briefly discuss approximation and simulation aspects for random fields.

The main topic of Chapter 3 will be the standard k-ϵ model for turbulence [32, 43]. It consists of a system of equations for functions

$$\mathrm{k} : \mathbb{R}^3 \times \mathbb{R}_+ \to \mathbb{R}_+, \quad \epsilon : \mathbb{R}^3 \times \mathbb{R}_+ \to \mathbb{R}_+, \quad \overline{\mathbf{U}} : \mathbb{R}^3 \times \mathbb{R}_+ \to \mathbb{R}^3,$$

where k and ϵ are related to $\mathbf{U}'$ by the requirements

$$\mathrm{k}(\mathbf{x}, \mathrm{t}) = \frac{1}{2}\mathbb{E}(\langle \mathbf{U}'(\mathbf{x}, \mathrm{t}), \mathbf{U}'(\mathbf{x}, \mathrm{t})\rangle), \quad \epsilon(\mathbf{x}, \mathrm{t}) = \nu\mathbb{E}\left(\left|\nabla \mathbf{U}'(\mathbf{x}, \mathrm{t})\right|_F^2\right).$$

Here, $\nu > 0$ denotes the kinematic viscosity of the air flow. The numerics of the k-ϵ model is implemented in many software solutions for Computational Fluid Dynamics (CFD). Therefore, we assume that we are given these functions at least numerically. The remaining task is an appropriate model for $\mathbf{U}'$ that satisfies the above requirements.

Taking into account theoretical considerations from turbulence theory, especially Kolmogorov's local isotropy hypothesis [26, 36, 59], Marheineke has developed a local model for the turbulent velocity fluctuations $\mathbf{U}'$ in [53], which will

be explained in Chapter 4.1. For a fixed $\mathbf{p} \in \mathbb{R}^3 \times \mathbb{R}_+$ the local model at $\mathbf{p}$ is given by a centered, homogeneous, spatially isotropic and incompressible, $\mathbb{R}^3$-valued Gaussian random field $\left(\mathbf{U}'_{\mathbf{p}}(\mathbf{x}, \mathrm{t})\right)_{(\mathbf{x},\mathrm{t})\in\mathbb{R}^3\times\mathbb{R}_+}$, whose covariance function parametrically depends on $\mathbf{p}$. In [30] we have derived an approximation $\mathbf{U}'_{\mathbf{p},N}$ of $\mathbf{U}'_{\mathbf{p}}$ by decoupling space and time in the covariance function and using the Central Limit Theorem. In Chapter 4.2 we will present a detailed construction of $\mathbf{U}'_{\mathbf{p},N}$. This approximation and an exploitation of the special covariance structure then permits the development of an efficient simulation algorithm for the local model, see [30] and Chapter 4.3 of this thesis. The key features (for turbulent spinning) of this algorithm are the following:

- given a finite set $D = \{(\mathbf{x}_1, \mathrm{t}_1), \ldots, (\mathbf{x}_N, \mathrm{t}_N)\} \subset \mathbb{R}^3 \times \mathbb{R}_+$ of evaluation points the computational effort for the evaluation of a single realization of our approximation in D is $\mathcal{O}(N)$, i.e., is linear in the number of points,
- the evaluation points need not to be known a priori.

These features permit an efficient simulation of the fiber dynamics in turbulent spinning, as described in Chapter 5. Based on the random fields $\mathbf{U}'_{\mathbf{p},N}$ we have further proposed two constructions for suitable random fields $\mathbf{U}'$, see Theorem 4.9, Chapter 4.4, and [30]. Both constructions fulfill the requirements on the kinetic turbulent energy k exactly, but the requirements on the dissipation rate ϵ only approximately. Moreover, these random fields can be simulated with the help of the simulation algorithm for the local fields with almost no loss in computational speed.

In Chapter 5 we finally use the constructed random fields in the simulation of turbulent spinning processes. A detailed model for the fiber dynamics for the spundbond process is a random PDAE model, see [53]. Here, a fiber of length $\ell(\mathrm{T}) > 0$ at time instance $\mathrm{T} > 0$ is described by an arclength-parametrized, time-dependent curve

$$\mathbf{r} : [0, \ell(\mathrm{T})] \times [0, \mathrm{T}] \times \Omega \to \mathbb{R}^3.$$

This means that $\mathbf{r}(\mathrm{s}, \mathrm{t}, \omega) \in \mathbb{R}^3$ describes the fiber position at arclength parameter s and time instance t for the corresponding realization $\mathbf{U}(\cdot, \omega)$ of the turbulent

velocity field. The system for the fiber dynamics reads (in short notation)

$$\begin{aligned} \partial_{\mathrm{tt}}\mathbf{r} &= \mathbf{f}_{in} + \mathbf{f}_{out}(\mathbf{U}) \\ |\partial_{\mathrm{s}}\mathbf{r}| &= 1, \end{aligned}$$

which essentially describes Newton's second law, i.e., the acceleration of the fiber is directly related to the inner force $\mathbf{f}_{in}$ and the outer force $\mathbf{f}_{out}$ influencing the motion of the fiber. The outer force $\mathbf{f}_{out}$ crucially depends on the the air velocity $\mathbf{U}$.

As already mentioned, one characteristic of the meltblown process are the huge fiber elongations. Up to now, there is a gap between the elongation measured in experiments and the elongation obtained by numerical simulations available in the literature. To quantify the elongation with the help of Monte Carlo methods, at first we use a simplification of a random PDE model, which is further outlined in Chapter 5.1. This simplification is a system of first order random ODEs in time for the jet position $\mathbf{r} : [0, \mathrm{T}] \times \Omega \to \mathbb{R}^3$, the jet velocity $\mathbf{v} : [0, \mathrm{T}] \times \Omega \to \mathbb{R}^3$, and the elongation $e : [0, \mathrm{T}] \times \Omega \to \mathbb{R}_+$. It reads

$$\begin{aligned} \frac{\mathrm{d}}{\mathrm{dt}}\mathbf{r} &= \mathbf{v} \\ \frac{\mathrm{d}}{\mathrm{dt}}\mathbf{v} &= e^{3/2}\,\mathrm{a}\,\boldsymbol{f}\left(\frac{\mathbf{v}}{|\mathbf{v}|}, \frac{1}{\sqrt{e}}\frac{\mathbf{U}(\mathbf{r},\mathrm{t}) - \mathbf{v}}{\mathrm{b}}\right) \\ \frac{\mathrm{d}}{\mathrm{dt}}e &= \frac{1}{\mathrm{v}_0}\,e^{3/2}\,\mathrm{a}\left|\boldsymbol{f}\left(\frac{\mathbf{v}}{|\mathbf{v}|}, \frac{1}{\sqrt{e}}\frac{\mathbf{U}(\mathbf{r},\mathrm{t}) - \mathbf{v}}{\mathrm{b}}\right)\right| \end{aligned}$$

with appropriate initial conditions and constants $a, b > 0$, see also [30]. The numerical results are very promising: whereas the numerical results available in the literature can only predict elongations up to order 10^4 we get an order of 10^5, which is closer to the elongation of order 10^6 measured in experiments. The simplification as well as our numerical results will be presented in Chapter 5.1. In Chapter 5.2 we will present the random PDAE model for spunbond in more detail. Because the numerical scheme for this system is already very demanding regarding computational speed we only address the issue of appropriate grid sizes (in space and time) to simulate fibers that are 'smooth' enough. At the end of Chapter 5.2 we will present our numerical results for the simulation of this model.

1.1 Notation

We denote by $\langle \cdot, \cdot \rangle$ the standard scalar product on $\mathbb{R}^d$ and by $|\cdot|$ the corresponding Euclidean norm. For matrices $A, B \in \mathbb{R}^{m \times n}$ we denote the Frobenius scalar product by $\langle \cdot, \cdot \rangle_F$, i.e., $\langle A, B \rangle_F = \sum_{i=1}^{m} \sum_{i=1}^{n} a_{ij} b_{ij}$ and by $|\cdot|_F$ the respective matrix norm. The trace of a matrix $A \in \mathbb{R}^{n \times n}$ is denoted by $tr(A) = \sum_{i=1}^{n} a_{ii}$. The set of all non-negative real numbers is given by $\mathbb{R}_+ = \{x \in \mathbb{R} : x \geq 0\}$. For functions $f : \mathbb{R}^3 \times \mathbb{R}_+ \to \mathbb{R}^{3\times 3}$, $g : \mathbb{R}^3 \times \mathbb{R}_+ \to \mathbb{R}^3$, and $h : \mathbb{R}^3 \times \mathbb{R}_+ \to \mathbb{R}$, for which the partial derivatives $\frac{\partial f_{ij}(x,t)}{\partial x_k}$, $\frac{\partial g_i(x,t)}{\partial x_k}$, $\frac{\partial h(x,t)}{\partial x_k}$, $x \in \mathbb{R}^3$, $t \in \mathbb{R}_+$, $i, j, k \in \{1, 2, 3\}$, exist we denote by

$$\operatorname{div}(f(x,t)) = \left(\sum_{j=1}^{3} \frac{\partial f_{1j}(x,t)}{\partial x_j}, \sum_{j=1}^{3} \frac{\partial f_{2j}(x,t)}{\partial x_j}, \sum_{j=1}^{3} \frac{\partial f_{3j}(x,t)}{\partial x_j} \right)^T$$

the divergence of f and by

$$\operatorname{div}(g(x,t)) = \sum_{j=1}^{3} \frac{\partial g_j(x,t)}{\partial x_j}$$

the divergence of g. By $\nabla g(x,t) \in \mathbb{R}^{3\times 3}$ we denote the Jacobian matrix of g, i.e., the matrix with the entries

$$(\nabla g(x,t))_{ij} = \frac{\partial g_i(x,t)}{\partial x_j}$$

and by

$$\nabla h(x,t) = \left(\frac{\partial h(x,t)}{\partial x_1}, \frac{\partial h(x,t)}{\partial x_2}, \frac{\partial h(x,t)}{\partial x_3} \right)^T$$

the gradient of h. That means if a function is $\mathbb{R}^{3\times 3}$-valued we use the first definition of div and if it is $\mathbb{R}^3$-valued we use the second definition.

CHAPTER 2

Gaussian Random Fields

In this chapter, we will give a brief introduction to the theory of Gaussian random fields and introduce the important concepts of homogenity, isotropy, and incompressibility, which will be used for the modeling of the turbulent velocity fields later on. Further we will give a short discussion on approximation and simulation aspects for random fields regarding this thesis. Literature and references to proofs are outlined in the text.

2.1 Definitions and Examples

In the sequel, $(\Omega, \mathcal{A}, P)$ denotes a probability space and $D \neq \emptyset$ any set.

Definition 2.1 (Normal distribution)**.** *A random variable $X : \Omega \to \mathbb{R}^d$ is called normally distributed with mean vector $m \in \mathbb{R}^d$ and covariance matrix $\Sigma \in \mathbb{R}^{d\times d}$ if X has the characteristic function*

$$\varphi_X(t) = \mathbb{E}(\exp(i\langle t, X\rangle)) = \exp\left(i\langle t, m\rangle - \frac{1}{2}\langle t, \Sigma t\rangle\right).$$

Remark 2.2. Let X be an $\mathbb{R}^d$-valued, normally distributed random variable, see Definition 2.1. Then X has the mean vector

$$m = (\mathbb{E}(X_1), \ldots, \mathbb{E}(X_d))^T$$

and the covariance matrix

$$\Sigma = (\mathbb{E}((X_i - \mathbb{E}(X_i))(X_j - \mathbb{E}(X_j))))_{i,j\in\{1,\dots,d\}}.$$

If $\det(\Sigma) > 0$, then the distribution of X has the Lebesgue density

$$f(x) = \frac{1}{\sqrt{(2\pi)^d \det(\Sigma)}} \exp\left(-\frac{1}{2}\langle x - m, \Sigma^{-1}(x-m)\rangle\right), \quad x \in \mathbb{R}^d.$$

Henceforth, we use the notation P_X for the distribution of a random variable X and the notation $P_X = \mathcal{N}_d(m, \Sigma)$ if X is a normally distributed, $\mathbb{R}^d$-valued random variable with mean vector m and covariance matrix Σ.

Theorem 2.3 (Existence of normal distribution)**.** *Let $m \in \mathbb{R}^d$ and a symmetric matrix $\Sigma \in \mathbb{R}^{d\times d}$ with $z^T\Sigma z \geq 0$ for all $z \in \mathbb{R}^d$ be given. Then there exists an $\mathbb{R}^d$-valued random variable X with $P_X = \mathcal{N}_d(m, \Sigma)$.*

A proof of this theorem can be found in [19, Theorem 9.5.7].

Definition 2.4 (Random field)**.** *A familiy $\xi = (\xi(x))_{x\in D}$ of $\mathbb{R}^d$-valued random variables on $(\Omega, \mathcal{A}, P)$ is called an $\mathbb{R}^d$-valued random field. In the case $D \subseteq \mathbb{R}$, ξ is also called an $\mathbb{R}^d$-valued stochastic process.*

Another term often used for 'random field' is the term 'random function'. This is motivated by the fact that the realizations $\xi(\cdot, \omega) : D \to \mathbb{R}^d$, $\omega \in \Omega$, of a random field ξ are elements of some function space $F(D)$ of $\mathbb{R}^d$-valued functions on D, i.e., $X : \Omega \to F(D)$, $X(\omega) = \xi(\cdot, \omega)$, defines a random function. Note that at this point we do not discuss the issue of measurability. This will be done in Chapter 2.2 to some extent. The previous observations lead us to the following definition.

Definition 2.5 (Continuity and differentiability)**.** *Let $\xi = (\xi(x))_{x\in D}$ be an $\mathbb{R}^d$-valued random field and $X(\omega) = \xi(\cdot, \omega)$ for $\omega \in \Omega$. Then ξ is called continuous if $X \in C(D)$ almost surely and p-times differentiable if X is p-times differentiable almost surely.*

In this work we deal with second-order fields, i.e., in the sequel we assume that every random field $(\xi(x))_{x\in D}$ under consideration satisfies

$$\mathbb{E}\left(|\xi(x)|^2\right) < \infty$$

for all $x \in D$. In this case, the mean function $m_\xi : D \to \mathbb{R}^d$,

$$m_\xi(x) = \mathbb{E}(\xi(x))$$

and the covariance function $K_\xi : D \times D \to \mathbb{R}^{d\times d}$,

$$K_\xi(x,y) = \mathbb{E}\left((\xi(x) - m_\xi(x))(\xi(y) - m_\xi(y))^T\right)$$

are well-defined, where the expectation applied to a vector or matrix is the expectation applied to its components.

Definition 2.6 (Gaussian random field)**.** *A real-valued random field $(\xi(x))_{x\in D}$ is called Gaussian if all finite-dimensional distributions are normal distributions, i.e., there exist $m \in \mathbb{R}^d$ and $\Sigma \in \mathbb{R}^{d\times d}$ such that*

$$P_{(\xi(x_1),\dots,\xi(x_d))} = \mathcal{N}_d(m,\Sigma)$$

for all $d \in \mathbb{N}$, $x_1,\dots,x_d \in D$. An $\mathbb{R}^d$-valued random field $(\xi(x))_{x\in D}$ is called Gaussian if the real-valued random field $(\eta_\alpha(x))_{x\in D}$ defined by

$$\eta_\alpha(x) = \langle \xi(x), \alpha\rangle$$

is Gaussian for every $\alpha \in \mathbb{R}^d$.

As we are interested in the modeling of random fields we address the question: can any given functions $m : D \to \mathbb{R}^d$ and $K : D \times D \to \mathbb{R}^{d\times d}$ be the mean and covariance function of a random field? At least for K we would expect some properties to be fulfilled, if we look at the definition of a covariance function. As we will see, necessary conditions on K are given by the following definition.

Definition 2.7. *A function $K : D \times D \to \mathbb{R}^{d\times d}$ is called nonnegative definite if*

$$\sum_{i=1}^{n}\sum_{j=1}^{n} z_i^T K(x_i,x_j) z_j \geq 0$$

for all $n \in \mathbb{N}$, $z_1,\dots,z_n \in \mathbb{R}^d$, $x_1,\dots,x_n \in D$, and symmetric if

$$K(x,y) = (K(y,x))^T$$

for all $x, y \in D$.

Clearly, the covariance function K_ξ of a random field $(\xi(x))_{x\in D}$ is symmetric. In addition, we have

$$\begin{aligned}\sum_{i=1}^{n}\sum_{j=1}^{n} z_i^T K_\xi(x_i,x_j)z_j &= \sum_{i=1}^{n}\sum_{j=1}^{n} z_i^T \mathbb{E}\left((\xi(x_i)-m_\xi(x_i))(\xi(x_j)-m_\xi(x_j))^T\right) z_j \\ &= \mathbb{E}\left(\sum_{i=1}^{n}\sum_{j=1}^{n} z_i^T(\xi(x_i)-m_\xi(x_i))(\xi(x_j)-m_\xi(x_j))^T z_j\right) \\ &= \mathbb{E}\left(\left|\sum_{i=1}^{n} z_i^T(\xi(x_i)-m_\xi(x_i))\right|^2\right) \geq 0,\end{aligned}$$

for all $n \in \mathbb{N}$, $z_1, \ldots, z_n \in \mathbb{R}^d$, $x_1, \ldots, x_n \in D$, i.e., K_ξ is nonnegative definite. That this conditions on K_ξ are also sufficient in the Gaussian case is the statement of the upcoming theorem. A proof for the real-valued case can be found in [19, p.443], an extension to the $\mathbb{R}^d$-valued case is straightforward.

Theorem 2.8 (Existence of Gaussian random fields)**.** *Let any index set D, any function m on D and a nonnegative definite, symmetric function K on $D \times D$ be given. Then there exists a Gaussian random field $\xi = (\xi(x))_{x\in D}$ with mean function m and covariance function K.*

Theorem 2.8 is essential to the theory of Gaussian random fields as it ensures the existence of a Gaussian field given any function m and a nonnegative definite, symmetric function K. In the following we show this on one example.

Example 2.9 (Brownian sheet)**.**
Let $D = [0,1]^s$ for $s \geq 1$ and $d = 1$. Define $m(x) = 0$ for all $x \in D$ and

$$K(x,y) = \prod_{i=1}^{s} \min(x_i, y_i)$$

for $x = (x_1, \ldots, x_s)^T, y = (y_1, \ldots, y_s)^T \in D$. Then it holds that

$$K(x,y) = K(y,x)$$

and with the notation $x_l = (x_{l,1}, \ldots, x_{l,s})$ for $x_l \in D$ we get

$$\begin{aligned}\sum_{i=1}^{n}\sum_{j=1}^{n} z_i K(x_i, x_j) z_j &= \sum_{i=1}^{n}\sum_{j=1}^{n} z_i z_j \prod_{k=1}^{s} \min(x_{i,k}, x_{j,k}) \\ &= \sum_{i=1}^{n}\sum_{j=1}^{n} z_i z_j \prod_{k=1}^{s} \int_D 1_{[0,x_{i,k}]}(x) 1_{[0,x_{j,k}]}(x)\, dx \\ &= \int_{[0,1]} \left| \sum_{i=1}^{n} z_i \prod_{k=1}^{s} 1_{[0,x_{i,k}]}(x) \right|^2 dx \geq 0\end{aligned}$$

for all $n \in \mathbb{N}$, $z_1, ..., z_n \in \mathbb{R}$, $x_1, ..., x_n \in D$. According to Theorem 2.8 there exists a Gaussian field $\xi = (\xi(x))_{x \in D}$ with

$$m_\xi(x) = 0, \quad K_\xi(x, y) = K(x, y), \quad x, y \in D,$$

which is called a Brownian sheet or a Brownian motion in the case $s = 1$. Figure 2.1 shows one realization of ξ with index set $D = [0, 1]^2$.

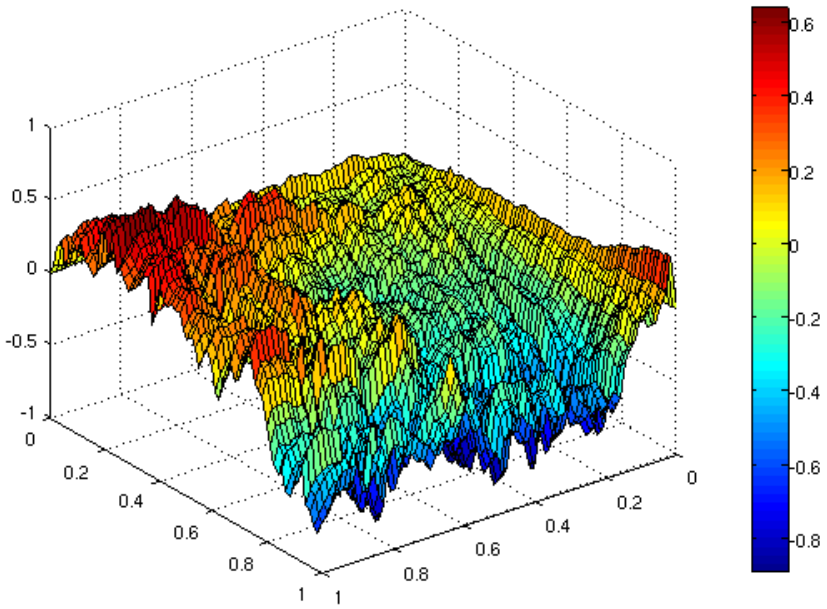

Figure 2.1: Realization of Brownian sheet on $[0, 1]^2$.

Remark 2.10. Let ξ be a Brownian sheet on $(\Omega, \mathcal{A}, P)$. Then there exists a continuous random field η on the same probability space, such that

$$P(\xi(x) = \eta(x)) = 1$$

for all $x \in D$. This is a consequence of the Kolmogorov-Chentsov Theorem, see, e.g., [34, p. 53 ff].

Let us now introduce the concept of homogenity. Note that we are only interested in the weak form of this and the following concepts (i.e., homogenity as property of the covariance function).

Definition 2.11 (Homogenity)**.** *An $\mathbb{R}^d$-valued random field $(\xi(x))_{x\in\mathbb{R}^s}$ with constant mean function is called homogeneous if*

$$K_\xi(x, y) = K_\xi(x - a, y - a)$$

for all $x, y, a \in \mathbb{R}^s$.

In particular it holds that $K_\xi(x, y) = K_\xi(x - y, 0)$ for a homogeneous random field ξ. The function B_ξ defined by $B_\xi(x) = K_\xi(x, 0)$ is often called autocovariance function of ξ. Analogously to Definition 2.7, a function $B : \mathbb{R}^s \to \mathbb{R}^{d\times d}$ is called nonnegative definite if

$$\sum_{i=1}^{n}\sum_{j=1}^{n} z_i^T B(x_i - x_j)z_j \geq 0$$

for all $n \in \mathbb{N}$, $z_1, \ldots, z_n \in \mathbb{R}^d$, $x_1, \ldots, x_n \in \mathbb{R}^s$. Clearly, the autocovariance function B_ξ of a homogeneous random field ξ is nonnegative definite and

$$B_\xi(x) = K_\xi(x, 0) = K_\xi(0, x)^T = K_\xi(-x, 0)^T = B_\xi(-x)^T. \tag{2.1.1}$$

It is easy to see that in reverse every nonnegative definite function $B : \mathbb{R}^s \to \mathbb{R}^{d\times d}$ with (2.1.1) is the autocovariance function of an $\mathbb{R}^d$-valued homogeneous random field. Let us gather additional facts about B_ξ. With help of the Cauchy-Schwarz inequality it holds for the components $B_\xi^{(i,j)}$ of B_ξ that

$$\left|B_\xi^{(i,j)}(x)\right| \leq \left|\sqrt{B_\xi^{(i,i)}(0)B_\xi^{(j,j)}(0)}\right|,$$

i.e., B_ξ is bounded. If further the diagonal elements $B_\xi^{(i,i)}$, $i \in \{1,\dots,d\}$, are continuous at 0, all components $B_\xi^{(i,j)}$, $i,j \in \{1,\dots,d\}$, are continuous everywhere because of

$$\begin{aligned}\left|B_\xi^{(i,j)}(x) - B_\xi^{(i,j)}(y)\right| &= \left|\mathbb{E}\left(\xi_i(x)\xi_j(0)\right) - \mathbb{E}\left(\xi_i(y)\xi_j(0)\right)\right| \\ &= \left|\mathbb{E}\left((\xi_i(x) - \xi_i(y))\xi_j(0)\right)\right| \\ &\le \sqrt{\mathbb{E}\left((\xi_i(x) - \xi_j(y))^2\right)\mathbb{E}\left(\xi_j(0)^2\right)} \\ &= \sqrt{2\left(B_\xi^{(i,i)}(0) - B_\xi^{(i,i)}(x-y)\right)B_\xi^{(j,j)}(0)} \longrightarrow 0\end{aligned}$$

for $y \to x$. In order to relate the continuity of B_ξ with a property of ξ we need the following definition.

Definition 2.12 (Mean-square continuity)**.** *A random field $(\xi(x))_{x\in\mathbb{R}^s}$ is called mean-square continuous if*

$$\lim_{y\to x} \mathbb{E}\left(\left|\xi(y) - \xi(x)\right|^2\right) = 0$$

for all $x \in \mathbb{R}^s$.

In terms of a homogeneous random field ξ we can now state that its autocovariance function is continuous at 0 if and only if ξ is mean-square continuous. This follows from the equality

$$\mathbb{E}\left((\xi_i(y) - \xi_i(x))^2\right) = 2\left(B_\xi^{(i,i)}(0) - B_\xi^{(i,i)}(x-y)\right)$$

for all $i \in \{1,\dots,d\}$.

For the following discussion we need some results from Fourier analysis. For proofs of the outlined statements we refer to [27, Chapter 2]. Let $g : \mathbb{R}^s \to \mathbb{R}$ be an integrable function. Then its Fourier transform is defined by

$$\mathcal{F}_g(\kappa) = \frac{1}{(2\pi)^s}\int_{\mathbb{R}^s} \exp(-i\langle\kappa, x\rangle)g(x)\,dx, \quad \kappa \in \mathbb{R}^s.$$

Let us formally introduce the inverse Fourier transform of g by

$$\mathcal{F}_g^{-1}(\kappa) = (2\pi)^s\mathcal{F}_g(-\kappa).$$

Under the assumption that $\mathcal{F}_g$ is also integrable we have

$$\mathcal{F}_{\mathcal{F}_g^{-1}} = \mathcal{F}_{\mathcal{F}_g}^{-1}$$

according to the Fourier inversion theorem. Analogously, we define the Fourier transform of a matrix-valued function to be the Fourier transform applied to all components. Clearly, $\mathcal{F}_g$ is bounded, as it holds

$$|\mathcal{F}_g(\kappa)| \leq \frac{1}{(2\pi)^s} \int_{\mathbb{R}^s} |g(x)| \, dx < \infty$$

for all $\kappa \in \mathbb{R}^s$. Moreover, $\mathcal{F}_g$ is continuous. The last fact we would like to present is the scaling property. It states that the function $\tau^a(g) = g(\frac{\cdot}{a})$, $a \in \mathbb{R}$, has the Fourier transform

$$\mathcal{F}_{\tau^a(g)}(\kappa) = \frac{1}{|a|^s} \mathcal{F}_g \left(\frac{\kappa}{a} \right).$$

If we now assume, that B_ξ is the autocovariance function of a homogenenous, mean-square continuous, $\mathbb{R}^d$-valued random field $(\xi(x))_{x \in \mathbb{R}^s}$ with $B_\xi \in L_1(\mathbb{R}^s)$ we can take its Fourier transform

$$f(\kappa) = \mathcal{F}_{B_\xi}(\kappa),$$

which is called spectral density of ξ and will play an important role throughout this work. From its definition it follows with (2.1.1) and the scaling property ($a = -1$) that

$$\begin{aligned} f(\kappa) &= \frac{1}{(2\pi)^s} \int_{\mathbb{R}^s} \exp(-i\langle \kappa, x \rangle) B_\xi(x) \, dx \\ &= \frac{1}{(2\pi)^s} \int_{\mathbb{R}^s} \exp(-i\langle \kappa, x \rangle) (B_\xi(-x))^T \, dx \\ &= \mathcal{F}_{\tau^{-1}(B_\xi^T)}(\kappa) \\ &= \mathcal{F}_{B_\xi^T}(-\kappa) = (f(-\kappa))^T. \end{aligned}$$

Moreover, it can be shown that $f(\kappa)$ is a nonnegative matrix for every $\kappa \in \mathbb{R}^s$, see [17, Theorem 1]. That the converse is also true is the statement of the next theorem, which is a result by Cramér [17, Theorem] and extends a theorem of Bochner [11, Satz 19] to the vector-valued case.

Theorem 2.13. *Let $f : \mathbb{R}^s \to \mathbb{R}^{d\times d}$ be an integrable function with*

$$f(\kappa) = (f(-\kappa))^T, \quad z^T f(\kappa) z \geq 0, \tag{2.1.2}$$

for all $\kappa \in \mathbb{R}^s$, $z \in \mathbb{R}^d$. Then there exists an $\mathbb{R}^d$-valued, homogeneous, mean-square continuous Gaussian random field ξ with autocovariance function B_ξ given by

$$B_\xi(x) = \int_{\mathbb{R}^s} \exp(i\langle \kappa, x\rangle) f(\kappa)\, d\kappa.$$

A theorem by Kruse [40, Theorem 2.34], which can be easily applied to vector-valued random fields, relates the differentiability of a homogeneous Gaussian random field to the trace of its spectral density.

Theorem 2.14. *Let $f : \mathbb{R}^s \to \mathbb{R}^{d\times d}$ be an integrable function, which satisfies* (2.1.2) *and*

$$\int_{\mathbb{R}^s} |\kappa|^2 \ln(1+|\kappa|)^\alpha \; tr(f(\kappa))\, d\kappa < \infty \tag{2.1.3}$$

for $\alpha > 3$. Then there exists a centered, homogeneous, differentiable Gaussian random field $(\xi(x))_{x\in\mathbb{R}^s}$ with spectral density f.

Let us now introduce the definition of mean-square differentiability, which will be needed in the following.

Definition 2.15 (Mean-square differentiability)**.** *Let $(\xi(x))_{x\in\mathbb{R}^s}$ be an $\mathbb{R}^d$-valued random field. Then ξ is called mean-square differentiable if there exists an $\mathbb{R}^{d\times s}$-valued, second-order random field $(D\xi(x))_{x\in\mathbb{R}^s}$ such that*

$$\lim_{h\to 0} \mathbb{E}\left(\left| \frac{\xi_i(x+he_j) - \xi_i(x)}{h} - D\xi^{(i,j)}(x) \right|^2 \right) = 0$$

for all $x \in \mathbb{R}^s$, $i \in \{1,\dots,d\}$, $j \in \{1,\dots,s\}$, and j-th unit vector e_j.

Clearly, every mean-square differentiable random field is also mean-square continuous. For a homogeneous, $\mathbb{R}^d$-valued random field $(\xi(x))_{x\in\mathbb{R}^s}$ and $i \in \{1,\dots,d\}$, $j \in \{1,\dots,s\}$, we define the real-valued random field $(\xi_{h,i,j}(x))_{x\in\mathbb{R}^s}$ by

$$\xi_{h,i,j}(x) = \frac{\xi_i(x+he_j) - \xi_i(x)}{h}.$$

Then $\xi_{h,i,j}$ is also homogeneous with autocovariance function

$$\begin{aligned} B_{\xi_{h,i,j}}(x) &= \frac{1}{h^2}\left(2B_{\xi_i}(x) - B_{\xi_i}(x+he_j) - B_{\xi_i}(x-he_j)\right) \\ &= \frac{1}{h^2}\left(2B_{\xi}^{(i,i)}(x) - B_{\xi}^{(i,i)}(x+he_j) - B_{\xi}^{(i,i)}(x-he_j)\right) \end{aligned}$$

If $B^{(i,i)}$ is twice differentiable then

$$\lim_{h\to 0} B_{\xi_{h,i,j}}(x) = -\frac{\partial^2 B_{\xi}^{(i,i)}(x)}{\partial x_j^2}.$$

Moreover, a homogeneous random field ξ is mean-square differentiable if and only if the diagonal elements of its autocovariance function B_ξ are twice differentiable at 0. In this case we have the relation

$$B_{D\xi^{(i,j)}}(x) = -\frac{\partial^2}{\partial x_j^2} B_{\xi}^{(i,i)}(x)$$

between the autocovariance function $B_{D\xi^{(i,j)}}$ of $D\xi^{(i,j)}$ and the autocovariance function $B_{\xi}^{(i,i)} = B_{\xi_i}$ of ξ_i. For details we refer to [60, Chapter 2] as well as for a proof in the real-valued case to [76, Chapter 2.6]. An extension to the vector-valued case works analogously. Note that differentiability as defined in Definition 3 does in general not imply the mean-square differentiability. For a counterexample, see, e.g., [76, p. 21-22].

Remark 2.16. Let ξ be an $\mathbb{R}^d$-valued, differentiable Gaussian random field with Jacobian matrix $\nabla\xi$. Then $\nabla\xi$ is also Gaussian, because the differentiation is a linear operator, see, e.g., [64, Chapter 9]. Particularly, every differentiable Gaussian random field ξ is also mean-square differentiable and $\nabla\xi$ coincides almost surely with the mean-square derivative $D\xi$.

Let us now come to another important concept besides homogenity that is called isotropy. In the following we focus on the three-dimensional case $s = 3$ because this is of special interest as we will see in the following chapters. Note that we only point out the facts that are important for us in the course of this thesis. For more information and proofs we refer to the work of Monin and Yaglom [60, Chapters 6-7] or the work of Marheineke [52, Chapter 1]. We begin with the definition of isotropy.

Definition 2.17 (Isotropy). *Let $\xi = (\xi(x))_{x\in\mathbb{R}^3}$ be an $\mathbb{R}^3$-valued, centered random field. Then ξ is called isotropic if*

$$K_\xi(x,y) = SK_\xi(S^Tx, S^Ty)S^T$$

for all $x, y \in \mathbb{R}^3$ and $S \in \mathbb{R}^{3\times3}$ with $S^T = S^{-1}$.

Before we come to the main theorem we state an additional definition. This will lead to a special form of the spectral density, see Theorem 2.19.

Definition 2.18 (Incompressibility). *An $\mathbb{R}^3$-valued random field $(\xi(x))_{x\in\mathbb{R}^3}$ is called incompressible if it is differentiable and*

$$\sum_{i=1}^{3} \frac{\partial \xi_i}{\partial x_i} = 0$$

almost surely.

As we will see in the next chapter, the incompressibility condition appears in the Navier-Stokes equations and will be further explained there. With the last definition in mind we can state the following.

Theorem 2.19. *Let $(\xi(x))_{x\in\mathbb{R}^3}$ be a mean-square differentiable, homogeneous, isotropic, and incompressible random field with integrable autocovariance function. Then its spectral density f satisfies*

$$f(\kappa) = \frac{1}{4\pi}\frac{E(|\kappa|)}{|\kappa|^2}\left(I - \frac{\kappa\kappa^T}{|\kappa|^2}\right) \tag{2.1.4}$$

with

$$E(\kappa) = \frac{1}{2}\kappa^2 \int_{S^2} tr(f(\kappa\sigma))\, d\sigma, \tag{2.1.5}$$

where $S^2 = \{x \in \mathbb{R}^3 : |x| = 1\}$.

A proof can be found in [52, p. 22-25]. The function E is called energy spectrum of the random field ξ and is crucial for the modeling of the turbulent velocity fields, as we will see later on. For an interpretation of E (in the sense of physics) we refer to Remark 4.2. From (2.1.5) it follows that E is a nonnegative function, because the diagonal elements $f^{(i,i)}(\kappa)$ of the nonnegative definite matrix $f(\kappa) \in \mathbb{R}^{d\times d}$

satisfy

$$f^{(i,i)}(\kappa) = e_i^T f(\kappa) e_i \geq 0,$$

where e_i denotes the i-th unit vector in $\mathbb{R}^d$. Before we end this section with an important corollary we state two useful relations, cf. [52, p. 28].

Lemma 2.20. *Let $(\xi(x))_{x\in\mathbb{R}^3}$ be a mean-square differentiable, homogeneous, isotropic, incompressible random field with energy spectrum E and let $\nabla\xi$ be the Jacobian matrix of ξ. Then*

$$\frac{1}{2}\mathbb{E}(\langle\xi(x),\xi(x)\rangle) = \int_0^\infty E(\kappa)\, d\kappa,$$
$$\mathbb{E}\left(|\nabla\xi(x)|_F^2\right) = 2\int_0^\infty \kappa^2 E(\kappa)\, d\kappa,$$

with Frobenius norm $|\cdot|_F$.

From the first equation of Lemma 2.20 it follows that the energy spectrum is an integrable function. As we are interested in the construction of random fields the question arises, which conditions on a function E suffice, such that f defined by (2.1.4) is the spectral density of a homogeneous, isotropic, and incompressible random field. We have already seen that E must necessarily be a nonnegative and integrable function. To ensure the differentiability of the corresponding random field ξ we can use Theorem 2.14. Inserting (2.1.4) into (2.1.3) we get together with (2.16) the following corollary, cf. [52, p. 27].

Corollary 2.21. *Let $E : \mathbb{R}_+ \to \mathbb{R}_+$ be an integrable function with*

$$\int_0^\infty (\ln(1+\kappa))^\alpha \kappa^2 E(\kappa)\, d\kappa < \infty$$

for $\alpha > 3$. Then there exists a homogeneous, isotropic, incompressible Gaussian random field $(\xi(x))_{x\in\mathbb{R}^3}$ with spectral density

$$f(\kappa) = \frac{1}{4\pi}\frac{E(|\kappa|)}{|\kappa|^2}\left(I - \frac{\kappa\kappa^T}{|\kappa|^2}\right).$$

2.2 Approximation and Simulation

In the previous section we have given an overview of the theory of Gaussian random fields and have introduced the important concepts of homogenity, isotropy, and incompressibility. Now we will give a short discussion on approximation and simulation aspects and point out the important facts regarding the topic of this thesis.

In general, random fields can not be simulated exactly. Therefore we need approximation schemes, which approximate the desired field in a certain sense. To understand what is meant by certain sense we first recapitulate basic definitions of different convergence concepts. After that we make clear in which of these concepts we are particularly interested and comment on where our focus lies in simulations.

Let $\xi = (\xi(x))_{x\in D}$ and $\xi_N = (\xi_N(x))_{x\in D}$, $N \in \mathbb{N}$, be random fields defined on a common probability space $(\Omega, \mathcal{A}, P)$ with measurable index set $D \subset \mathbb{R}^s$, $s \in \mathbb{N}$. We can think of ξ as our desired random field and of ξ_N as appropriate approximation scheme. Before we come to the next definition let us recall that a measurable function $\xi : D \to \mathbb{R}^s$ is an element of $L_p(D)$, $p \in [1, \infty[$, if

$$|\xi|_{L_p(D)} = \left(\int_D |\xi(x)|^p \ dx \right)^{1/p} < \infty.$$

With this in mind we can define the following.

Definition 2.22 (L_p-convergence)**.** *Let ξ_N, $\xi \in L_p(D)$ for all $N \in \mathbb{N}$. We say that ξ_N converges to ξ in L_p, $p \in [1, \infty[$, if*

$$\lim_{N\to\infty} \mathbb{E}\left(|\xi - \xi_N|^p_{L_p(D)} \right) = 0.$$

Let us now assume that the realizations of ξ and ξ_N are elements of some separable Banach space $(X, |\cdot|_X)$, e.g., $X = C(D)$ provided with the supremum norm and compact subset D. Then ξ and ξ_N define distributions P_ξ, P_{ξ_N} on $(X, \mathcal{X})$ by

$$P_\xi(A) = P(\{\xi \in A\}),\ P_{\xi_N}(A) = P(\{\xi_N \in A\}),$$

for $A \in \mathcal{X}$, where $\mathcal{X}$ denotes the Borel σ-algebra of X. In this case we can define the following.

Definition 2.23 (Convergence in probability and in distribution)**.** *We say that ξ_N converges to ξ in probabilty if*

$$\lim_{N\to\infty} P\left(\{|\xi_N - \xi|_X > \epsilon\}\right) = 0$$

for all $\epsilon > 0$, and that ξ_N converges in distribution to ξ if

$$\lim_{N\to\infty} \int_X f \, dP_{\xi_N} = \int_X f \, dP_\xi$$

for all bounded and continuous functions f on X.

The latter convergence concept is also known as weak convergence of the measures P_{ξ_N} to P_ξ. With the notation $\xi_N \xrightarrow{d} \xi$ for the convergence in distribution we can define the following.

Definition 2.24 (Convergence of finite-dimensional distributions)**.** *We say the finite-dimensional distributions of $(\xi_N)_{N\in\mathbb{N}}$ converge to the finite-dimensional distributions of ξ if*

$$(\xi_N(x_1), \ldots, \xi_N(x_n)) \xrightarrow{d} (\xi(x_1), \ldots, \xi(x_n)), \quad N \to \infty,$$

for all $n \in \mathbb{N}$, $x_1, \ldots, x_n \in D$.

Remark 2.25. It is well-known that the L_p-convergence implies convergence in probability, which itself implies convergence in distribution. The convergence in distribution implies the convergence of the finite-dimensional distributions.

As we have seen there are different concepts to approximate random fields. In this thesis we are interested in the approximation and simulation of finite-dimensional distributions of a given (i.e., we know its mean and covariance function) Gaussian random field ξ such that the covariance function K_ξ of ξ coincides with the covariance function K_{ξ_N} of an approximation ξ_N, i.e.,

$$K_{\xi_N}(x, y) = K_\xi(x, y),$$

for $N \in \mathbb{N}$, $x, y \in D$. Our priority lies on the exact reproduction of the covariance function whereas a sufficient approximation of the finite-dimensional distribution is only a secondary property.

For Gaussian random fields there exists a method that simulates the exact finite-dimensional distributions in given points based on the Cholesky decomposition of the covariance matrix, see, e.g., [7, Chapter XI]. However, this method has two major drawbacks, which serve as an good example of what we are trying to avoid in our forthcoming simulations.

As we have already mentioned in the introduction, in the simulation of turbulent spinning processes hundreds of fibers are simulated in parallel and we want to evaluate one realization of the turbulent velocity field at every fiber point. Therefore one crucial simulation aspect is the computational speed, i.e., how fast we are able to evaluate one realization in different points. As the number of points is very high in spinning processes, methods like Cholesky are inappropriate. Another main aspect in turbulent spinning is that the points, in which we want to evaluate a realization of the random field are not known in advance. Thus any simulation method, which needs to know this information a priori induces further approximation errors through interpolation.

In summary, we are interested in a simulation algorithm, which is fast, sufficiently accurate (in the sense described above), and is able to evaluate realizations of the given random field on-demand, i.e., the points do not need to be known a priori.

CHAPTER 3

Turbulence Modeling

In the last chapter we have introduced Gaussian random fields in general, and we have studied specific properties like homogenity, isotropy, and incompressibility. Now we combine the random field theory and ideas from physics, particularly from the turbulence theory, to get first requirements on a random velocity field model, which will be further developed in Chapter 4. Standard references that cover both, basic random field theory and turbulence theory, are the works [59] and [60] by Monin and Yaglom. We remind the reader of our convention that every random field under consideration is a second-order field.

Notation 3.1 (Dimensional vs Dimensionless Quantity)**.** *We typeset vector-valued and matrix-valued quantities in bold-faced letters, dimensional quantities (in the sense of physics) in Roman style (e.g.,* $\mathbf{x}$*,* t*), and the corresponding dimensionless quantities in Italic style (e.g.,* $\boldsymbol{x}$*,* t*) throughout the following.*

As already mentioned in the introduction of this thesis we are interested in the efficient simulation of turbulent air flows to determine the force, which influences the motion of fibers in turbulent spinning processes. From an algorithmic point of view, given a spatial point $\mathbf{x} \in \mathbb{R}^3$ and a time instance $\mathrm{t} \geq 0$, we want to know the velocity vector $\mathbf{U}(\mathbf{x}, \mathrm{t}) \in \mathbb{R}^3$, which serves as an input parameter for an appropriate force model (cf. Chapter 5). Therefore, we need an idea how to model a turbulent velocity field $\mathbf{U} = (\mathbf{U}(\mathbf{x}, \mathrm{t}))_{(\mathbf{x},\mathrm{t}) \in \mathbb{R}^3 \times \mathbb{R}_+}$. This will lead us to

the Navier-Stokes equations, which in general describe the motion of Newtonian fluids like air and water, and will be described in the sequel. A detailed derivation of these equations can be found in [63]. Note that in the sequel we make some assumptions motivated by the background in physics that are needed to describe the general ideas.

We start with a deterministic model for the velocity $\mathbf{U} : \mathbb{R}^3 \times \mathbb{R}_+ \to \mathbb{R}^3$ and the pressure $\mathrm{P} : \mathbb{R}^3 \times \mathbb{R}_+ \to \mathbb{R}$. Let us assume that $\mathbf{U}$ is twice differentiable with respect to $\mathbf{x}$, differentiable with respect to t and that P is differentiable with respect to $\mathbf{x}$. We further make the assumption that $\mathbf{U}$ and P satisfy the incompressible Navier-Stokes equations for a Newtonian fluid with constant density $\rho > 0$ and constant dynamic viscosity $\mu > 0$. This system consists of two equations for $\mathbf{U}$ and P together with appropriate boundary conditions. How to choose the boundary conditions is neither necessary to understand the ideas, nor in the focus of this thesis. The first equation, which represents the incompressibility of $\mathbf{U}$, is the so-called continuity equation

$$\mathrm{div}(\mathbf{U}(\mathbf{x}, \mathrm{t})) = 0. \tag{3.0.1}$$

An understanding of an incompressible flow is, that applying pressure does not change the fluid density. In general, air flows are not incompressible. However, the air flows we are interested in have a low Mach number (< 0.3) that is the ratio of the absolute flow velocity and the speed of sound in the medium, and small pressure changes. Thus, they can be handled as incompressible. For more details we refer to [63, Chapter 10]. The second equation is the momentum equation

$$\rho \left(\frac{\partial \mathbf{U}(\mathbf{x}, \mathrm{t})}{\partial \mathrm{t}} + \mathrm{div} \left(\mathbf{U}(\mathbf{x}, \mathrm{t}) \mathbf{U}(\mathbf{x}, \mathrm{t})^T \right) \right) = -\nabla \mathrm{P}(\mathbf{x}, \mathrm{t}) + \mathrm{div}(2\mu \mathbf{S}(\mathbf{x}, \mathrm{t})) \tag{3.0.2}$$

with strain-rate tensor $\mathbf{S}(\mathbf{x}, \mathrm{t}) = \frac{1}{2} \left(\nabla \mathbf{U}(\mathbf{x}, \mathrm{t}) + \nabla \mathbf{U}(\mathbf{x}, \mathrm{t})^T \right)$. It describes the conservation of momentum according to Newton's second law. Note that up to now it is not clear whether there exists a smooth, physically reasonable solution to the system (3.0.1), (3.0.2). Therefore different solution concepts have been developed, some of which are described in [24], [46].

As we are dealing with turbulent flows, we make the second assumption that randomness enters the system at some point. Here, we only give an intuition on

how a deterministic system can exhibit a random character. For a more detailed discussion on this phenomenon we refer to [59, Chapter 1]. It has been observed in experiments that under certain conditions on the flow, the velocity at any point $(\mathbf{x}, \mathrm{t})$ differs significantly when it is measured several times under almost identical conditions (in real experiments we always have to expect some deviations). In [69], Reynolds pointed out that we can expect a random behaviour of the flow if its dimensionless Reynolds number

$$Re = \frac{\rho \mathrm{u} \mathrm{l}}{\mu},$$

exceeds a critical number, which depends on the experimental setting. Here, u, $\mathrm{l} \in \mathbb{R}_+$ are a typical speed and lengthscale (think of a simulation of a flow with density ρ, dynamic viscosity μ, and absolute velocity u in a spatial domain of the form $[0, \mathrm{l}]^3$). An example for the Reynolds number regime in a turbulent spinning process is given in [56] where $Re = 10^7$.

Remark 3.2 (Reynolds number similarity)**.** The Reynolds number completely describes a flow (except for boundary and initial values), i.e., if two flows have the same Reynolds number they will show a similar behaviour. This is the so-called Reynolds number similarity, see, e.g., [67, Chapter 2], [24, Chapter 1].

A mathematical formulation of the previous observations could be, that at some initial state the air velocity is given by an $\mathbb{R}^3$-valued random field $(\mathbf{U}_0(\mathbf{x}))_{\mathbf{x}\in\mathbb{R}^3}$ on a probability space $(\Omega, \mathcal{A}, P)$, i.e.,

$$\mathbf{U}(\mathbf{x}, 0) = \mathbf{U}_0(\mathbf{x}), \quad \mathbf{x} \in \mathbb{R}^3.$$

Accordingly, $\mathbf{U}$ and P are random fields on $(\Omega, \mathcal{A}, P)$. For numerical simulations this would mean, given a realization of $\mathbf{U}_0$, we would get a realization of $\mathbf{U}$ and P by numerically solving equations (3.0.1) and (3.0.2) together with appropriate boundary conditions.

At the end of Chapter 2, we have stated that we are interested in simulation methods, which are fast, regarding computational speed and are sufficiently accurate. There are different simulation approaches for $\mathbf{U}$ based on the Navier-Stokes equations. Direct numerical simulation (DNS) methods provide the highest ac-

curacy as one tries to numerically solve the equations (3.0.1), (3.0.2), together with appropriate boundary conditions, e.g., by pseudo-spectral methods in case of homogeneous turbulence (turbulence that can be modeled by homogeneous random fields), see [62]. Therefore, we have to ensure that the velocity field is resolved properly, which leads to an enourmous amount of computational calculations. In fact, it can be shown that the number N of spatial grid points sufficient for a numerical scheme, resolving the finest turbulence structures, scales with the Reynolds number of the flow. More specifically, lower and upper bounds for N are of order

$$Re^{9/4},$$

see, e.g., [24, Chapters I, II]. This shows that we have to take care which approach to choose in order to get a fast and sufficiently accurate simulation method. For more information on simulation approaches like DNS or Large Eddy Simulation (LES) we refer to [67, Chapters 9-13] and for discussions about accuracy to [67, Chapters 9.3, 11.10, 13.7].

In the following, we focus on a turbulence model based on the Reynolds-Averaged Navier-Stokes equations. This will lead to a deterministic system for quantities $\overline{\mathbf{U}}$, k, and ϵ that will be explained in Chapter 3.2 and can be interpreted as input parameters for a random velocity field model.

3.1 Reynolds-Averaged Navier-Stokes Equations

In this section we state the original idea of Reynolds [69] in terms of random fields. Let us assume that $\mathbf{U} = (\mathbf{U}(\mathbf{x}, \mathrm{t}))_{(\mathbf{x},\mathrm{t})\in\mathbb{R}^3\times\mathbb{R}_+}$ and $\mathrm{P} = (\mathrm{P}(\mathbf{x}, \mathrm{t}))_{(\mathbf{x},\mathrm{t})\in\mathbb{R}^3\times\mathbb{R}_+}$ are random fields on a common probability space $(\Omega, \mathcal{A}, P)$, which solve the Navier-Stokes equations (3.0.1), (3.0.2) almost surely. Thus, we implicitly assume that $\mathbf{U}$ is twice differentiable with respect to $\mathbf{x}$, differentiable with respect to t and that P is differentiable with respect to $\mathbf{x}$. To derive the Reynolds-averaged Navier-Stokes (RANS) equations we additionally assume that we are allowed to change the order of differentiation and expectation of both $\mathbf{U}$ and P, e.g.,

$$\mathbb{E}(\mathrm{div}(\mathbf{U}(\mathbf{x}, \mathrm{t}))) = \mathrm{div}(\mathbb{E}(\mathbf{U}(\mathbf{x}, \mathrm{t}))).$$

Let us denote the mean functions of $\mathbf{U}$ and P by

$$\overline{\mathbf{U}}(\mathbf{x},\mathrm{t}) = \mathbb{E}(\mathbf{U}(\mathbf{x},\mathrm{t})), \quad \overline{\mathrm{P}}(\mathbf{x},\mathrm{t}) = \mathbb{E}(\mathrm{P}(\mathbf{x},\mathrm{t})).$$

By setting

$$\mathbf{U}'(\mathbf{x},\mathrm{t}) = \mathbf{U}(\mathbf{x},\mathrm{t}) - \overline{\mathbf{U}}(\mathbf{x},\mathrm{t}), \quad \mathrm{P}'(\mathbf{x},\mathrm{t}) = \mathrm{P}(\mathbf{x},\mathrm{t}) - \overline{\mathrm{P}}(\mathbf{x},\mathrm{t}),$$

we get centered random fields, which are also called fluctuations.

The idea of Reynolds in the random field context is to take the expectation of the Navier-Stokes equations, i.e.,

$$\begin{aligned} \mathbb{E}(\mathrm{div}(\mathbf{U}(\mathbf{x},\mathrm{t}))) &= 0 \qquad (3.1.1)\\ \mathbb{E}\left(\rho\left(\frac{\partial \mathbf{U}(\mathbf{x},\mathrm{t})}{\partial \mathrm{t}} + \mathrm{div}(\mathbf{U}(\mathbf{x},\mathrm{t})\mathbf{U}(\mathbf{x},\mathrm{t})^T)\right)\right) &= \mathbb{E}(-\nabla \mathrm{P}(\mathbf{x},\mathrm{t}) + \mathrm{div}(2\mu\mathbf{S}(\mathbf{x},\mathrm{t}))), \end{aligned}$$

insert the decompositions

$$\mathbf{U}(\mathbf{x},\mathrm{t}) = \overline{\mathbf{U}}(\mathbf{x},\mathrm{t}) + \mathbf{U}'(\mathbf{x},\mathrm{t}), \quad \mathrm{P}(\mathbf{x},\mathrm{t}) = \overline{\mathrm{P}}(\mathbf{x},\mathrm{t}) + \mathrm{P}'(\mathbf{x},\mathrm{t}), \qquad (3.1.2)$$

when needed, and use the assumption, that we are allowed to change the order of differentiation and expectation to derive the RANS equations for the mean-flow $\overline{\mathbf{U}}$. As we will see, the RANS equations are not closed because of the appearance of the so-called Reynolds stress tensor

$$\boldsymbol{\tau}(\mathbf{x},\mathrm{t}) = -\rho\,\mathbb{E}\left(\mathbf{U}'(\mathbf{x},\mathrm{t})\mathbf{U}'(\mathbf{x},\mathrm{t})^T\right) = -\rho\,\mathbf{K}_{\mathbf{U}'}((\mathbf{x},\mathrm{t}),(\mathbf{x},\mathrm{t})) \in \mathbb{R}^{3\times 3}, \qquad (3.1.3)$$

where $\mathbf{K}_{\mathbf{U}'}$ denotes the covariance function of $\mathbf{U}'$. It can be interpreted as a force caused by the fluctuations acting on the mean-flow $\overline{\mathbf{U}}$, and has to be modeled by further equations. This will lead us to the k-ϵ model, a turbulence model designed to close the RANS equations.

As an example for deriving the RANS equations we show how to rewrite the term

$$\mathbb{E}\left(\rho\mathrm{div}\left(\mathbf{U}(\mathbf{x},\mathrm{t})(\mathbf{U}(\mathbf{x},\mathrm{t}))^T\right)\right). \qquad (3.1.4)$$

Inserting (3.1.2) into (3.1.4) and omitting the parameter dependence $(\mathbf{x}, \mathrm{t})$ we get

$$\begin{aligned}\mathbb{E}\left(\rho\mathrm{div}(\mathbf{U}\mathbf{U}^T)\right) = \mathbb{E}\left(\rho\mathrm{div}\left(\overline{\mathbf{U}}\ \overline{\mathbf{U}}^T\right)\right) + \mathbb{E}\left(\rho\mathrm{div}\left(\mathbf{U}'\mathbf{U}'^T\right)\right) \\ + \mathbb{E}\left(\rho\mathrm{div}\left(\mathbf{U}'\overline{\mathbf{U}}^T\right)\right) + \mathbb{E}\left(\rho\mathrm{div}\left(\overline{\mathbf{U}}\mathbf{U}'^T\right)\right).\end{aligned}$$

Using the assumptions and the fact that $\mathbf{U}'$ is centered we further get

$$\mathbb{E}\left(\rho\mathrm{div}\left(\mathbf{U}'\overline{\mathbf{U}}^T\right)\right) = \rho\mathrm{div}\left(\mathbb{E}\left(\mathbf{U}'\right)\overline{\mathbf{U}}^T\right) = 0,$$

so that

$$\mathbb{E}\left(\rho\mathrm{div}\left(\mathbf{U}\mathbf{U}^T\right)\right) = \rho\mathrm{div}\left(\overline{\mathbf{U}}\ \overline{\mathbf{U}}^T\right) - \mathrm{div}(\boldsymbol{\tau}),$$

with Reynolds stress tensor $\boldsymbol{\tau}$ given by (3.1.3). Analogously, we can rewrite the remaining terms of (3.1.1), which will result in the RANS equations

$$\mathrm{div}\left(\overline{\mathbf{U}}(\mathbf{x}, \mathrm{t})\right) = 0 \tag{3.1.5}$$

$$\rho\left(\frac{\partial\overline{\mathbf{U}}(\mathbf{x}, \mathrm{t})}{\partial \mathrm{t}} + \mathrm{div}\left(\overline{\mathbf{U}}(\mathbf{x}, \mathrm{t})\overline{\mathbf{U}}(\mathbf{x}, \mathrm{t})^T\right)\right) = -\nabla\overline{\mathrm{P}}(\mathbf{x}, \mathrm{t}) + \mathrm{div}\left(2\mu\overline{\mathbf{S}}(\mathbf{x}, \mathrm{t}) + \boldsymbol{\tau}(\mathbf{x}, \mathrm{t})\right)$$

with mean strain-rate tensor

$$\overline{\mathbf{S}}(\mathbf{x}, \mathrm{t}) = \frac{1}{2}\left(\nabla\overline{\mathbf{U}}(\mathbf{x}, \mathrm{t}) + \nabla\overline{\mathbf{U}}(\mathbf{x}, \mathrm{t})^T\right) \in \mathbb{R}^{3\times 3}.$$

In summary, we have made the following assumptions on $\mathbf{U}$ and P to derive the RANS equations, which will be also used in next section:

- $\mathbf{U}$ is twice differentiable with respect to $\mathbf{x}$, differentiable with respect to t, P is differentiable with respect to $\mathbf{x}$, and $\mathbf{U}$, P solve the Navier-Stokes equations (3.0.1), (3.0.2) almost surely.
- We are allowed to change the order of differentiation and expectation of both $\mathbf{U}$ and P.

If these assumptions held, then $\overline{\mathbf{U}}$, $\overline{\mathrm{P}}$, and $\boldsymbol{\tau}$ would solve the RANS equations (3.1.5). As already mentioned, this system is not closed because we now have three unknowns $\overline{\mathbf{U}}$, $\overline{\mathrm{P}}$, and $\boldsymbol{\tau}$ but only two equations. Thus, we need further equations to close the system, which is a key problem in turbulence modeling

and will be addressed in the next section in form of the standard k-ϵ model. For details on the physics of this model we refer to the outlined literature and works.

3.2 The k-ϵ Model

In the turbulence literature, e.g., [67], there is mainly a distinction between two classes of RANS-based turbulence models: the so-called Reynolds-stress models, which mainly consist of solving an equation for $\boldsymbol{\tau}$, and the turbulent viscosity models, which are based on the turbulent viscosity hypothesis by Boussinesq [13], i.e.,

$$\boldsymbol{\tau}(\mathbf{x},\mathrm{t}) = \mu_T(\mathbf{x},\mathrm{t})\overline{\mathbf{S}}(\mathbf{x},\mathrm{t}) - \frac{2}{3}\rho\mathrm{k}(\mathbf{x},\mathrm{t})I \tag{3.2.1}$$

with a yet to be specified turbulent eddy viscosity

$$\mu_T : \mathbb{R}^3 \times \mathbb{R}_+ \to \mathbb{R}_+,$$

turbulent kinetic energy

$$\mathrm{k} : \mathbb{R}^3 \times \mathbb{R}_+ \to \mathbb{R}_+,$$

and unit matrix $I \in \mathbb{R}^{3\times 3}$. The standard k-$\epsilon$ model [32] by Jones and Launder, further refined in [43] by Launder and Sharma, belongs to the class of turbulent viscosity models. In this model, the turbulent eddy viscosity μ_T is specified as

$$\mu_T(\mathbf{x},\mathrm{t}) = \rho C_\mu \frac{\mathrm{k}^2(\mathbf{x},\mathrm{t})}{\epsilon(\mathbf{x},\mathrm{t})}, \quad C_\mu = 0.09,$$

with dissipation rate

$$\epsilon : \mathbb{R}^3 \times \mathbb{R}_+ \to \mathbb{R}_+.$$

In particular, k is defined as the turbulent kinetic energy of the fluctuations $\mathbf{U}'$ per unit mass, i.e.,

$$\mathrm{k}(\mathbf{x},\mathrm{t}) = \frac{1}{2}\mathbb{E}(\langle \mathbf{U}'(\mathbf{x},\mathrm{t}), \mathbf{U}'(\mathbf{x},\mathrm{t})\rangle),$$

and ϵ as the dissipation per unit mass, i.e.,

$$\epsilon(\mathbf{x}, \mathrm{t}) = \nu \mathbb{E}\left(\left|\nabla \mathbf{U}'(\mathbf{x}, \mathrm{t})\right|_F^2\right), \tag{3.2.2}$$

with constant kinematic viscosity $\nu = \mu/\rho$. The dissipation is the rate at which the turbulent kinetic energy is converted into thermal energy.

The RANS system (3.1.5) together with (3.2.1) will form a closed system, if we have additional equations for k and ϵ. An equation for k can be derived by considering the equation

$$\mathbb{E}\left(\rho\left\langle\left(\frac{\partial \mathbf{U}}{\partial \mathrm{t}} + \operatorname{div}\left(\mathbf{U}\mathbf{U}^T\right)\right), \mathbf{U}'\right\rangle\right) = \mathbb{E}(\langle -\nabla \mathrm{P} + \operatorname{div}(2\mu \mathbf{S}), \mathbf{U}'\rangle)$$

i.e., we formally take the scalar product of both sides of the momentum equation (3.0.2) with $\mathbf{U}'$ and take the expectation. This leads to the equation

$$\begin{aligned}\rho\left(\frac{\partial \mathrm{k}}{\partial \mathrm{t}} + \langle \overline{\mathbf{U}}, \nabla \mathrm{k}\rangle\right) =& \langle \boldsymbol{\tau}, \nabla \overline{\mathbf{U}}\rangle_F - \rho\epsilon \\ &+ \mu \operatorname{div}(\nabla \mathrm{k}) + \operatorname{div}\left(\mathbb{E}\left(-\frac{\rho}{2}\left(\langle \mathbf{U}', \mathbf{U}'\rangle \mathbf{U}' - \mathrm{P}'\mathbf{U}'\right)\right)\right)\end{aligned} \tag{3.2.3}$$

for the turbulent kinetic energy k. Because of the term

$$\mathbb{E}\left(-\frac{\rho}{2}\left(\langle \mathbf{U}', \mathbf{U}'\rangle \mathbf{U}' - \mathrm{P}'\mathbf{U}'\right)\right)$$

equation (3.2.3) would induce additional unknowns. Thus, it is further replaced by

$$\mathbb{E}\left(-\frac{\rho}{2}\left(\langle \mathbf{U}', \mathbf{U}'\rangle \mathbf{U}' - \mathrm{P}'\mathbf{U}'\right)\right) = \frac{\mu_T}{\sigma_\mathrm{k}} \operatorname{div}(\nabla \mathrm{k})$$

with empirical closure coefficient $\sigma_k = 1$. Instead of (3.2.3) we therefore consider the equation

$$\rho\left(\frac{\partial \mathrm{k}}{\partial \mathrm{t}} + \langle \overline{\mathbf{U}}, \nabla \mathrm{k}\rangle\right) = \langle \boldsymbol{\tau}, \nabla \overline{\mathbf{U}}\rangle_F - \rho\epsilon + \operatorname{div}\left(\left(\mu + \frac{\mu_T}{\sigma_\mathrm{k}}\right)\nabla \mathrm{k}\right)$$

for an approximation of k. Analogously to the previous considerations, we could try to get an exact equation for ϵ, but because 'the standard model equation for ϵ is best viewed as being entirely empirical', according to Pope [67, p.375], we only

state the equation for an approximation of ϵ. It reads

$$\rho\left(\frac{\partial\epsilon}{\partial \mathrm{t}} + \langle\overline{\mathbf{U}}, \nabla\epsilon\rangle\right) = C_{\epsilon 1}\frac{\epsilon}{\mathrm{k}}\langle\boldsymbol{\tau}, \nabla\overline{\mathbf{U}}\rangle_F - C_{\epsilon 2}\rho\frac{\epsilon^2}{\mathrm{k}} + \operatorname{div}\left(\left(\mu + \frac{\mu_T}{\sigma_\epsilon}\right)\nabla\epsilon\right)$$

with $C_{\epsilon 1} = 1.44$, $C_{\epsilon 2} = 1.92$, and $\sigma_\epsilon = 1.3$. Note the similarity between the two equations for approximations of k and ϵ. As we have seen the previous derivations are rather heuristic. For discussions on the model we refer to [67, Chapter 10.4.3, Chapter 11.10]. Putting things together, we get the following model.

Model 3.3. *Let the dynamic viscosity $\mu > 0$ and the fluid density $\rho > 0$ be given. Then the system for $\overline{\mathbf{U}} : \mathbb{R}^3 \times \mathbb{R}_+ \to \mathbb{R}^3$, $\overline{\mathrm{P}} : \mathbb{R}^3 \times \mathbb{R}_+ \to \mathbb{R}$, $\mathrm{k} : \mathbb{R}^3 \times \mathbb{R}_+ \to \mathbb{R}_+$, and $\epsilon : \mathbb{R}^3 \times \mathbb{R}_+ \to \mathbb{R}_+$ is given by*

$$\begin{aligned}
&\operatorname{div}(\overline{\mathbf{U}}) = 0\\
&\rho\left(\frac{\partial\overline{\mathbf{U}}}{\partial \mathrm{t}} + \operatorname{div}\left(\overline{\mathbf{U}}\ \overline{\mathbf{U}}^T\right)\right) = -\nabla\overline{\mathrm{P}} + \operatorname{div}\left(\left(2\mu + \rho C_\mu\frac{\mathrm{k}^2}{\epsilon}\right)\overline{\mathbf{S}} - \frac{2}{3}\rho\mathrm{k}I\right)\\
&\rho\left(\frac{\partial\mathrm{k}}{\partial \mathrm{t}} + \langle\overline{\mathbf{U}}, \nabla\mathrm{k}\rangle\right) = \langle\boldsymbol{\tau}, \nabla\overline{\mathbf{U}}\rangle_F - \rho\epsilon + \operatorname{div}\left(\left(\mu + \rho\frac{C_\mu}{\sigma_\mathrm{k}}\frac{\mathrm{k}^2}{\epsilon}\right)\nabla\mathrm{k}\right)\\
&\rho\left(\frac{\partial\epsilon}{\partial \mathrm{t}} + \langle\overline{\mathbf{U}}, \nabla\epsilon\rangle\right) = C_{\epsilon 1}\frac{\epsilon}{\mathrm{k}}\langle\boldsymbol{\tau}, \nabla\overline{\mathbf{U}}\rangle_F - C_{\epsilon 2}\rho\frac{\epsilon^2}{\mathrm{k}} + \operatorname{div}\left(\left(\mu + \rho\frac{C_\mu}{\sigma_\epsilon}\frac{\mathrm{k}^2}{\epsilon}\right)\nabla\epsilon\right)
\end{aligned}$$

with empirical closure coefficients

$$C_\mu = 0.09, \quad \sigma_k = 1, \quad C_{\epsilon 1} = 1.44, \quad C_{\epsilon 2} = 1.92, \quad \sigma_\epsilon = 1.3.$$

Let us now forget all the made assumptions. We have derived a deterministic system for functions k, ϵ, and $\overline{\mathbf{U}}$, which is widely used in the field of Computational Fluid Dynamics (CFD) and therefore implemented in many software solutions. The purpose of our simulation approach is now the following: we get the functions k, ϵ, and $\overline{\mathbf{U}}$ for a specific flow domain by a CFD simulation software (cf. Figure 5.2 in Chapter 5.1). Then the previous considerations motivate the idea to interpret $\overline{\mathbf{U}}$ as mean-flow, k as turbulent kinetic energy and ϵ as dissipation of (yet to be modeled) incompressible fluctuations $\mathbf{U}'$.

Summing up, we have given the parameters (at least numerically)

- fluid density $\rho > 0$, kinematic viscosity $\mu > 0$, functions $\mathrm{k} : \mathbb{R}^3 \times \mathbb{R}_+ \to \mathbb{R}_+$, $\epsilon : \mathbb{R}^3 \times \mathbb{R}_+ \to \mathbb{R}_+$, $\overline{\mathbf{U}} : \mathbb{R}^3 \times \mathbb{R}_+ \to \mathbb{R}^3$,

and want to construct a random field $\mathbf{U}'$ representing the fluctuations such that

- $\mathbf{U}'$ is spatially incompressible,
- $\mathbb{E}(\langle \mathbf{U}'(\mathbf{x},\mathrm{t}), \mathbf{U}'(\mathbf{x},\mathrm{t})\rangle)$ and $\mathbb{E}\left(|\nabla \mathbf{U}'(\mathbf{x},\mathrm{t})|_F^2\right)$ exist and are finite for all $(\mathbf{x},\mathrm{t}) \in \mathbb{R}^3 \times \mathbb{R}_+$,
- $\mathrm{k}(\mathbf{x},\mathrm{t}) = \frac{1}{2}\mathbb{E}(\langle \mathbf{U}'(\mathbf{x},\mathrm{t}), \mathbf{U}'(\mathbf{x},\mathrm{t})\rangle), \quad \epsilon(\mathbf{x},\mathrm{t}) = \nu\mathbb{E}\left(|\nabla \mathbf{U}'(\mathbf{x},\mathrm{t})|_F^2\right)$.

Having constructed the random field $\mathbf{U}'$, we get the actual turbulent velocity $\mathbf{U}$ by

$$\mathbf{U}(\mathbf{x},\mathrm{t}) = \overline{\mathbf{U}}(\mathbf{x},\mathrm{t}) + \mathbf{U}'(\mathbf{x},\mathrm{t}).$$

Note that at this point it is not clear if such a random field $\mathbf{U}'$ exists in the first place. This issue will be addressed in the next chapter where we will also describe a refined random field model for the fluctuations based on the standard k-ϵ model and will develop an efficient simulation algorithm, which fulfills our simulation requirements, cf. Chapter 2.2.

CHAPTER 4

A Velocity Field Model and its Simulation

On top of the k-ϵ model Marheineke has developed a model for the velocity fluctations $\mathbf{U}'$ in [53]. This model is based on a Global-from-Local-Assumption according to that the local velocity fluctuations (fine-scale structure) are modeled as homogeneous, spatially isotropic and incompressible Gaussian random fields that are superposed to form the large-scale structure of the global turbulence. This assumption is motivated by Kolmogorov's local isotropy hypothesis [26, 36, 59]: certain theoretical considerations concerning the energy transfer through the eddy-size spectrum from larger to the smaller eddies lead to the conclusion that the fine-scale structure of anisotropic turbulent flows is almost homogeneous and isotropic.

This chapter is divided into four parts. In the first section we will describe the local velocity field model that has been developed in [53]. It will be shown that the energy spectrum of the local random velocity field is especially characterized by one single parameter ζ, which is obtained by the underlying k-ϵ model. After this we will show how to construct a random field that has exactly the covariance function of the the local velocity random field, is approximately Gaussian (in the sense of finite-dimensional distributions, see Chapter 2.2), and permits the development of a fast simulation algorithm, which then will be described in Section 4.3. In the last part we will propose constructions for global velocity fields based on the local random fields, which fulfill the requirements of the k-ϵ model in

a global sense, see Theorem 4.9. Note that parts of this chapter are strongly oriented on [30]. In the following we take $\mathbb{R}^4$ as index set for the random fields under consideration and interpret t as time parameter.

4.1 The Local Model

Let the constant fluid density $\rho > 0$, dynamic viscosity $\mu > 0$, and functions $\mathrm{k} : \mathbb{R}^3 \times \mathbb{R}_+ \to \mathbb{R}_+$, $\epsilon : \mathbb{R}^3 \times \mathbb{R}_+ \to \mathbb{R}_+$, $\overline{\mathbf{U}} : \mathbb{R}^3 \times \mathbb{R}_+ \to \mathbb{R}^3$ be given, which satisfy the equations in Model 3.3. To every $\mathbf{p} \in \mathbb{R}^3 \times \mathbb{R}_+$ we associate a centered, homogeneous, spatially isotropic and incompressible, $\mathbb{R}^3$-valued Gaussian random field $\mathbf{U}'_{\mathbf{p}} = \left(\mathbf{U}'_{\mathbf{p}}(\mathbf{x}, \mathrm{t})\right)_{(\mathbf{x},\mathrm{t})\in\mathbb{R}^4}$ on a common probability space $(\Omega, \mathcal{A}, P)$ such that

$$\frac{1}{2}\,\mathbb{E}\left(\langle \mathbf{U}'_{\mathbf{p}}(\mathbf{p}), \mathbf{U}'_{\mathbf{p}}(\mathbf{p})\rangle\right) = \mathrm{k}(\mathbf{p}), \quad \nu\,\mathbb{E}\left(\left|\nabla \mathbf{U}'_{\mathbf{p}}(\mathbf{p})\right|_F^2\right) = \epsilon(\mathbf{p}), \tag{4.1.1}$$

with kinematic viscosity $\nu = \mu/\rho > 0$. Note that we implicitly assume the existence of $\mathbf{U}'_{\mathbf{p}}$, since we show how to construct it later on.

Remark 4.1. Because $\mathbf{U}'_{\mathbf{p}}$ is Gaussian and spatially incompressible the random field $(\nabla \mathbf{U}'_{\mathbf{p}}(\mathbf{x}, \mathrm{t}))_{(\mathbf{x},\mathrm{t})\in\mathbb{R}^4}$ exists and is Gaussian too, see Remark 2.16. Hence, the second relation in (4.1.1) is well-defined because $\mathbb{E}\left(\left|\nabla \mathbf{U}'_{\mathbf{p}}(\mathbf{p})\right|_F^2\right)$ is finite.

The homogenity of $\mathbf{U}'_{\mathbf{p}}$ implies that its covariance function $\mathbf{K}_{\mathbf{p}}$ satisfies

$$\mathbf{K}_{\mathbf{p}}((\mathbf{x}_1, \mathrm{t}_1), (\mathbf{x}_2, \mathrm{t}_2)) = \mathbf{K}_{\mathbf{p}}((\mathbf{x}_1 - \mathbf{x}_2, \mathrm{t}_1 - \mathrm{t}_2), (\mathbf{0}, 0)).$$

Thus, the functions $\mathbb{E}\left(\langle \mathbf{U}'_{\mathbf{p}}(\cdot), \mathbf{U}'_{\mathbf{p}}(\cdot)\rangle\right)$ and $\mathbb{E}\left(\left|\nabla \mathbf{U}'_{\mathbf{p}}(\cdot)\right|_F^2\right)$ are constant. In view of (4.1.1) it follows

$$\frac{1}{2}\,\mathbb{E}\left(\langle \mathbf{U}'_{\mathbf{p}}(\mathbf{x}, \mathrm{t}), \mathbf{U}'_{\mathbf{p}}(\mathbf{x}, \mathrm{t})\rangle\right) = \mathrm{k}(\mathbf{p}), \quad \nu\,\mathbb{E}\left(\left|\nabla \mathbf{U}'_{\mathbf{p}}(\mathbf{x}, \mathrm{t})\right|_F^2\right) = \epsilon(\mathbf{p}), \tag{4.1.2}$$

for all $(\mathbf{x}, \mathrm{t}) \in \mathbb{R}^4$. Because $\mathbf{U}'_{\mathbf{p}}$ is spatially isotropic its spatial autocovariance function $\boldsymbol{\gamma}_{\mathbf{p}} : \mathbb{R}^3 \to \mathbb{R}^{3\times 3}$,

$$\boldsymbol{\gamma}_{\mathbf{p}}(\mathbf{x}) = \mathbf{K}_{\mathbf{p}}((\mathbf{x}, 0), (\mathbf{0}, 0))$$

satisfies

$$\boldsymbol{\gamma}_{\mathbf{p}}(\mathbf{x}) = \boldsymbol{S}\boldsymbol{\gamma}_{\mathbf{p}}\left(\boldsymbol{S}^T\mathbf{x}\right)\boldsymbol{S}^T$$

for all $\boldsymbol{S} \in \mathbb{R}^{3\times 3}$ with $\boldsymbol{S}^T = \boldsymbol{S}^{-1}$, cf. Definition 2.17.

Remark 4.2 (Energy spectrum)**.** If $\boldsymbol{\gamma}_{\mathbf{p}}$ is integrable then its Fourier transform is of the form

$$\mathcal{F}_{\boldsymbol{\gamma}_{\mathbf{p}}}(\boldsymbol{\kappa}) = \frac{1}{4\pi}\frac{E_{\mathbf{p}}(|\boldsymbol{\kappa}|)}{|\boldsymbol{\kappa}|^2}\left(\boldsymbol{I} - \frac{\boldsymbol{\kappa}\boldsymbol{\kappa}^T}{|\boldsymbol{\kappa}|^2}\right), \quad \boldsymbol{\kappa} \in \mathbb{R}^3,$$

with integrable energy spectrum $\mathrm{E}_{\mathbf{p}} : \mathbb{R}_+ \to \mathbb{R}_+$, see Theorem 2.19. In this case, we have

$$\mathrm{k}(\mathbf{p}) = \int_0^\infty \mathrm{E}_{\mathbf{p}}(\kappa)\, d\kappa$$

according to Lemma 2.20 and (4.1.1). Interpreting k as turbulent kinetic energy, the function $\mathrm{E}_{\mathbf{p}}$ gives us the energy distribution of the fluctuations among all wave numbers κ, see also [60, Chapter 6].

In the forthcoming explanations we focus on dimensionless quantities. Thus, we make $\mathbf{U}'_{\mathbf{p}}$ dimensionless using the typical turbulent length and time

$$\mathrm{l}_T(\mathbf{p}) = \frac{\mathrm{k}^{3/2}(\mathbf{p})}{\epsilon(\mathbf{p})}, \quad \mathrm{t}_T(\mathbf{p}) = \frac{\mathrm{k}(\mathbf{p})}{\epsilon(\mathbf{p})},$$

corresponding to $\mathbf{p}$, i.e.,

$$\mathbf{U}'_{\mathbf{p}}(\mathbf{x}, \mathrm{t}) = \mathrm{k}^{1/2}(\mathbf{p})\, \boldsymbol{U}'_{\mathbf{p}}\left(\frac{\mathbf{x}}{\mathrm{l}_T(\mathbf{p})}, \frac{\mathrm{t}}{\mathrm{t}_T(\mathbf{p})}\right). \tag{4.1.3}$$

This yields

$$\frac{1}{2}\,\mathbb{E}\left(\langle \boldsymbol{U}'_{\mathbf{p}}(\boldsymbol{x},t), \boldsymbol{U}'_{\mathbf{p}}(\boldsymbol{x},t)\rangle\right) = 1, \quad \mathbb{E}\left(\left|\nabla \boldsymbol{U}'_{\mathbf{p}}(\boldsymbol{x},t)\right|_F^2\right) = \frac{1}{\zeta(\mathbf{p})}, \tag{4.1.4}$$

for the dimensionless field $\boldsymbol{U}'_{\mathbf{p}}$ with dimensionless viscosity

$$\zeta(\mathbf{p}) = \frac{\nu\epsilon(\mathbf{p})}{\mathrm{k}^2(\mathbf{p})} \in \mathbb{R}_+.$$

Remark 4.3 (Dimensionless viscosity ζ)**.** In his first hypothesis of similarity [36, p. 12], Kolmogorov introduced the so-called Kolmogorov length

$$\eta = \left(\frac{\nu^3}{\epsilon}\right)^{1/4}$$

for a turbulent flow with kinematic viscosity ν and dissipation ϵ. The Kolmogorov length characterizes the smallest turbulent length scales, whereas

$$\mathrm{l}_T = \frac{\mathrm{k}^{3/2}}{\epsilon}$$

characterizes the largest turbulent length scales, see, e.g., [67, Chapter 6.1]. Because

$$\zeta = \left(\frac{\eta}{\mathrm{l}_T}\right)^{4/3}, \tag{4.1.5}$$

it can be interpreted as ratio of turbulent fine-scale and large-scale length. Later on we will make use of this interpretation and relation (4.1.5).

In the following we will shortly describe the construction of the local $\mathbb{R}^{3\times3}$-valued covariance function $\boldsymbol{K}_{\mathbf{p}}$. For the detailed derivation of the original model with frozen turbulence pattern we refer to [53], extensions on the temporal correlations are studied and incorporated in [56]. For more informations about turbulence and its evolution see [26, 33, 50, 56] and references within.

In a homogeneous turbulent flow, the covariance function $\boldsymbol{K}_{\mathbf{p}}$ is invariant with regard to spatial and temporal translations and hence depends only on the differences of the arguments. The evolution of the autocovariance function of $\boldsymbol{U}'_{\mathbf{p}}$ is modeled by an advection-driven vortex structure that is naturally decaying over time (alleviated frozen turbulence). Taylor's hypothesis of frozen turbulence pattern [78], i.e., fluctuations arise due to so-called turbulence pattern that are transported by the mean flow without changing their structure, is based on the observation that the rate of decay of the mean properties is rather slow with respect to the time scale of the fluctuating fine-scale structures. The superposition with a natural temporal decay function φ is essential for describing suspensions of particles or filaments in turbulent flows, since otherwise small light objects tending to move with the mean flow field would experience permanently the same

non-varying fluctuations.

So, we assume $\boldsymbol{K}_{\mathbf{p}}$ is given by

$$\boldsymbol{K}_{\mathbf{p}}(\boldsymbol{x}+\boldsymbol{x_1}, t+t_1, \boldsymbol{x_1}, t_1) = \boldsymbol{\gamma}_{\mathbf{p}}\left(\boldsymbol{x} - \overline{\boldsymbol{U}}_{\mathbf{p}} t\right)\varphi(t) \tag{4.1.6}$$

with spatial autocovariance function $\boldsymbol{\gamma}_{\mathbf{p}}$, a temporal decay function $\varphi : \mathbb{R}_+ \to \mathbb{R}$ (see Model 4.5), and mean flow velocity $\overline{\boldsymbol{U}}_{\mathbf{p}}$. The latter is also made dimensionless with respect to the typical turbulent length and time in consistency to (4.1.3), i.e.,

$$\overline{\boldsymbol{U}}_{\mathbf{p}} = \frac{1}{\mathrm{k}^{1/2}(\mathbf{p})}\overline{\mathbf{U}}(\mathbf{p}).$$

In case of spatially incompressible and isotropic turbulence, $\boldsymbol{\gamma}_{\mathbf{p}}$ can be constructed by a single scalar-valued function, see Corollary 2.21. In terms of the spectral density being its Fourier transform $\mathcal{F}_{\boldsymbol{\gamma}_{\mathbf{p}}}$, this function is known as energy spectrum $E_{\mathbf{p}} : \mathbb{R}_+ \to \mathbb{R}_+$ that has been well-studied theoretically and experimentally in the last century,

$$\mathcal{F}_{\boldsymbol{\gamma}_{\mathbf{p}}}(\boldsymbol{\kappa}) = \frac{1}{4\pi}\frac{E_{\mathbf{p}}(|\boldsymbol{\kappa}|)}{|\boldsymbol{\kappa}|^2}\left(\boldsymbol{I} - \frac{\boldsymbol{\kappa}\boldsymbol{\kappa}^T}{|\boldsymbol{\kappa}|^2}\right), \quad \boldsymbol{\kappa} \in \mathbb{R}^3, \tag{4.1.7}$$

with unit matrix $\boldsymbol{I} \in \mathbb{R}^{3\times 3}$. Based on dimensional analysis Kolmogorov has derived not only the characteristic ranges but also the typical behavior of the spectrum which agrees with later coming physical concepts and experiments, cf. Kolmogorov's 5/3-law and his hypothesis of local isotropy [26, 36]. Gathering the existing knowledge about $E_{\mathbf{p}}$, an appropriate model has to satisfy Kolmogorov's 5/3-law as well as the requirements (4.1.4) of the k-ϵ turbulence model, i.e.,

$$\begin{aligned} &\int_0^\infty (\ln(1+\kappa))^\alpha \kappa^2 E_{\mathbf{p}}(\kappa)\,\mathrm{d}\kappa < \infty \text{ for } \alpha > 3, \\ &\int_0^\infty E_{\mathbf{p}}(\kappa)\,\mathrm{d}\kappa = 1, \quad \int_0^\infty \kappa^2 E_{\mathbf{p}}(\kappa)\,\mathrm{d}\kappa = \frac{1}{2\zeta(\mathbf{p})}. \end{aligned} \tag{4.1.8}$$

The first relation ensures the differentiability of $\boldsymbol{U}'_{\mathbf{p}}$, see Corollary 2.21. The other relations correspond to the definitions of the kinetic turbulent energy k and dissipation rate ϵ in its nondimensionalized form (4.1.4), because due to

Lemma 2.20 we have

$$1 = \frac{1}{2}\,\mathbb{E}\left(\langle \boldsymbol{U}'_{\mathbf{p}}(\boldsymbol{x},t), \boldsymbol{U}'_{\mathbf{p}}(\boldsymbol{x},t)\rangle\right) = \int_0^\infty E_{\mathbf{p}}(\kappa)\, d\kappa,$$
$$\frac{1}{2\zeta(\mathbf{p})} = \frac{1}{2}\mathbb{E}\left(\left|\nabla \boldsymbol{U}'_{\mathbf{p}}(\boldsymbol{x},t)\right|_F^2\right) = \int_0^\infty \kappa^2 E_{\mathbf{p}}(\kappa)\, d\kappa.$$

Figure 4.1 shows the typical form of a energy spectrum. For further details, see [53, p. 1713]. The conditions (4.1.8) on $E_{\mathbf{p}}$ allow for a family of functions that can be adapted to experiments. In particular, $E_{\mathbf{p}}$ and $\boldsymbol{\gamma}_{\mathbf{p}}$ only depend on $\zeta(\mathbf{p})$. Therefore we write

$$E_{\zeta(\mathbf{p})} = E_{\mathbf{p}}, \quad \boldsymbol{\gamma}_{\zeta(\mathbf{p})} = \boldsymbol{\gamma}_{\mathbf{p}},$$

throughout the following.

Model 4.4 (Energy Spectrum [53, 56])**.** *The energy spectrum of the local field* $\boldsymbol{U}'_{\mathbf{p}}$ *is constructed as function* $E_{\zeta(\mathbf{p})} \in C^2(\mathbb{R}_+)$*,*

$$E_{\zeta(\mathbf{p})}(\kappa) = C_{\mathrm{K}} \begin{cases} \kappa_1^{-5/3} \sum_{j=4}^{6} a_j \left(\frac{\kappa}{\kappa_1}\right)^j & \kappa < \kappa_1 \\ \kappa^{-5/3} & \kappa_1 \le \kappa \le \kappa_2 \\ \kappa_2^{-5/3} \sum_{j=7}^{9} b_j \left(\frac{\kappa}{\kappa_2}\right)^{-j} & \kappa_2 < \kappa \end{cases} \tag{4.1.9}$$

where the $\zeta(\mathbf{p})$*-dependent transition wave numbers* κ_1 *and* κ_2 *are implicitly given by*

$$\int_0^\infty E_{\zeta(\mathbf{p})}(\kappa)\,\mathrm{d}\kappa = 1, \quad \int_0^\infty \kappa^2\, E_{\zeta(\mathbf{p})}(\kappa)\,\mathrm{d}\kappa = \frac{1}{2\zeta(\mathbf{p})}. \tag{4.1.10}$$

The regularity parameters are $a_4 = 230/9$*,* $a_5 = -391/9$*,* $a_6 = 170/9$*,* $b_7 = 209/9$*,* $b_8 = -352/9$*,* $b_9 = 152/9$*, and the Kolmogorov constant is* $C_{\mathrm{K}} = 1/2$*.*

The integral conditions in (4.1.10) can be reformulated as nonlinear system for κ_1 and κ_2 in $\zeta = \zeta(\mathbf{p})$

$$\hat{a}_1 \kappa_1^{-2/3} - \hat{b}_1 \kappa_2^{-2/3} = C_K^{-1}, \quad -\hat{a}_2 \kappa_1^{4/3} + \hat{b}_2 \kappa_2^{4/3} = (2C_K\zeta)^{-1}, \tag{4.1.11}$$

with positive parameters

$$\hat{a}_1 = \frac{3}{2} + \sum_{j=4}^{6} \frac{a_j}{j+1}, \quad \hat{a}_2 = \frac{3}{4} - \sum_{j=4}^{6} \frac{a_j}{j+3},$$

$$\hat{b}_1 = \frac{3}{2} - \sum_{j=7}^{9} \frac{b_j}{j-1}, \quad \hat{b}_2 = \frac{3}{4} + \sum_{j=7}^{9} \frac{b_j}{j-3}.$$

The condition $0 < \kappa_1 < \kappa_2 < \infty$ is equivalent to $0 < \zeta < \zeta_{crit} = (2C_K^3(\hat{b}_2 - \hat{a}_2)(\hat{b}_1 - \hat{a}_1)^2)^{-1} \approx 3.86$. The bounds on ζ (where we have $\kappa_1 = \kappa_2 = (C_K(\hat{a}_1 - \hat{b}_1))^{3/2}$ for $\zeta = \zeta_{crit}$ and $\kappa_1 = (C_K\hat{a}_1)^{3/2}$, $\kappa_2 = \infty$ for $\zeta = 0$) are no practically relevant restrictions, since the general turbulence theory assumes the ratio of fine-scale and large-scale length to satisfy $\zeta = \epsilon\nu/\mathrm{k}^2 \ll 1$.

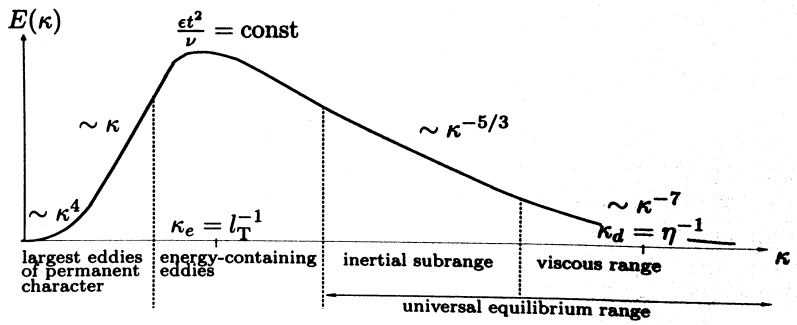

Figure 4.1: [53] Sketch of energy spectrum for isotropic turbulence.

Model 4.5 (Temporal Correlations)**.** *The natural decay of the temporal correlations is modeled as* $\varphi \in C^\infty(\mathbb{R}_+)$

$$\varphi(t) = \exp\left(\frac{-t^2}{2\tau_l^2}\right), \quad \mathcal{F}_\varphi(s) = \frac{\tau_l}{\sqrt{2\pi}} \exp\left(\frac{-\tau_l^2 s^2}{2}\right), \quad \tau_l = 0.212. \tag{4.1.12}$$

The temporal covariance function φ satisfies $\varphi(0) = 1$, which implies that the integral of its Fourier transform $\mathcal{F}_\varphi$ is normalized. We use an exponential decay with respect to the turbulent large-scale time with $\tau_l = 0.212$, see, e.g., [48, 66] and references within.

4.2 Modeling the Covariance Structure of the Local Velocity Fields

In this section we will show how to construct a random field that has exactly the covariance function (4.1.6) of the local velocity field $\boldsymbol{U}'_{\mathrm{p}}$ and can be simulated efficiently. As we are interested in a Gaussian field we will use the Central Limit Theorem to approximate the desired normal distribution. In view of the prescribed

data (covariance/spectral function) there exist various approximation/simulation procedures in the literature, e.g., Karhunen-Loeve expansion, Cholesky decomposition, circulant embedding for a given covariance function [15] or spectral, Fourier, Fourier-wavelet methods for a given spectral density [21, 29, 41]; for an overview see [7, 38] and references within. We will use a technique that takes advantage of the special structure of the given data and turns out to be exact in the covariance and very efficient as we will comment on. Note that we do not address the issue of existence of all occurring random fields and stochastic processes as we construct them later on. To shorten the notation we write $\zeta = \zeta(\mathbf{p})$ in the following.

Considering the covariance function (4.1.6), we separate the spatial and temporal arguments by introducing a new Gaussian random field $\boldsymbol{V}_\mathbf{p} = (\boldsymbol{V}_\mathbf{p}(\boldsymbol{x}, t))_{(\boldsymbol{x},t)\in\mathbb{R}^4}$ defined by

$$\boldsymbol{V}_\mathbf{p}(\boldsymbol{x}, t) = \boldsymbol{U}'_\mathbf{p}\left(\boldsymbol{x} + \overline{\boldsymbol{U}}_\mathbf{p} t, t\right), \quad (\boldsymbol{x}, t) \in \mathbb{R}^4,$$

from which $\boldsymbol{U}'_\mathbf{p}$ can be easily regained. Then $\boldsymbol{V}_\mathbf{p}$ is also centered and homogeneous with covariance function

$$\begin{aligned} \boldsymbol{K}_{\boldsymbol{V}_\mathbf{p}}((\boldsymbol{x}_1, t_1), (\boldsymbol{x}_2, t_2)) &= \mathbb{E}\left(\boldsymbol{V}_\mathbf{p}(\boldsymbol{x}_1, t_1)\boldsymbol{V}_\mathbf{p}(\boldsymbol{x}_2, t_2)^T\right) \\ &= \mathbb{E}\left(\boldsymbol{U}'_\mathbf{p}\left(\boldsymbol{x}_1 + \overline{\boldsymbol{U}}_\mathbf{p} t_1, t_1\right)\boldsymbol{U}'_\mathbf{p}\left(\boldsymbol{x}_2 + \overline{\boldsymbol{U}}_\mathbf{p} t_2, t_2\right)^T\right) \\ &= \boldsymbol{\gamma}_\zeta(\boldsymbol{x}_1 - \boldsymbol{x}_2)\,\varphi(t_1 - t_2). \end{aligned} \tag{4.2.1}$$

The form of $\boldsymbol{K}_{\boldsymbol{V}_\mathbf{p}}$ leads to the following idea: let $\boldsymbol{\xi}_\zeta = (\boldsymbol{\xi}_\zeta(\boldsymbol{x}))_{\boldsymbol{x}\in\mathbb{R}^3}$ be an $\mathbb{R}^3$-valued random field and $\psi = (\psi(t))_{t\in\mathbb{R}}$ be a real-valued stochastic process, which are centered and stochastically independent with covariance functions

$$\boldsymbol{K}_{\xi_\zeta}(\boldsymbol{x}_1, \boldsymbol{x}_2) = \boldsymbol{\gamma}_\zeta(\boldsymbol{x}_1 - \boldsymbol{x}_2), \quad K_\psi(t_1, t_2) = \varphi(t_1 - t_2). \tag{4.2.2}$$

Defining a random field $\boldsymbol{V}_\zeta$ by

$$\boldsymbol{V}_\zeta(\boldsymbol{x}, t) = \boldsymbol{\xi}_\zeta(\boldsymbol{x})\,\psi(t),$$

$\boldsymbol{V}_\zeta$ and $\boldsymbol{V}_\mathbf{p}$ possess the same covariance function (4.2.1). As we are interested in

a Gaussian field, we consider

$$\boldsymbol{V}_{\zeta,N}(\boldsymbol{x},t) = \frac{1}{\sqrt{N}} \sum_{l=1}^{N} \boldsymbol{V}_{\zeta}^{(l)}(\boldsymbol{x},t), \quad N \in \mathbb{N}, \tag{4.2.3}$$

in which $\boldsymbol{V}_{\zeta}^{(l)}$, $l = 1, ..., N$, are independent copies of $\boldsymbol{V}_{\zeta}$. The Central Limit Theorem ensures then the convergence in distribution

$$\boldsymbol{V}_{\zeta,N}(\boldsymbol{x},t) \xrightarrow{d} \mathcal{N}(\boldsymbol{0}, \boldsymbol{\gamma}(\boldsymbol{0})\varphi(0))$$

for every $(\boldsymbol{x},t) \in \mathbb{R}^4$ as N tends to infinity. Due to the multi-dimensional Central Limit Theorem, for any choice of $n \in \mathbb{N}$ and $(\boldsymbol{x}_1,t_1),\ldots,(\boldsymbol{x}_n,t_n) \in \mathbb{R}^4$, the joint distribution of $\boldsymbol{V}_{\zeta,N}(\boldsymbol{x}_1,t_1),\ldots,\boldsymbol{V}_{\zeta,N}(\boldsymbol{x}_n,t_n)$, converges in distribution to a normal distribution on $\mathbb{R}^{3n}$. We conclude that $\boldsymbol{V}_{\zeta,N}$ is a centered random field with covariance (4.2.1), which is approximately Gaussian (in the sense of finite-dimensional distributions) if N is large. In the following we will show how to construct a random field $\boldsymbol{\xi}_{\zeta}$ and a stochastic process ψ with the covariance functions (4.2.2) such that an efficient simulation of $\boldsymbol{V}_{\zeta,N}$ is possible.

For the construction of $\boldsymbol{\xi}_{\zeta}$ we exploit the special structure of its spectral density $\mathcal{F}_{\boldsymbol{\gamma}_{\zeta}}$ in (4.1.7). Let $\boldsymbol{\eta}_{\zeta} = (\boldsymbol{\eta}_{\zeta}(t))_{t\in\mathbb{R}}$ be a centered, homogeneous, and $\mathbb{R}^3$-valued stochastic process with spectral density given by

$$\boldsymbol{f}_{\boldsymbol{\eta}_{\zeta}}(\kappa) = \frac{E_{\zeta}(|\kappa|)}{2}\boldsymbol{I}, \quad \kappa \in \mathbb{R}, \tag{4.2.4}$$

i.e., its components $\eta_{\zeta,i}$, $i \in \{1,2,3\}$, are pairwise uncorrelated processes with the same spectral density

$$f_{\eta_{\zeta,i}}(\kappa) = \frac{E_{\zeta}(|\kappa|)}{2}.$$

The following statement by Majda [49, p. 1156] is essential for our forthcoming simulation algorithm (see Algorithm 4.8 in the next section).

Theorem 4.6. *Let $\boldsymbol{\eta}_{\zeta} = (\boldsymbol{\eta}_{\zeta}(t))_{t\in\mathbb{R}}$ be a centered, homogeneous, and $\mathbb{R}^3$-valued stochastic process with spectral density given by* (4.2.4) *and let $\boldsymbol{Z}$ be a uniformly distributed random vector on the unit sphere $S^2 = \{\boldsymbol{x} \in \mathbb{R}^3 : |\boldsymbol{x}| = 1\}$. Under the*

assumption that $\boldsymbol{\eta}_\zeta, \boldsymbol{Z}$ *are independent, the* $\mathbb{R}^3$*-valued random field* $(\boldsymbol{\xi}_\zeta(\boldsymbol{x}))_{\boldsymbol{x}\in\mathbb{R}^3}$ *that is defined by*

$$\boldsymbol{\xi}_\zeta(\boldsymbol{x}) = \left(\boldsymbol{I} - \boldsymbol{Z}\boldsymbol{Z}^T\right)\boldsymbol{\eta}_\zeta(\langle \boldsymbol{x}, \boldsymbol{Z}\rangle), \quad \boldsymbol{x}\in\mathbb{R}^3,$$

with unit matrix $\boldsymbol{I}\in\mathbb{R}^{3\times 3}$ *has the covariance function* $\boldsymbol{\gamma}_\zeta$*.*

Proof. Let $\boldsymbol{\eta}_\zeta$ be defined on a probability space $(\Omega_1, \mathcal{A}_1, P_1)$ and $\boldsymbol{Z}$ on a probability space $(\Omega_2, \mathcal{A}_2, P_2)$. We define $\boldsymbol{\xi}_\zeta(\boldsymbol{x})$ on the product space

$$(\Omega_1\times\Omega_2, \mathcal{A}_1\otimes\mathcal{A}_2, P_1\otimes P_2)$$

by

$$\boldsymbol{\xi}_\zeta(\boldsymbol{x})(\omega_1,\omega_2) = \left(\boldsymbol{I} - \boldsymbol{Z}(\omega_2)\boldsymbol{Z}(\omega_2)^T\right)\boldsymbol{\eta}_\zeta(\langle \boldsymbol{x}, \boldsymbol{Z}(\omega_2)\rangle)(\omega_1),$$

where $\omega_1\in\Omega_1$, $\omega_2\in\Omega_2$, $\boldsymbol{x}\in\mathbb{R}^3$. With $\boldsymbol{P}(\boldsymbol{y}) = \left(\boldsymbol{I} - \boldsymbol{y}\boldsymbol{y}^T\right)$ it holds that

$$\begin{aligned}
&\mathbb{E}_{P_1\otimes \mathrm{P}_2}\left(\boldsymbol{\xi}_\zeta(\boldsymbol{x}_1)\boldsymbol{\xi}_\zeta(\boldsymbol{x}_2)^T\right)\\
&\quad= \int_{\Omega_2} \boldsymbol{P}(\boldsymbol{Z}(\omega_2))\boldsymbol{K}_{\eta_\zeta}(\langle \boldsymbol{x}_1-\boldsymbol{x}_2, \boldsymbol{Z}(\omega_2)\rangle, 0)\boldsymbol{P}(\boldsymbol{Z}(\omega_2))\; P_2(d\omega_2)\\
&\quad= \int_{\Omega_2} \boldsymbol{P}(\boldsymbol{Z}(\omega_2))\mathcal{F}^{-1}_{\boldsymbol{f}_{\eta_\zeta}}(\langle \boldsymbol{x}_1-\boldsymbol{x}_2, \boldsymbol{Z}(\omega_2)\rangle)\boldsymbol{P}(\boldsymbol{Z}(\omega_2))\; P_2(d\omega_2)\\
&\quad= \frac{1}{4\pi}\int_{S^2} \boldsymbol{P}(\sigma)\left(\int_{\mathbb{R}} e^{i\kappa\langle \boldsymbol{x}_1-\boldsymbol{x}_2,\sigma\rangle} E_\zeta(|\kappa|)\boldsymbol{I}\; d\kappa\right)\boldsymbol{P}(\sigma)\; d\sigma\\
&\quad= \frac{1}{4\pi}\int_{\mathbb{R}} E_\zeta(|\kappa|)\left(\int_{S^2} e^{i\kappa\langle \boldsymbol{x}_1-\boldsymbol{x}_2,\sigma\rangle}\boldsymbol{P}(\sigma)\; d\sigma\right)\; d\kappa\\
&\quad= \frac{1}{4\pi}\int_{\mathbb{R}} E_\zeta(|\kappa|)\left(\int_{\boldsymbol{\phi}(K)} e^{i\kappa\langle \boldsymbol{x}_1-\boldsymbol{x}_2,\sigma\rangle}\boldsymbol{P}(\sigma)\; d\sigma\right)\; d\kappa
\end{aligned}$$

with $K = [0,2\pi]\times[-\frac{\pi}{2},\frac{\pi}{2}]$ and $\boldsymbol{\phi}(u,v) = [\cos(u)\cos(v), \sin(u)\cos(v), \sin(v)]^T$. Hence,

$$\begin{aligned}
&\mathbb{E}_{P_1\otimes \mathrm{P}_2}\left(\boldsymbol{\xi}_\zeta(\boldsymbol{x}_1)\boldsymbol{\xi}_\zeta(\boldsymbol{x}_2)^T\right)\\
&\quad= \frac{1}{4\pi}\int_{\mathbb{R}} \frac{E_\zeta(|\kappa|)}{|\kappa|^2}\int_0^{2\pi}\int_{-\frac{\pi}{2}}^{\frac{\pi}{2}} e^{i\langle \boldsymbol{x}_1-\boldsymbol{x}_2,\kappa\phi(u,v)\rangle}\boldsymbol{P}(\boldsymbol{\phi}(u,v))\cdot|\kappa|^2\cos(v)\; dv\; du\; d\kappa.
\end{aligned}$$

With the substitution

$$\boldsymbol{g}(\kappa, u, v) = \kappa\boldsymbol{\phi}(u, v) = \boldsymbol{k},\ |\det \boldsymbol{g}'(\kappa, u, v)| = |\kappa|^2 \cos(v),$$

we get $|\kappa| = |\boldsymbol{k}|$ and hence

$$\begin{aligned}\mathbb{E}_{P_1 \otimes \mathrm{P}_2}\left(\boldsymbol{\xi}_\zeta(\boldsymbol{x}_1)\boldsymbol{\xi}_\zeta(\boldsymbol{x}_2)^T\right) &= \int_{\mathbb{R}^3} e^{i\langle \boldsymbol{x}_1 - \boldsymbol{x}_2, \boldsymbol{k}\rangle} \frac{1}{4\pi} \frac{E_\zeta(|\boldsymbol{k}|)}{|\boldsymbol{k}|^2} \boldsymbol{P}\left(\frac{\boldsymbol{k}}{|\boldsymbol{k}|}\right)\, d\boldsymbol{k} \\ &= \gamma_\zeta(\boldsymbol{x}_1 - \boldsymbol{x}_2).\end{aligned}$$

□

Since the components of $\boldsymbol{\eta}_\zeta$ are pairwise uncorrelated, it is sufficient to focus on the construction of one component $\eta_{\zeta,i}$ in order to construct the whole field $\boldsymbol{\xi}_\zeta$. Following [41], this can be done in the subsequent manner: as $E_\zeta(\kappa) \geq 0$ for all $\kappa \geq 0$ and

$$\int_{\mathbb{R}} f_{\eta_{\zeta,i}}(\kappa)\, \mathrm{d}\kappa = \int_0^\infty E_\zeta(\kappa)\, \mathrm{d}\kappa = 1,$$

the function $f_{\eta_{\zeta,i}}$ is a continuous probability density on $\mathbb{R}$. Choosing a random variable R_ζ with this probability density and two standard normally distributed random variables X and Y, such that X, Y, R_ζ are stochastically independent, the complex-valued process $(\eta_{\zeta,C}(t))_{t\in\mathbb{R}}$ defined by

$$\eta_{\zeta,C}(t) = A\exp(iR_\zeta t), \quad A = X + iY,$$

has the spectral density $2f_{\eta_{\zeta,i}}$, as a simple calculation with the conjugate-complex $\overline{\eta_{\zeta,C}}$ shows

$$\mathbb{E}(\eta_{\zeta,C}(t + t_1)\,\overline{\eta_{\zeta,C}}(t_1)) = \mathbb{E}\left(A\overline{A}\right)\mathbb{E}\left(\exp(iR_\zeta t)\right) = 2\int_{\mathbb{R}} \exp(i\kappa t)\, f_{\eta_{\zeta,i}}(\kappa)\, \mathrm{d}\kappa.$$

By taking its real or imaginary part we obtain a real-valued process with the desired spectral density $f_{\eta_{\zeta,i}}$. The so constructed process $\eta_{\zeta,i}$ ($\eta_{\zeta,i} = \mathrm{Re}(\eta_{\zeta,C})$ or $\eta_{\zeta,i} = \mathrm{Im}(\eta_{\zeta,C})$) has obviously almost surely differentiable realizations and hence the same holds for $\boldsymbol{\xi}_\zeta$.

A construction of the time process ψ can be achieved analogously to $\eta_{\zeta,i}$. We

define a new process $(\psi_{\tau_l}(t))_{t\in\mathbb{R}}$ by

$$\psi_{\tau_l}(t) = \psi(\tau_l t)$$

having the covariance function

$$\mathbb{E}(\psi_{\tau_l}(t+t_1)\psi_{\tau_l}(t)) = \varphi(\tau_l t),$$

cf. (4.1.12). Consequently, its spectral density is

$$f_{\psi_{\tau_l}}(s) = \frac{1}{\tau_l}\mathcal{F}_\varphi\left(\frac{s}{\tau_l}\right) = \frac{1}{\sqrt{2\pi}}\exp\left(-\frac{s^2}{2}\right).$$

As $f_{\psi_{\tau_l}}$ is the probability density of the standard normal distribution, we take three independent, standard normally distributed random variables R, X, Y, and define a complex-valued process $(\psi_C(t))_{t\in\mathbb{R}}$ by

$$\psi_C(t) = A\exp(iRt), \quad A = X + iY.$$

Then, the process $\psi = \mathrm{Re}(\psi_C(\cdot/\tau_l))$ or $\psi = \mathrm{Im}(\psi_C(\cdot/\tau_l))$ has the desired covariance function φ and almost surely differentiable realizations.

In summary, we get an approximation $\boldsymbol{U}'_{\mathbf{p},N}$ of $\boldsymbol{U}'_{\mathbf{p}}$ by

$$\boldsymbol{U}'_{\mathbf{p},N}(\boldsymbol{x},t) = \frac{1}{\sqrt{N}}\sum_{l=1}^{N}\boldsymbol{\xi}_\zeta^{(l)}\left(\boldsymbol{x} - \overline{\boldsymbol{U}}_{\mathbf{p}}t\right)\psi^{(l)}(t),$$

for $N \in \mathbb{N}, (\boldsymbol{x},t) \in \mathbb{R}^4$, with help of the previous constructions. In view of (4.1.3) we get the dimensional velocity $\mathbf{U}'_{\mathbf{p},N}$ by

$$\mathbf{U}'_{\mathbf{p},N}(\mathrm{x},\mathrm{t}) = \mathrm{k}^{1/2}(\mathbf{p})\,\boldsymbol{U}'_{\mathbf{p},N}\left(\frac{\mathbf{x}}{\mathrm{l}_T(\mathbf{p})}, \frac{\mathrm{t}}{\mathrm{t}_T(\mathbf{p})}\right)$$

with

$$\mathrm{l}_T(\mathbf{p}) = \frac{\mathrm{k}^{3/2}(\mathbf{p})}{\epsilon(\mathbf{p})}, \quad \mathrm{t}_T(\mathbf{p}) = \frac{\mathrm{k}(\mathbf{p})}{\epsilon(\mathbf{p})}.$$

In the next section we will develop an efficient simulation algorithm for $\boldsymbol{U}'_{\mathbf{p},N}$.

4.3 Simulation of the Local Model

The construction strategy for $\boldsymbol{\xi}_\zeta$ uses the isotropic form of the spectral density and traces the construction of a random field back to the construction of a real-valued stochastic process, which involves an enormous reduction of the computational effort. For the simulation of the real-valued process $\eta_{\zeta,i}$ with known spectral density, various (approximate) Fourier methods could be applied. However, this approach of introducing the complex-valued surrogate process via three random variables is not only exact but also efficient. The simulation and evaluation can be performed flexibly regarding the needs. In contrast to the a priori fixed discretization in the Fourier methods, this adaptivity yields advantages concerning memory and computation costs for the forthcoming simulations of the jets dynamics. The same holds true for the time process ψ. Here, one could certainly think of direct methods on top of the covariance, but their performance suffers from an a priori discretization and high computational effort (for example the effort for a Cholesky decomposition is $\mathcal{O}(n^3)$, n number of grid points), see also the discussion at the end of Chapter 2.2.

Let us assume we want to evaluate a realization of $\boldsymbol{U}'_{\mathbf{p},N}$ in M evaluation points. Then the effort of our simulation algorithm is $\mathcal{O}(M)$ for a fixed N (if we additionally allow that N varies, the effort is $\mathcal{O}(MN)$). For every $\boldsymbol{U}'_{\mathbf{p},N}$ we have to generate $9N$ standard normally and $3N$ $f_{\eta_{\zeta,i}}$-distributed random numbers as well as N uniformly distributed vectors on S^2. Thereby, the realization of the $f_{\eta_{\zeta,i}}$-distributed random variables is the most expensive part. These variables depend on the considered flow situation as $f_{\eta_{\zeta,i}}(\kappa) = E_\zeta(|\kappa|)/2$ with $\zeta = \epsilon\nu/\mathrm{k}^2$ at point $\mathbf{p}$. In the following we will show how to simulate them. For details on the techniques, see, e.g., [7, 61].

Because $f_{\eta_{\zeta,i}}$ is symmetric it suffices to simulate an $\mathbb{R}_+$-valued random variable Y_ζ with probability density $f_{Y_\zeta}(\kappa) = E_\zeta(\kappa)$. If we set

$$X = \begin{cases} -Y_\zeta, & U < 1/2, \\ Y_\zeta, & U \geq 1/2, \end{cases}$$

where U is uniform distributed on $[0,1]$, such that U, Y_ζ are independent, then X has the probability density $f_{\eta_{\zeta,i}}$. So, in the following we will focus on the

simulation of Y_ζ.

For an exact simulation of Y_ζ we could use the classical acceptance-rejection method by von Neumann [82], taking the density $g_{a,b}$ of the Gamma distribution with parameters $a, b > 0$, which is given by

$$g_{a,b}(x) = \frac{1}{b^a \Gamma(a)} x^{a-1} \exp\left(-\frac{x}{b}\right), \quad x \in \mathbb{R}_+,$$

$\Gamma(a) = \int_0^\infty t^{a-1} \exp(-t)\, dt$, as reference density. However, we have no algorithmic solution for determining the parameters a and b of the reference density for a given ζ. Nevertheless, we show an example of appropriate parameters a and b with $\zeta = 0.05$ as example. By solving the nonlinear system (4.1.11) with an implemented MATLAB routine, we could get a plot of the energy spectrum corresponding to ζ. By testing various values for a and b we get that

$$f_Y(x) \leq C g_{1.4,2}(x), \quad C = 3,$$

for all $x \in \mathbb{R}_+$, which is shown in Figure 4.2. In view of the globalization strategy

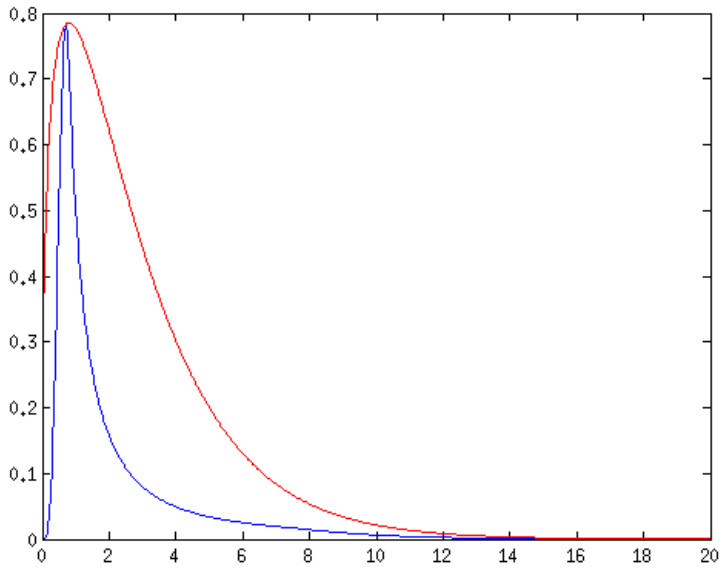

Figure 4.2: Energy spectrum for $\zeta = 0.05$ (*blue*) and density $g_{1.4,2}$ (*red*).

(4.4.1) in the following section this 'graphical solution' is not appropriate.

Therefore we prefer a simulation with the inversion method. Let

$$F_{Y_\zeta}(x) = \int_0^x E_\zeta(\kappa)\, d\kappa, \quad x \in \mathbb{R}_+,$$

be the distribution function of Y_ζ and let U be uniform distributed on $[0, 1]$. By determining X, which solves

$$F_{Y_\zeta}(X) = U, \tag{4.3.1}$$

we get a random variable X with density f_{Y_ζ}. Because the inverse function of F_{Y_ζ} is not known analytically this method involves approximation errors by solving equation (4.3.1) numerically. In Figure 4.3 we have plotted the energy spectrum for $\zeta = 0.05$ against the kernel density estimate of an independent sample

$$X = (X_1, \ldots, X_{40000})$$

drawn with help of (4.3.1). For the density estimation we have used a Gaussian kernel. The differences between the energy spectrum and the estimated density are negligible for our purposes.

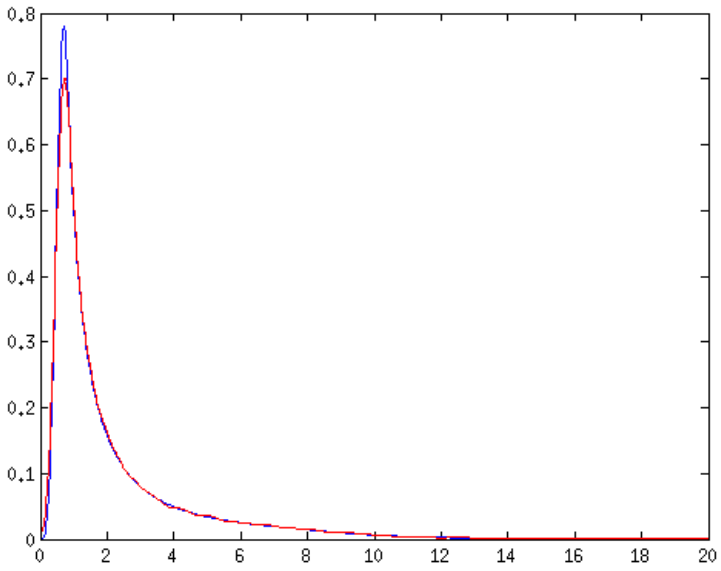

Figure 4.3: Energy spectrum for $\zeta = 0.05$ (*blue*) and estimated density of X (*red*).

Remark 4.7. As for the stochastic simulation (cf. Algorithm 4.8), a random vector $\boldsymbol{Z}$, which is uniformly distributed on the unit sphere S^2 can be simulated by help of three independent, standard normally distributed random variables X_1, X_2, X_3, according to $\boldsymbol{Z} = (X_1, X_2, X_3)^T/R$ with $R = \sqrt{X_1^2 + X_2^2 + X_3^2}$.

Let us now state the simulation algorithm for the simulation of the approximation $\boldsymbol{U}'_{\mathbf{p},N}$.

Algorithm 4.8 (Simulation algorithm)**.**

Input: *$N \in \mathbb{N}$, local point $\mathbf{p}$, evaluation point $(\boldsymbol{x}, t)$, kinematic viscosity ν, flow data at point $\mathbf{p}$:* k, ϵ, $\overline{\mathbf{U}}$

Output: *realization of $\boldsymbol{U}'_{\mathbf{p},N}$ at $(\boldsymbol{x}, t)$*

A.1 Determine the dimensionless local flow parameters:
$\zeta = \epsilon\nu/\mathrm{k}^2$ *and* $\overline{\boldsymbol{U}} = \overline{\mathbf{U}}/\sqrt{\mathrm{k}}$

A.2 Generate independent random numbers, $l = 1, \ldots, N$:

- $\boldsymbol{Z}^{(l)}$*:*
  N samples according to the uniform distribution on the sphere S^2 by scaling method
- $R^{(l)}_{\zeta,j}$*, $j = 1, 2, 3$:*
  $3N$ samples according to the density $f_{\eta_{\zeta,i}}$ by the inversion method (obtain $f_{\eta_{\zeta,i}}(\kappa) = E_\zeta(|\kappa|)/2$ by solving the nonlinear system (4.1.11))
- $X^{(l)}_{\xi,j}$*,* $Y^{(l)}_{\xi,j}$*, $j = 1, 2, 3$, as well as* $R^{(l)}_{\psi}$*,* $X^{(l)}_{\psi}$*,* $Y^{(l)}_{\psi}$*:*
  $9N$ samples according to the standard normal distribution

B.1 Compute realizations, $l = 1, \ldots, N$:

- *spatial field* $\boldsymbol{\xi}^{(l)}_\zeta$*:*

$$\boldsymbol{\xi}^{(l)}_\zeta(\boldsymbol{x}) = \left(\boldsymbol{I} - \boldsymbol{Z}^{(l)}\left(\boldsymbol{Z}^{(l)}\right)^T\right)\boldsymbol{\eta}^{(l)}_\zeta\left(\left\langle \boldsymbol{x}, \boldsymbol{Z}^{(l)}\right\rangle\right)$$

with

$$\eta^{(l)}_{\zeta,j}\left(\left\langle \boldsymbol{x}, \boldsymbol{Z}^{(l)}\right\rangle\right) = \mathrm{Re}\left(\left(X^{(l)}_{\xi,j} + iY^{(l)}_{\xi,j}\right)\exp\left(iR^{(l)}_{\zeta,j}\left\langle \boldsymbol{x}, \boldsymbol{Z}^{(l)}\right\rangle\right)\right)$$

for $j = 1, 2, 3$

- *time process* $\psi^{(l)}$*:*

$$\psi^{(l)}(t) = \mathrm{Re}\left(\left(X_\psi^{(l)} + iY_\psi^{(l)}\right)\exp\left(iR_\psi^{(l)}t/\tau_l\right)\right), \quad \tau_l = 0.212$$

B.2 Calculate

$$\boldsymbol{U}'_{\mathbf{p},N}(\boldsymbol{x},t) = \frac{1}{\sqrt{N}}\sum_{l=1}^{N}\boldsymbol{\xi}_\zeta^{(l)}\left(\boldsymbol{x} - \overline{\boldsymbol{U}}t\right)\psi^{(l)}(t)$$

Algorithm 4.8 consists of two parts, A - the initialization with the generation of random numbers and B - the computation and evaluation. Hence, to evaluate the same sample at a different collection of points $(\boldsymbol{x_i}, t_i)$, only part B need to be executed while the initialization with the random numbers of part A should be stored. Simulating the local velocity fluctuations, the finite-dimensional distributions of $\boldsymbol{V}_{\zeta,N}$ and $\boldsymbol{U}'_{\mathbf{p},N}$ are close to a multivariate normal distribution for large N according to the Central Limit Theorem. For the assessment of the multivariate normality on a fixed set of points $\{(\boldsymbol{x}_1,t_1),\ldots,(\boldsymbol{x}_d,t_d)\} \subset \mathbb{R}^4$ we apply the statistical test by Royston [72], [73], which we evaluate by help of the respective MATLAB routine [79]. Table 4.1 shows the rejection frequencies at the significance level 0.05 for different values of the variate size d and the random field parameter N. We use here 1000 Monte Carlo replications and a sample size of 50.

$N\backslash d$	1	2	3	4	5	6
10	0.357	0.416	0.439	0.461	0.497	0.518
30	0.108	0.15	0.184	0.187	0.19	0.182
50	0.098	0.102	0.12	0.143	0.183	0.126
70	0.069	0.079	0.072	0.087	0.117	0.124
100	0.082	0.076	0.096	0.091	0.085	0.108
150	0.094	0.099	0.093	0.101	0.109	0.125

Table 4.1: Rejection frequencies of Royston's test.

The rejection frequency among the 1000 replications turns out to be a robust quantity that stays approximately the same for $N \geq 50$. Hence, we use $N = 50$ in (4.2.3) for the forthcoming simulations. The observed rejection frequency of 10% is acceptable for us since the Gaussian distribution is a secondary property. Our main interest is the accurate construction of the covariance structure.

Having the simulation algorithm it is straightforward to generate realizations of $\boldsymbol{U}'_{\mathbf{p},N}$ with a given ζ. Let us set the turbulent kinetic energy and dissipation rate to be $\mathrm{k} = \epsilon = 1$. Then, by varying ζ this would mean we vary the viscosity, because $\zeta = \epsilon\nu/\mathrm{k}^2 = \nu$. Figure 4.4 illustrates the numerical result of a realization of $\boldsymbol{U}'_{\mathbf{p},N}$ with $\zeta = 10^{-3}$ and $\mathrm{k} = \epsilon = 1$.

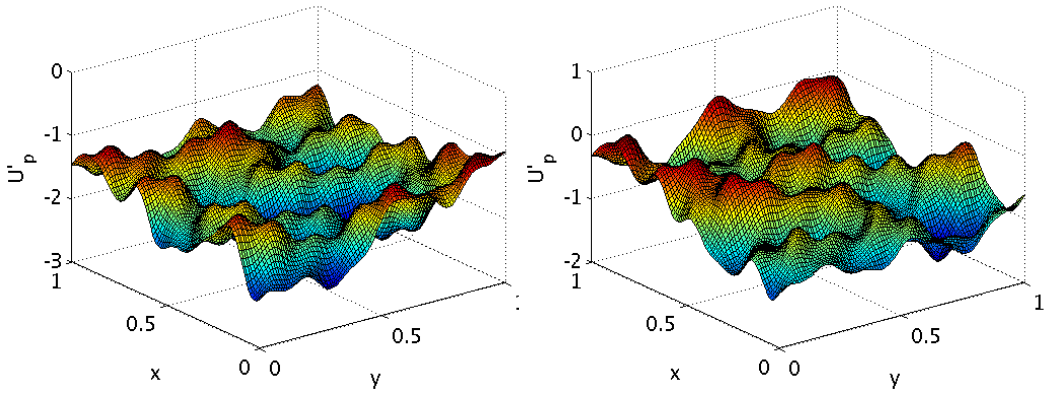

Figure 4.4: Realization of a component of $\boldsymbol{U}'_{\mathbf{p},N}$ with $\zeta = 10^{-3}$, plotted over two-dimensional space at certain times.

What would we expect from a numerical result of a realization of $\boldsymbol{U}'_{\mathbf{p},N}$ with a smaller ζ, e.g., $\zeta = 10^{-4}$? By (4.1.5) in Remark 4.3 this would mean we decrease the Kolmogorov length η, because under the assumption that $\mathrm{k} = \epsilon = 1$ it holds

$$\eta = \zeta^{3/4}.$$

In Figure 4.5 we can see the effect, i.e., the realization exposes a more 'fine-scaled structure'.

4.4 Globalization Strategy

In [53] the authors proposed the construction of a random field $\mathbf{U}'$ that satisfies the requirements of the k-ϵ turbulence model (4.1.1) in an integral sense. In [30] it is pointed out that this construction is not appropriate for the simulation of turbulent spinning processes. Thus, in [30] we have proposed the following construction

$$\mathbf{U}'_N(\mathbf{x},\mathrm{t}) = \mathrm{k}^{1/2}(\mathbf{x},\mathrm{t})\,\boldsymbol{U}'_{(\mathbf{x},\mathrm{t}),N}\left(\frac{\epsilon(\mathbf{x},\mathrm{t})}{\mathrm{k}^{3/2}(\mathbf{x},\mathrm{t})}\,\mathbf{x}, \frac{\epsilon(\mathbf{x},\mathrm{t})}{\mathrm{k}(\mathbf{x},\mathrm{t})}\,\mathrm{t}\right), \quad N \in \mathbb{N}, \tag{4.4.1}$$

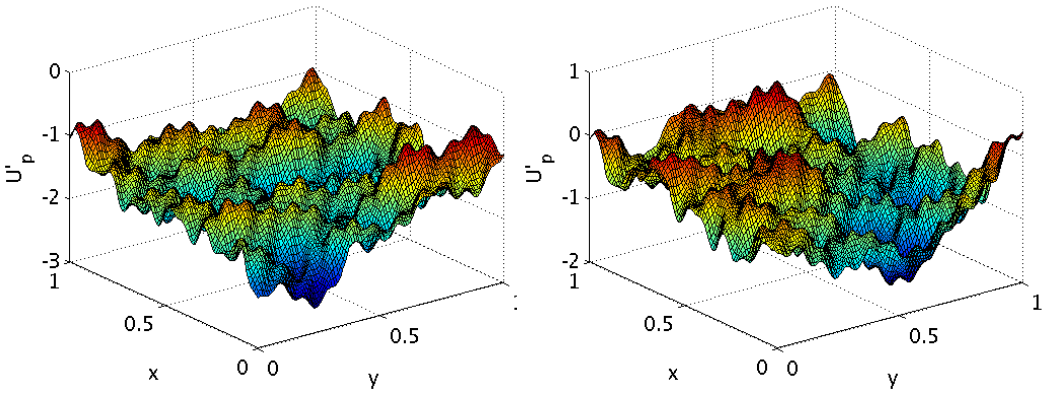

Figure 4.5: Realization of a component of $\boldsymbol{U}'_{\mathbf{p},N}$ with $\zeta = 10^{-4}$, plotted over two-dimensional space at certain times.

for a global velocity field using the space- and time-dependent flow fields for kinetic turbulent energy and dissipation rate known from the k-ϵ simulation. The construction (4.4.1) has to be understood in the following manner: in view of Algorithm 4.8 we do not directly generate the $f_{\eta_{\zeta,i}}$-distributed random numbers in part A. Instead we only generate independent realizations $U(\omega_1), \ldots, U(\omega_n)$ of a uniform in $[0,1]$ distributed random variable U needed for the inversion method. Then in part B of the algorithm we generate independent $f_{\eta_{\zeta,i}}$-distributed random numbers $X(\omega_1), \ldots, X(\omega_n)$ with help of the actual ζ at $(\mathbf{x}, \mathrm{t})$, i.e., $X(\omega_i)$ has to solve the equation

$$\int_0^{X(\omega_i)} E_{\zeta(\mathbf{x},\mathrm{t})}(\kappa)\, d\kappa = U(\omega_i),$$

cf. (4.3.1). Considering the family of the local fluctuation fields $\boldsymbol{U}'_{\mathbf{p},N}$, the global velocity fluctuation $\mathbf{U}'_N$ equals here pointwise the respective local fluctuation. By the globalization the local properties of isotropy and homogeneity vanish, and $\mathbf{U}'_N$ represents the actual turbulence structure. Moreover, we can state the following.

Theorem 4.9. *Let* $\mathbf{U}'_N$ *be defined by* (4.4.1). *Then* $\mathbf{U}'_N$ *fulfills the conditions on the kinetic turbulent energy exactly, i.e.,*

$$\frac{1}{2}\,\mathbb{E}(\langle \mathbf{U}'_N(\mathbf{x},\mathrm{t}), \mathbf{U}'_N(\mathbf{x},\mathrm{t})\rangle) = \mathrm{k}(\mathbf{x},\mathrm{t})$$

for all $(\mathbf{x},\mathrm{t}) \in \mathbb{R}^4$.

Proof. With

$$\mathrm{l}_T(\mathbf{x},\mathrm{t}) = \frac{\mathrm{k}^{3/2}(\mathbf{x},\mathrm{t})}{\epsilon(\mathbf{x},\mathrm{t})}, \quad \mathrm{t}_T(\mathbf{x},\mathrm{t}) = \frac{\mathrm{k}(\mathbf{x},\mathrm{t})}{\epsilon(\mathbf{x},\mathrm{t})},$$

it follows with help of (4.1.4)

$$\begin{aligned}
&\frac{1}{2}\,\mathbb{E}(\langle \mathbf{U}'_N(\mathbf{x},\mathrm{t}), \mathbf{U}'_N(\mathbf{x},\mathrm{t})\rangle) \\
&\quad = \mathrm{k}(\mathbf{x},\mathrm{t})\,\frac{1}{2}\,\mathbb{E}\left(\left\langle \boldsymbol{U}'_{(\mathbf{x},\mathrm{t}),N}\left(\frac{\mathbf{x}}{\mathrm{l}_T(\mathbf{x},\mathrm{t})}, \frac{\mathrm{t}}{\mathrm{t}_T(\mathbf{x},\mathrm{t})}\right), \boldsymbol{U}'_{(\mathbf{x},\mathrm{t}),N}\left(\frac{\mathbf{x}}{\mathrm{l}_T(\mathbf{x},\mathrm{t})}, \frac{\mathrm{t}}{\mathrm{t}_T(\mathbf{x},\mathrm{t})}\right)\right\rangle\right) \\
&\quad = \mathrm{k}(\mathbf{x},\mathrm{t})
\end{aligned}$$

for all $(\mathbf{x},\mathrm{t}) \in \mathbb{R}^4$. □

The condition on the dissipation rate containing the spatial derivatives is valid up to an error of order $\mathcal{O}(\zeta_0)$ where the constant $\zeta_0 = \epsilon_0\nu_0/\mathrm{k}_0^2 \ll 1$ represents the typical ratio of turbulent fine-scale and large-scale length. The parameter ζ_0 can also be interpreted as the reciprocal of the turbulent Reynolds number. The error estimate is based on the assumption that changes in the behaviour of k and ϵ mainly appear on the large scale and not on the fine scale. This motivates an asymptotic consideration with the multi-scale ansatz $\mathrm{k}(\mathbf{x},\mathrm{t}) = \mathrm{k}_0 + \mathrm{k}_1(\zeta_0\mathbf{x},\mathrm{t})$ (and analogously for ϵ, ν), yielding the result. See [30], Remark 14, for the validity of this assumption in the melt-blowing process.

Since the whole field $\zeta(\mathbf{x},\mathrm{t}) = \nu\epsilon(\mathbf{x},\mathrm{t})/\mathrm{k}^2(\mathbf{x},\mathrm{t})$ is very small in turbulent flows (see, e.g., Figure 5.3 for a turbulent air stream in a melt-blowing process), construction (4.4.1) might be further simplified to

$$\mathbf{U}'_{c,N}(\mathbf{x},\mathrm{t}) = \mathrm{k}^{1/2}(\mathbf{x},\mathrm{t})\,\boldsymbol{U}'_{c,N}\left(\frac{\epsilon(\mathbf{x},\mathrm{t})}{\mathrm{k}^{3/2}(\mathbf{x},\mathrm{t})}\,\mathbf{x}, \frac{\epsilon(\mathbf{x},\mathrm{t})}{\mathrm{k}(\mathbf{x},\mathrm{t})}\,\mathrm{t}\right). \tag{4.4.2}$$

such that $\zeta(c) = \zeta$ is small, e.g., $\zeta = 10^{-4}$. The difference to (4.4.1) is that we only generate the $f_{\eta_{\zeta,i}}$-distributed random numbers for one ζ, which of course can be done in part A of Algorithm 4.8. This avoids the solving of different nonlinear systems (4.1.11) and the multiple application of the inversion method for all the required ζ in the respective points (see Algorithm 4.8, Step A.2), which involves a further decrease of computational costs. Analogously to the proof of Theorem 4.9

we get

$$\frac{1}{2}\,\mathbb{E}(\langle \mathbf{U}'_{c,N}(\mathbf{x},\mathrm{t}), \mathbf{U}'_{c,N}(\mathbf{x},\mathrm{t})\rangle) = \mathrm{k}(\mathbf{x},\mathrm{t})$$

exactly with a similar argument as before for the dissipation rate ϵ.

Remark 4.10. In [30] the construction (4.4.2) is considered with $\zeta = 0$. To get differentiable realizations of the velocity field the authors cut off the energy spectrum in simulations appropriately .

With (4.4.1) and (4.4.2) we have proposed two constructions for the global velocity fluctuations $\mathbf{U}'$ that can be simulated very efficiently. Note that the random field defined by (4.4.1) is in general not Gaussian whereas the field defined by (4.4.2) is Gaussian. In the next chapter we will use the both constructions for the simulation of turbulent spinning processes.

CHAPTER 5

Turbulent Spinning

In turbulent spinning processes like melt-blowing and spunbond very thin liquid fiber jets are spun due to high-velocity air streams. The characteristics of melt-blowing are the huge jet elongations (jet thinning) that are obtained by the stretching due to turbulent air flows. In spunbond there is no stretching but an additionally bonding step after the fiber laydown (e.g., by applying heated rolls) that fuses the fibers together. Because melt-blowing and spunbond are similar processes we only describe the former in more detail. For more information about spunbond we refer to [51]. Note that parts of this chapter are strongly oriented on [30].

Melt-blowing is a process for manufacturing very thin thermoplastic fibers, whose commercial importance steadily increases. It dates back to Wente's work in the 1950s at the Naval Research Laboratory in the USA [83]. For an overview on the technology we refer to [51, 65]. In a melt-blowing process, a molten stream of polymer is extruded from the spinneret into a forwarding high-velocity air stream. The aerodynamic force rapidly attenuates the polymer jet from a diameter d_0 of approximately 500 micrometers at the nozzle down to final diameters d that can be as small as 0.5 micrometers. The values of the speed are very high. Since air and polymer are nearly of the same temperature, the gas prevents polymer solidification at distances close to the die. So fibers are produced that are orders of

magnitude smaller than the fibers of a conventional melt-spinning process where the stretching is caused by a mechanical force due to a take-up wheel. The elongation

$$e = \frac{\mathrm{A}_0}{\mathrm{A}} = \frac{\mathrm{d}_0^2}{\mathrm{d}^2}$$

in melt-blowing is of order 10^6, that means a reduction of 10^3 in diameter d and of 10^6 in cross-sectional area

$$\mathrm{A} = \frac{\pi \mathrm{d}^2}{4}.$$

The index $_0$ indicates the quantities at the nozzle. Melt-blown fibers make excellent filters. They have a high insulating value, moreover they show high cover, surface area and potentially high strength per unit weight.

The optimization of the fabric and the manufacturing process requires the understanding of the fiber structure development in melt-blowing [14]. To gain insight in fiber jet attenuation (thinning) and cooling several on-line measurements have been performed during the last years (see, e.g., [74, 88] and for measurements on jet diameter and temperature [9, 80], jet velocity components [85], frequency and amplitude of jet vibrations [16, 75], nonwoven webs [45] etc.). But, until now there is a clear, unsolved discrepancy between experiments and mathematical models / simulations. The numerical results presented in the literature coincide quite well with the measurements under conditions of a conventional melt-spinning process with moderate elongation of order 10^2, but absolutely underestimate the jet attenuation in orders of magnitude for industrial melt-blowing processes, [74, 80, 89]. The reason might lie in the fact that the underlying mathematical models have been originally developed for melt-spinning processes, dealing with mass, momentum and energy balances for a steady (longitudinal) spinning threadline, cf. first publications [35, 58] in the 1960s or for an overview [90]. Up to now the studies have been extended to viscous and viscoelastic fluids with inclusion of heat transfer, inertial and air drag effects and with regard of jet dynamics, vibrations and bending instabilities. It is an area of active research as recent articles show, see for example [22, 55–57, 68, 75, 77, 86, 87] and references within. However, in the used steady considerations, the jet cross-sectional area A

and absolute speed v of the fiber are related according to

$$v_0 A_0 = vA$$

for an incompressible fluid, such that the computed elongation is obviously restricted by the velocity $\mathbf{U}$ of the acting air stream, i.e.,

$$e = \frac{v}{v_0} < \frac{|\mathbf{U}|_\infty}{v_0}. \tag{5.0.1}$$

This also holds true for advanced melt-blowing simulations with a turbulence model for the high-velocity air stream when only the mean flow field information is taken into account [89]. The computed elongation is hence of order 10^4 – in contrast to the measured order of 10^6. Latest experiments [74, 75] indicate the relevance of the turbulent fluctuations for the jet thinning.

In Chapter 5.1 we present a random PDE model for melt-blowing. Because the numerics for this system are very demanding regarding computational speed we use a simplification of this model to quantify the elongation with help of Monte Carlo methods. Thereby, we use the constructed random fields (4.4.1), (4.4.2), and an aerodynamic drag force, see (5.1.1). The simplification as well as the numerical results will be presented in Chapter 5.1. We will see that we are getting a step closer towards the in experiments measured elongation of order 10^6. In Chapter 5.2 we will describe a random PDAE model for spundbond, which has been developed by Marheineke and Wegener in [53]. For the numerics of this model we will address the issue of choosing appropriate grid sizes to simulate fibers that are smooth enough in a certain sense, which will be described later on.

5.1 Simplified Random ODE Model

In [53, 56] the authors have developed a model framework for the dynamics of a long slender object (fiber) in a turbulent flow in terms of a random aerodynamic drag force $\mathbf{f}$ in a one-way-coupling. The drag force

$$\mathbf{f} : S^2 \times \mathbb{R}^3 \times \mathbb{R}_+ \times \mathbb{R}_+ \times \mathbb{R}_+ \to \mathbb{R}^3$$

depends on the objects tangent $\boldsymbol{\tau} \in S^2$, the relative velocity $\mathbf{w}$ between air flow and object, the kinematic viscosity $\nu > 0$, the fluid density $\rho > 0$, and the diameter $\mathrm{d} > 0$ of the object. A nondimensionalization of $\mathbf{f}$ by

$$\mathbf{f}(\boldsymbol{\tau}, \mathbf{w}, \nu, \rho, \mathrm{d}) = \frac{\rho\nu^2}{\mathrm{d}} \boldsymbol{f}\left(\boldsymbol{\tau}, \frac{\mathrm{d}}{\nu}\mathbf{w}\right), \quad \mathbf{w} = \frac{\nu}{\mathrm{d}}\boldsymbol{w}, \tag{5.1.1}$$

yields a reduction of dependencies, where the dimensional quantities $\mathbf{f}$, $\mathbf{w}$ are scaled by help of the typical length d, mass $\rho\mathrm{d}^3$, and time d^2/ν that are induced by object and flow. Thus, the dimensionless drag force

$$\boldsymbol{f} : S^2 \times \mathbb{R}^3 \to \mathbb{R}^3$$

only depends on object's tangent $\boldsymbol{\tau}$ as well as on the relative velocity $\boldsymbol{w}$ between air flow and object. If the object under consideration can be described by a circular cylinder the drag can be particularly represented in terms of normal and tangential resistance functions r_n, r_τ,

$$\boldsymbol{f}(\boldsymbol{\tau}, \boldsymbol{w}) = w_n r_n(w_n)\boldsymbol{n} + w_\tau r_\tau(w_n)\boldsymbol{\tau},$$

with

$$w_\tau = \langle \boldsymbol{w}, \boldsymbol{\tau} \rangle, \quad w_n = \sqrt{\boldsymbol{w}^2 - w_\tau^2}, \quad \boldsymbol{n} = \frac{\boldsymbol{w} - w_\tau \boldsymbol{\tau}}{w_n},$$

see [56].

Model 5.1 (Resistance Coefficients for Drag [56])**.** *The normal and tangential resistance coefficients are modeled as* $r_n, r_\tau \in C^1(\mathbb{R}_+)$

$$r_n(w_n) = \begin{cases} \sum_{j=0}^{3} q_{n,j}\, w_n^j & w_n \le w_0 \\ 4\pi/S \left(1 - \frac{S^2 - S/2 + 5/16}{32S} w_n^2\right) & w_0 \le w_n < w_1 \\ \exp\left(\sum_{j=0}^{3} p_{n,j} \ln^j w_n\right) w_n & w_1 \le w_n < w_2 \\ 2\sqrt{w_n} + 0.5 w_n & w_2 \le w_n \end{cases}$$

$$r_\tau(w_n) = \begin{cases} \sum_{j=0}^{3} q_{\tau,j}\, w_n^j & w_n \le w_0 \\ 4\pi/\left(2S-1\right) \left(1 - \frac{2S^2 - 2S + 1}{16(2S-1)} w_n^2\right) & w_0 \le w_n < w_1 \\ \exp\left(\sum_{j=0}^{3} p_{\tau,j} \ln^j w_n\right) w_n & w_1 \le w_n < w_2 \\ \gamma\sqrt{w_n} & w_2 \le w_n. \end{cases}$$

With regularization parameter $0 \leq \delta < 3.5 \cdot 10^{-2}$ *and*

$$r_n^\star = (4\pi \ln(4/\delta) - \pi)/\ln^2(4/\delta), \quad r_\tau^\star = (2\pi \ln(4/\delta) + \pi/2)/\ln^2(4/\delta),$$

the transition points are

$$w_0 = 2\,(\exp(2.0022) - 4\pi/r_n^\star), \quad w_1 = 0.1, \quad w_2 = 100.$$

Moreover $\gamma = 2$ *and* $S = S(w_n) = 2.0022 - \ln w_n$. *The regularity parameters are given by*

$$\begin{aligned} &q_{n,0} = r_n^*, \quad q_{\tau,0} = r_\tau^*, \quad p_{n,0} = 1.6911, && p_{\tau,0} = 1.1552, \\ &q_{n,1} = 0, \quad q_{\tau,1} = 0, \quad p_{n,1} = -6.7222 \cdot 10^{-1}, && p_{\tau,1} = -6.8479 \cdot 10^{-1}, \end{aligned}$$

and

$$\begin{aligned} q_{n,2} &= (3r_n(w_0) - w_0 r_n'(w_0) - 3r_n^\star)/w_0^2, && p_{n,2} = 3.3287 \cdot 10^{-2}, \\ q_{\tau,2} &= (3r_\tau(w_0) - w_0 r_\tau'(w_0) - 3r_\tau^\star)/w_0^2, && p_{\tau,2} = 1.4884 \cdot 10^{-2}, \\ q_{n,3} &= (-2r_i(w_0) + w_0 r_n'(w_0) + 2r_n^\star)/w_0^3, && p_{n,3} = 3.5015 \cdot 10^{-3}, \\ q_{\tau,3} &= (-2r_\tau(w_0) + w_0 r_\tau'(w_0) + 2r_\tau^\star)/w_0^3, && p_{\tau,3} = 7.4966 \cdot 10^{-4}. \end{aligned}$$

Remark 5.2. The resistance coefficients r_n, r_τ are composed of Oseen theory, Taylor heuristic as well as numerical simulations and matched to Stokes expansions of higher order $r_n^\star$, $r_\tau^\star$ for $w_n \ll 1$. Model 5.1 has been derived for a steady flow around a cylinder and validated experimentally. It holds true for all incident flow directions and over a wide range of Reynolds numbers – even in the turbulent regime when time-averaged quantities are considered. By evaluating the tangent $\boldsymbol{\tau}$ and relative velocity $\boldsymbol{w}$ locally it was extended to handle dynamic situations (analogously to Stokes drag extensions for moving particles in flows). Its application to simulating melt-spinning processes yields satisfactory results, see, e.g., [4]. In turbulent spinning processes the air flow velocity fluctuates over time and space. Since the fibers follow the flow field, the relative velocity is of moderate size but still varying. In view of the underlying original assumptions this should be kept in mind when dealing with the drag model. In the sequel we use $\delta = 10^{-3}$.

In the following we investigate the jet dynamics due to the aerodynamic drag force (5.1.1) taking into account the turbulent velocity fluctuations $\mathbf{U}'$. Thereby, we use a simplified model that consists of a system of first order random ODEs in time for jet position $\mathbf{r}$, jet velocity $\mathbf{v}$, and elongation e. Let the velocity fluctuations be defined on a probability space $(\Omega, \mathcal{A}, P)$. For the simplification we proceed from a random PDE model. In this model a fiber is described by an arclength-parametrized, time-dependent curve

$$\mathbf{r} : [0, \ell(\mathrm{T})] \times [0, \mathrm{T}] \times \Omega \to \mathbb{R}^3$$

in Lagrangian formulation. We assume that the length $\ell(\mathrm{t})$ of the fiber at time instance t is given by

$$\ell(\mathrm{t}) = \mathrm{v}_0 \mathrm{t}$$

where $\mathrm{v}_0 > 0$ denotes the exit speed at the nozzle. We further assume that at time instance t the fiber leaves the nozzle at arclength parameter $s = \ell(t)$, see also Figure 5.8 in Chapter 5.2. Neglecting inner stresses, we obtain a system for the jet position $\mathbf{r} : [0, \ell(\mathrm{T})] \times [0, \mathrm{T}] \times \Omega \to \mathbb{R}^3$, the jet velocity

$$\mathbf{v} : [0, \ell(\mathrm{T})] \times [0, \mathrm{T}] \times \Omega \to \mathbb{R}^3,$$

and the elongation

$$e : [0, \ell(\mathrm{T})] \times [0, \mathrm{T}] \times \Omega \to \mathbb{R}_+$$

in the time interval $[0, \mathrm{T}]$ with time dependent boundary conditions. It reads

$$\begin{aligned} \partial_{\mathrm{t}} \mathbf{r}(\mathrm{s}, \mathrm{t}) &= \mathbf{v}(\mathrm{s}, \mathrm{t}) \\ \varrho \mathrm{A}_0 \, \partial_{\mathrm{t}} \mathbf{v}(\mathrm{s}, \mathrm{t}) &= e(\mathrm{s}, \mathrm{t}) \mathbf{f} \left(\frac{\partial_{\mathrm{s}} \mathbf{r}(\mathrm{s}, \mathrm{t})}{e(\mathrm{s}, \mathrm{t})}, \mathbf{U}(\mathbf{r}(\mathrm{s}, \mathrm{t}), \mathrm{t}) - \mathbf{v}(\mathrm{s}, \mathrm{t}), \nu, \rho, \frac{\mathrm{d}_0}{\sqrt{e(\mathrm{s}, \mathrm{t})}} \right) \\ e(\mathrm{s}, \mathrm{t}) &= |\partial_{\mathrm{s}} \mathbf{r}(\mathrm{s}, \mathrm{t})| \\ \mathbf{r}(\ell(\mathrm{t}), \mathrm{t}) &= \mathbf{r_0}, \quad \partial_{\mathrm{s}} \mathbf{r}(\ell(\mathrm{t}), \mathrm{t}) = \boldsymbol{\tau_0}, \quad \mathbf{v}(\ell(\mathrm{t}), \mathrm{t}) = \mathrm{v}_0 \boldsymbol{\tau_0} \end{aligned} \tag{5.1.2}$$

with nozzle position $\mathbf{r_0} \in \mathbb{R}^3$, diameter $\mathrm{d}_0 > 0$ ($\mathrm{A}_0 = \pi \mathrm{d}_0^2/4$), exit speed $\mathrm{v}_0 > 0$ in direction $\boldsymbol{\tau_0} \in S^2$, as well as jet density $\varrho > 0$. Thereby, the constructed

velocity field $\mathbf{U} = \overline{\mathbf{U}} + \mathbf{U}'$ carries the randomness into the dynamic system via construction (4.4.1) or (4.4.2). Particularly, (5.1.2) is a deterministic system for each realization of $\mathbf{U}'$. Certainly, gravitational forces could be included, but they play a negligibly small role in the considered process. In the drag force we approximate the jet tangent (containing the spatial derivative) by the direction of the jet velocity, i.e.,

$$\boldsymbol{\tau} = \frac{\partial_{\mathrm{s}}\mathbf{r}}{e} = \frac{\mathbf{v}}{|\mathbf{v}|}, \tag{5.1.3}$$

and motivate an evolution equation for the elongation e from the steady situation where $e = |\mathbf{v}|/\mathrm{v}_0$ (cf. (5.0.1)). Differentiation yields then

$$\partial_{\mathrm{t}} e = \frac{\langle \boldsymbol{\tau}, \partial_{\mathrm{t}}\mathbf{v}\rangle}{\mathrm{v}_0},$$

containing stretching and compressing. However, instead of being compressed the instationary jet tends to evade and to move according to the flow field where it is stretched. Hence, we propose

$$\partial_{\mathrm{t}} e = \frac{|\partial_{\mathrm{t}}\mathbf{v}|}{\mathrm{v}_0}, \tag{5.1.4}$$

see also [30]. As consequence of (5.1.3)

$$\partial_s \mathbf{r}(\ell(\mathrm{t}), \mathrm{t}) = e(\ell(\mathrm{t}), \mathrm{t}) \frac{\mathbf{v}(\ell(\mathrm{t}), \mathrm{t})}{|\mathbf{v}(\ell(\mathrm{t}), \mathrm{t})|},$$

hence the boundary condition $\partial_{\mathrm{s}}\mathbf{r}(\ell(\mathrm{t}), \mathrm{t}) = \boldsymbol{\tau_0}$ of (5.1.2) is equivalent to

$$e(\ell(\mathrm{t}), \mathrm{t}) = 1$$

because $\mathrm{v}_0 > 0$, $|\boldsymbol{\tau_0}| = 1$. Having replaced all partial derivates with respect to s and adding (5.1.4) we get the parametrized random ODE system

$$\begin{aligned} \partial_{\mathrm{t}}\mathbf{r}_{\mathrm{s}}(\mathrm{t}) &= \mathbf{v}_{\mathrm{s}}(\mathrm{t}) \\ \varrho \mathrm{A}_0\, \partial_{\mathrm{t}}\mathbf{v}_{\mathrm{s}}(\mathrm{t}) &= e_{\mathrm{s}}(\mathrm{t})\mathbf{f}\left(\frac{\mathbf{v}_{\mathrm{s}}(\mathrm{t})}{|\mathbf{v}_{\mathrm{s}}(\mathrm{t})|}, \mathbf{U}(\mathbf{r}_{\mathrm{s}}(\mathrm{t}), \mathrm{t}) - \mathbf{v}_{\mathrm{s}}(\mathrm{t}), \nu, \rho, \frac{\mathrm{d}_0}{\sqrt{e_{\mathrm{s}}(\mathrm{t})}}\right) \\ \partial_{\mathrm{t}} e_s(\mathrm{t}) &= \frac{|\partial_{\mathrm{t}}\mathbf{v}_s(\mathrm{t})|}{\mathrm{v}_0} \end{aligned} \tag{5.1.5}$$

$$\mathbf{r}_{\ell(\mathrm{t})}(\mathrm{t}) = \mathbf{r_0}, \quad e_{\ell(\mathrm{t})}(\mathrm{t}) = 1, \quad \mathbf{v}_{\ell(\mathrm{t})}(\mathrm{t}) = \mathrm{v}_0 \boldsymbol{\tau_0}.$$

With

$$\mathbf{r}_{\ell(0)}(0) = \mathbf{r_0}, \quad e_{\ell(0)}(0) = 1, \quad \mathbf{v}_{\ell(0)}(0) = \mathrm{v}_0 \boldsymbol{\tau_0}$$

we get the following system for $\mathbf{r}_{\ell(0)}$, $\mathbf{v}_{\ell(0)}$, and $e_{\ell(0)}$ (i.e., $\mathrm{s} = \ell(0) = 0$ in (5.1.5)) omitting the index $\ell(0)$.

Model 5.3 (Simplified random ODE model)**.** *Let $\mathbf{U}'$ be defined on a probabilty space $(\Omega, \mathcal{A}, P)$. Let the constant air density $\rho > 0$, kinematic viscosity $\nu > 0$, as well as the jet density $\varrho > 0$ and diameter $\mathrm{d}_0 > 0$ be given. The model for the jet position $\mathbf{r} : [0, \mathrm{T}] \times \Omega \to \mathbb{R}^3$, the jet velocity $\mathbf{v} : [0, \mathrm{T}] \times \Omega \to \mathbb{R}^3$, and the elongation $e : [0, \mathrm{T}] \times \Omega \to \mathbb{R}_+$ in the time interval $[0, \mathrm{T}]$ reads*

$$\begin{aligned}
&\frac{\mathrm{d}}{\mathrm{dt}}\mathbf{r}(\mathrm{t}) = \mathbf{v}(\mathrm{t}) \\
&\frac{\mathrm{d}}{\mathrm{dt}}\mathbf{v}(\mathrm{t}) = e^{3/2}(\mathrm{t})\,\frac{4}{\pi}\frac{\rho\nu^2}{\varrho \mathrm{d}_0^3}\,\boldsymbol{f}\left(\frac{\mathbf{v}(\mathrm{t})}{|\mathbf{v}(\mathrm{t})|}, \frac{\mathrm{d}_0}{\nu\sqrt{e(\mathrm{t})}}\left(\mathbf{U}(\mathbf{r}(\mathrm{t}), \mathrm{t}) - \mathbf{v}(\mathrm{t})\right)\right) \\
&\frac{\mathrm{d}}{\mathrm{dt}}e(\mathrm{t}) = e^{3/2}(\mathrm{t})\,\frac{1}{\mathrm{v}_0}\frac{4}{\pi}\frac{\rho\nu^2}{\varrho \mathrm{d}_0^3}\left|\boldsymbol{f}\left(\frac{\mathbf{v}(\mathrm{t})}{|\mathbf{v}(\mathrm{t})|}, \frac{\mathrm{d}_0}{\nu\sqrt{e(\mathrm{t})}}\left(\mathbf{U}(\mathbf{r}(\mathrm{t}), \mathrm{t}) - \mathbf{v}(\mathrm{t})\right)\right)\right|
\end{aligned} \tag{5.1.6}$$

The initial conditions are

$$\mathbf{r}(0) = \mathbf{r_0}, \quad \mathbf{v}(0) = \mathrm{v}_0 \boldsymbol{\tau_0}, \quad e(0) = 1.$$

with nozzle position $\mathbf{r_0} \in \mathbb{R}^3$ and exit speed $\mathrm{v}_0 > 0$ in direction $\boldsymbol{\tau_0} \in S^2$.

The model (5.1.6) describes the path and behavior of a single jet point whose motion is exclusively driven by a turbulent air flow. Note that the simplified model is free of any rheology, but it contains the effect of the flow fluctuations, which turns out to be of main relevance for the jet thinning. Material properties and nozzle conditions influence marginally.

Remark 5.4 (Numerical Treatment)**.** For the forthcoming numerical investigations of the random ordinary differential system (5.1.6) the k-ϵ simulations of the underlying turbulent flow field are performed with the software ANSYS Fluent. The CFD data is provided by the Fraunhofer ITWM, Kaiserslautern. The fiber

jet dynamics are computed in MATLAB using the standard ODE-solver `ode45.m`. The routine is an implementation of an explicit Runge-Kutta method of fourth (or respectively, fifth) order with adaptive time step control. The normally and uniformly distributed random numbers that are required for the simulation of the turbulent velocity fluctuations $\mathbf{U}'$ are generated with the MATLAB-functions `randn()` and `rand()`.

5.1.1 Numerical Results

We investigate the dynamics and behavior of a fiber jet in a flow situation that is usual for melt-blowing, [51, 65]. Temperature effects are neglected for simplicity. The air stream is directed vertically downwards and enters the domain of interest via a thin slot die, cf. Figure 5.1. Since the mean quantities of the

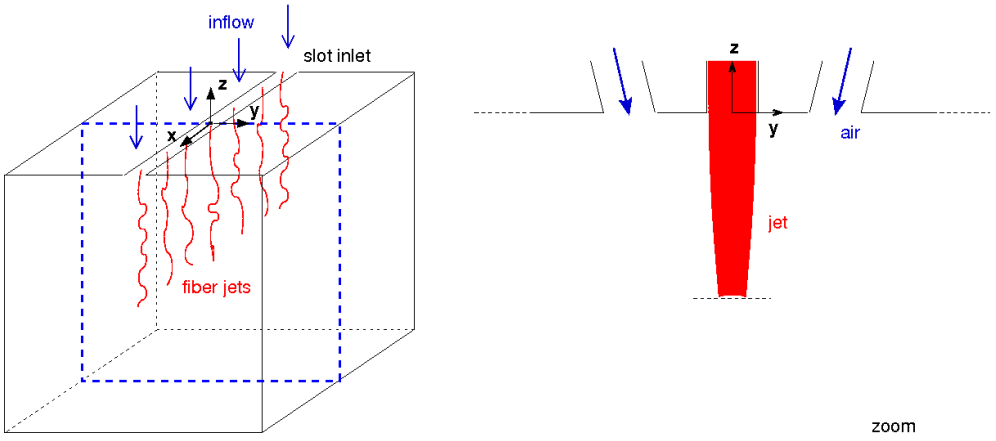

Figure 5.1: [30] Sketch of flow domain with immersed fiber jets. A two-dimensional cut (y-z-plane, marked by dashed line) is representative due to the given homogeneity in x-direction. For details on possible geometries see, e.g., [51, 65].

turbulent air stream are time-independent and homogeneous in direction of the slot (x-direction), we perform stationary k-ϵ simulations for a representative two-dimensional cut showing the y-z-plane. In the set-up the mean flow is symmetric with respect to the z-axis (y = 0). Figure 5.2 shows the respective flow fields for the mean velocity components, kinetic turbulent energy and dissipation rate. In addition

$$\rho = 1\,[\mathrm{kg/m^3}], \quad \nu = 1.5 \cdot 10^{-5}\,[\mathrm{m^2/s}].$$

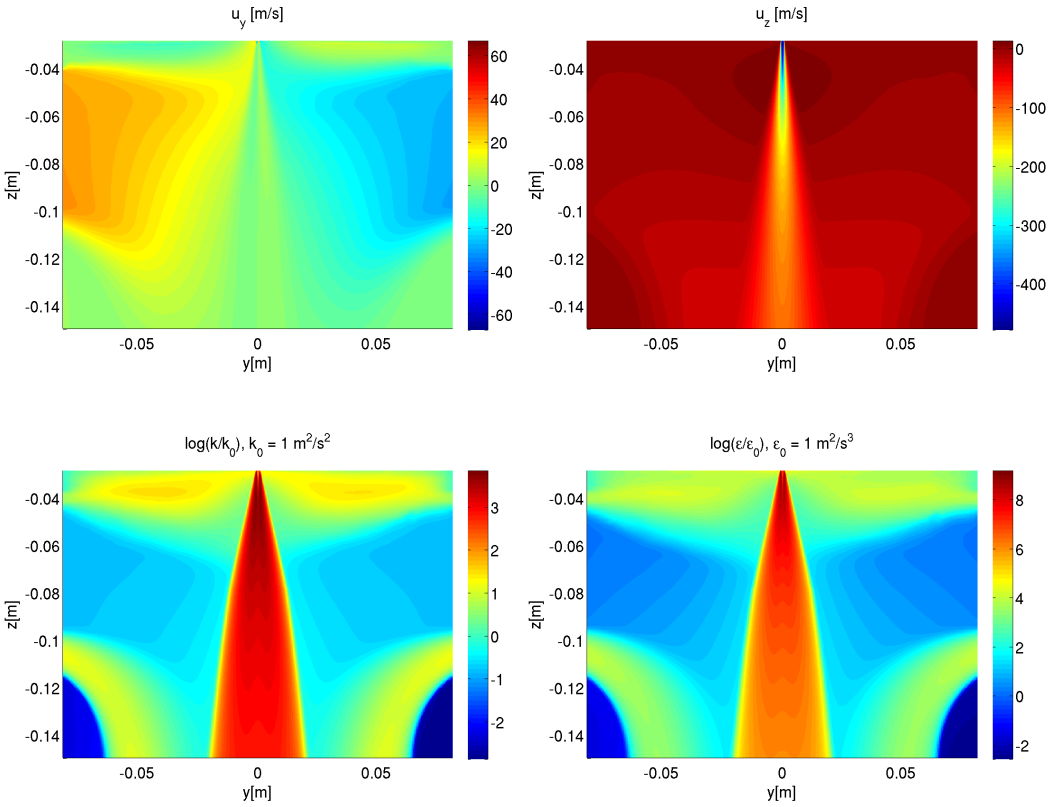

Figure 5.2: k-ϵ simulation of the representative 2d flow domain. *Top:* components of mean velocity $\overline{\mathbf{U}}$ in y- and z-direction. *Bottom:* turbulent kinetic energy k and dissipation rate ϵ in logarithmic plots.

A distinct free air jet develops that is supersonic at the inlet slot (here approximately: $\left|\overline{\mathbf{U}}\right| = 400$ [m/s], $k = 10^3$ [m^2/s^2], $\epsilon = 10^8$ [m^2/s^3]) and becomes subsonic within some centimeters away. So, the occurring typical turbulent length and time scales lie in a wide range, i.e.,

$$l_T = \frac{k^{3/2}}{\epsilon} \in \left]10^{-4}, 10^{-2}\right[\text{ [m]}, \quad t_T = \frac{k}{\epsilon} \in \left]10^{-5}, 10^{-3}\right[\text{ [s]}.$$

But, approximately $\zeta = 10^{-4}$ in the whole free air stream, as visualized in Figure 5.3. At the boundaries of the flow domain we observe side effects coming from the geometry (e.g., in the lower corners). However, these play no role for the dynamics of the fiber jet. Consequently, the simplified construction (4.4.2) with $\zeta = 10^{-4}$ for the simulation of the random velocity field is acceptable and applied.

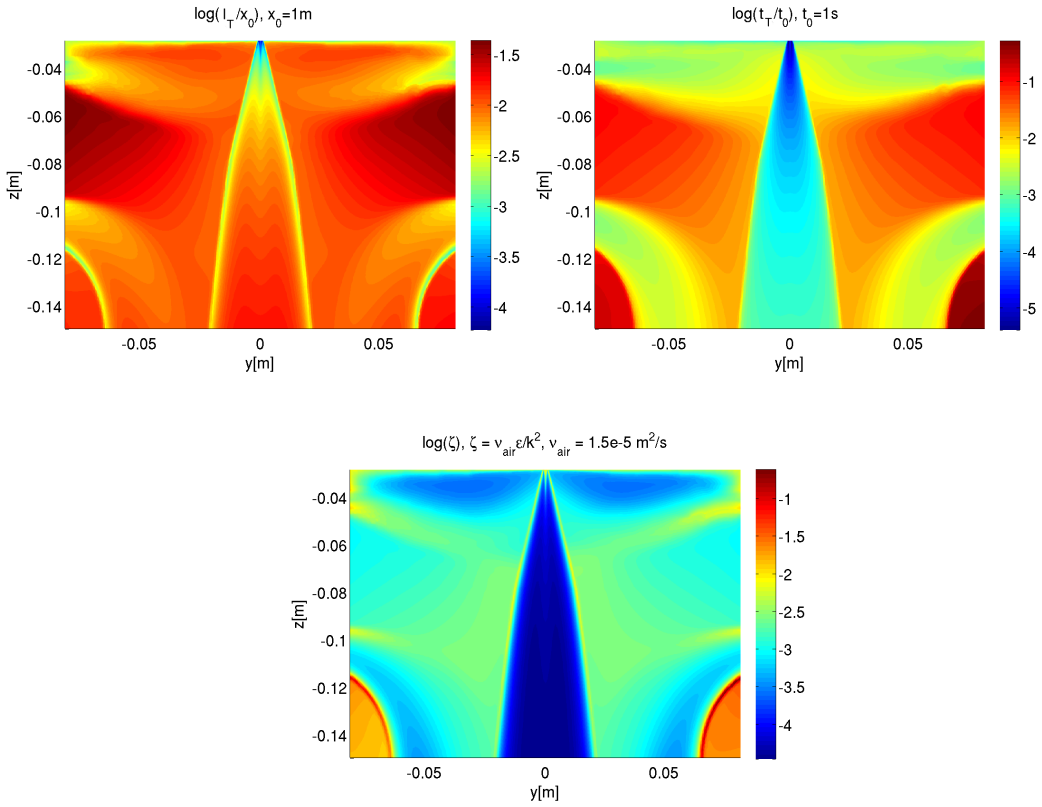

Figure 5.3: Turbulent scales corresponding to Figure 5.2 in logarithmic plots. *Top:* turbulent large-scale length $l_T = k^{3/2}/\epsilon$ and time $t_T = k/\epsilon$. *Bottom*: ratio of fine and large scales $\zeta = \epsilon\nu/k^2$.

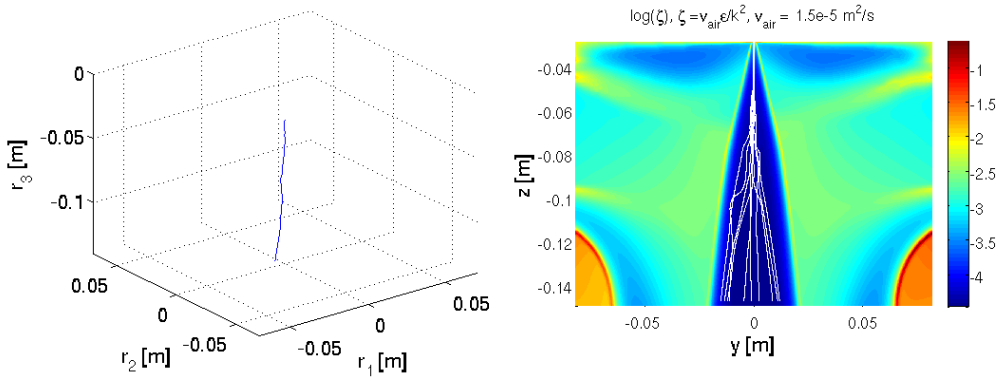

Figure 5.4: Fiber dynamics driven by turbulent aerodynamic drag force. *Left:* random trajectory $\mathbf{r}$. *Right:* projection of several trajectories into y-z-plane (white curves). They are located in the distinct free air stream where approximately $\zeta = 10^4$.

The immersed fiber jet to be spun in (negative) z-direction is initialized at the slot die (spinning nozzle) with

$$\mathrm{v}_0 = 10^{-2}\ [\mathrm{m/s}], \quad \mathrm{d}_0 = 4 \cdot 10^{-4}\ [\mathrm{m}], \quad \varrho = 7 \cdot 10^2\ [\mathrm{kg/m^3}],$$

and simulated for the time interval $[0, \mathrm{T}]$ with $\mathrm{T} = 10^{-3}$ [s]. The fiber jet moves exclusively in the distinct region of the free air stream, see Figure 5.4. Thereby, its motion is determined strongly by the mean flow pulling the fiber jet straight downwards, on the one hand. On the other hand the flow fluctuations cause a slight bouncing. The fiber velocity follows and finally adjusts to the flow velocity, as we can see in Figure 5.5. In the temporal evolution the fiber point starts from the nozzle where the impact of the turbulence is at the strongest. The velocity fluctuations act here on tiny length and time scales causing a quick acceleration and a very strong stretching of the jet. When the fiber point is some centimeters away from the nozzle after 0.2-0.3 milliseconds, the turbulence attenuates and the turbulent scales become larger (Figures 5.3 and 5.7). In particular, $\mathrm{t_T}$ and the jet's reaction time coincide which can be concluded from the velocity curves that match. Also the elongation stagnates.

Figure 5.6 shows the estimated probability density functions of the elongation at three depicted heights $\mathrm{r}_3 = -0.033, -0.066, -0.1$ [m]. They are estimated via kernel density estimation with a Gaussian kernel by help of 1000 independent realizations of $\mathbf{U}'$. We clearly observe the essential effect of the turbulent velocity fluctuations and the random aerodynamic drag force model on the jet thinning (especially in the first centimeters / tenths of milliseconds). The computed elongation rises up to a mean of $1.6 \cdot 10^5$ at T (here approximately: $\mathrm{r}_3 = -0.14$ [m]) with a minimum elongation of $8 \cdot 10^4$ and a maximum elongation of $3.56 \cdot 10^5$ among the 1000 realizations (for the construction (4.4.1) with non-constant ζ and the same initial seeds we have the mean elongation $1.59 \cdot 10^5$ with minimum $8.17 \cdot 10^4$ and maximum $4.03 \cdot 10^5$). In comparison, the numerical result neglecting the fluctuations (i.e., use of $\mathbf{U} = \overline{\mathbf{U}}$ in (5.1.6)) is approximately 10^4 which perfectly corresponds to the theoretical considerations on stationary turbulence stating that $e = |\mathbf{v}| / \mathrm{v}_0$ with $\mathbf{v} = \overline{\mathbf{U}}$ (approximately) holds. The reason for this difference lies in the nonlinearity of the drag force (5.1.1) so that the fluctuations produce a disproportionate extension. The fact that Zeng et al. [89] have obtained

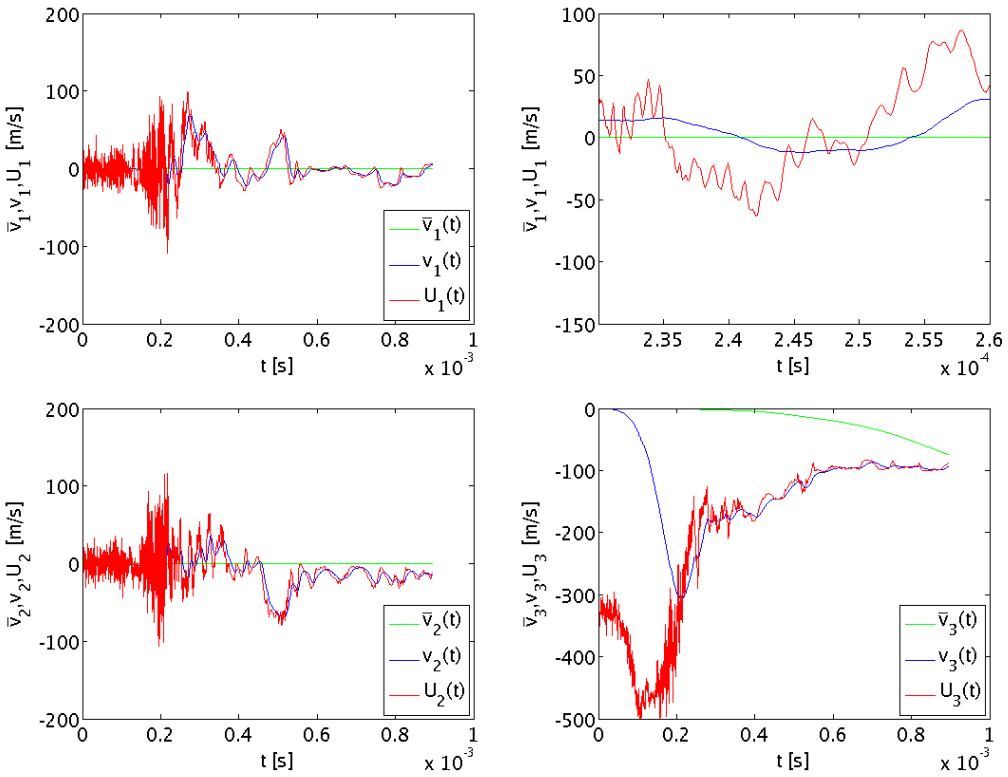

Figure 5.5: Temporal evolution of fiber $\mathbf{v}$ (blue) and air flow velocity $\mathbf{U} = \overline{\mathbf{U}} + \mathbf{U}'$ (red) experienced by the random trajectory of Fig. 5.4 (left); component-wise visualization. The plot *top-right* is a zoom in the v_1, U_1-components (x-direction). In addition, the fiber velocity due to the mean air flow velocity $\overline{\mathbf{U}}$ – neglecting the fluctuations and considering $\mathbf{U} = \overline{\mathbf{U}}$ in (5.1.6) – is illustrated ($\bar{\mathbf{v}}$, green line).

the same order 10^4 of elongation for an viscoelastic spring-beam jet model in a mean turbulent flow field (where $\mathbf{U} = \overline{\mathbf{U}}$ is considered) clearly stresses that the turbulent fluctuations are the major dominant effect for the large jet attenuation. Material models (rheology) and inner stresses in contrast seem to be of minor relevance. Moreover, it is worth to mention, that the random ODE-model (5.1.6) – as simple as it is – already predicts qualitatively appropriately all jet thinning stages observed in the experiments. However, proper quantitative estimates can be only expected according to the measurements [9] when temperature dependencies (e.g., temperature-dependent viscosity) are included.

Remark 5.5. Some concluding remarks on computational aspects:

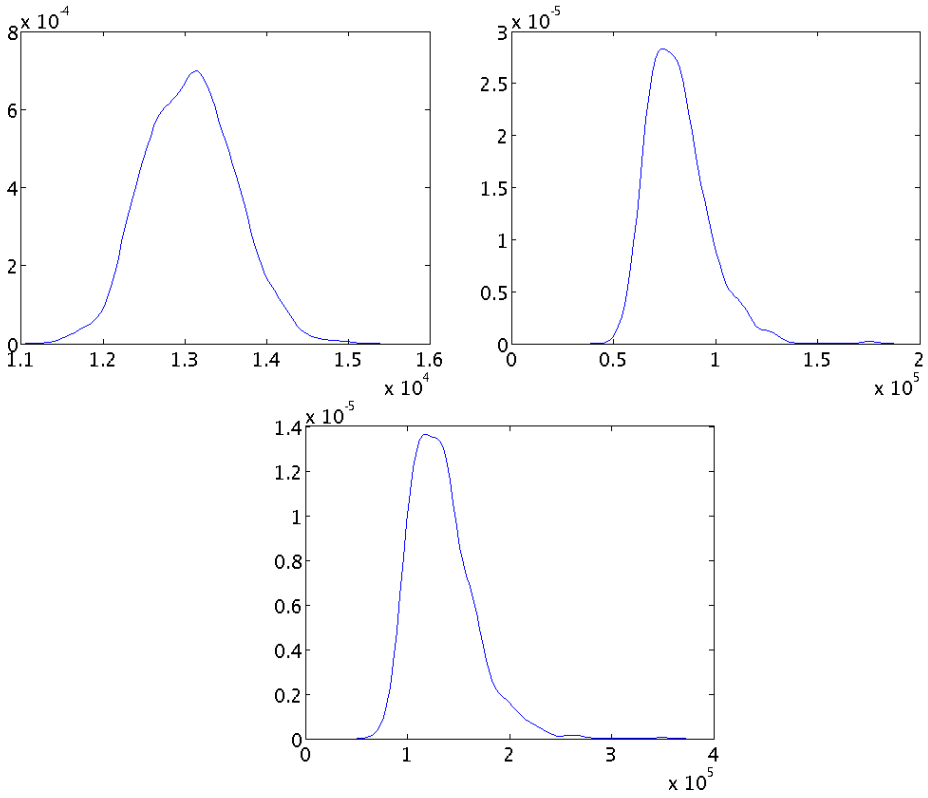

Figure 5.6: Probability density of e at depicted heights $r_3 = -0.033, -0.066, -0.1$ [m] (z-direction; from left to right) estimated with kernel density estimator.

- The adaptive time step control of the ODE-solver (cf. Remark 5.4) ensures the correct resolution of the turbulent scales since the chosen step size Δt is always clearly smaller than t_T and l_T/v_{rel}, $v_{rel} = \left|\overline{\mathbf{U}} - \mathbf{v}\right|$, cf. Figure 5.7. This implies the smooth numerical approximation of the jet quantities, see, e.g., the visualization of the velocity components in Figure 5.5.

- The simulation of a fiber trajectory in $[0, T]$, $T = 10^{-3}$ [s] takes a CPU-time of approximately 50 seconds for the globalization strategy (4.4.2) with constant ζ and a CPU-time of approximately 80 seconds for the strategy (4.4.1) with varying ζ on a 2.7 GHz Intel Core i5 processor.

- The computational effort of the simulation algorithm for the turbulent velocity fluctuations $\mathbf{U}'$ splits into initialization and continuous run. Whereas the costs for the initial generation of the set of random numbers are independent of the discretization and negligibly small (0.1 CPU-seconds for $N = 50$), the costs for the continuous run are linear in the time discretization

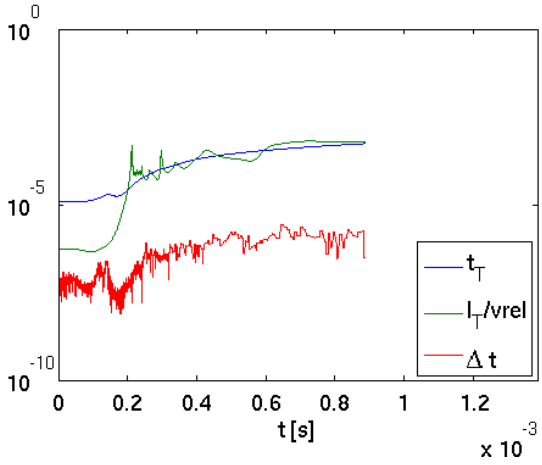

Figure 5.7: Adaptive time step choice Δt for (5.1.6) in comparison to turbulent time scales $t_T = k/\epsilon$ and $l_T/v_{rel} = k^{3/2}/(\epsilon v_{rel})$ with $v_{rel} = \left|\overline{\mathbf{U}} - \mathbf{v}\right|$ experienced at the jet position $\mathbf{r}(t)$ of Fig. 5.4.

and add up to approximately 88% of the total costs for solving the random ODE system (5.1.6). On the first glance this seems to be incredibly much but the reason lies in the necessary processing of the underlying flow data (e.g., sorting, interpolation of flow data are required). So far, no further attention has been paid to the data processing that is done with standard MATLAB routines. But its performance will be optimized in future which promises a drastical speed-up.

Summing up, the numerical results are very promising. They raise hope that the proposed approach with the random aerodynamic drag force is capable of predicting the large elongations that are measured in industrial melt-blowing processes, presupposing an appropriate Cosserat model for the viscous, non-isothermal fiber jet. In addition, the computational effort seems to be manageable since the effort of the simulation algorithm for the turbulent velocity fluctuations is linear in time and space discretization.

5.2 Random PDAE Model

In this section we describe a random PDAE model for the motion of a fiber immersed in a turbulent airflow disregarding the effect of the fiber on the flow, which has been developed in [53]. Therefore, let the fluctuations $\mathbf{U}'$ be defined on

a probability space $(\Omega, \mathcal{A}, P)$. Due to its slender geometry a fiber can be modeled by an arclength-parametrized, time-dependent curve

$$\mathbf{r} : [0, \ell] \times [0, \mathrm{T}] \times \Omega \to \mathbb{R}^3$$

according to the special Cosserat theory [2]. We assume that the fiber is inextensible, hence the length of the fiber at time instance $\mathrm{t} > 0$ is given by

$$\ell(\mathrm{t}) = \mathrm{v}_0 \mathrm{t}$$

with exit speed $\mathrm{v}_0 > 0$ at the nozzle. At time instance $\mathrm{t} > 0$ the fiber leaves the nozzle at arclength parameter $\mathrm{s} = \ell(\mathrm{t})$ and the fiber ending is at $\mathrm{s} = 0$, cf. Figure 5.8.

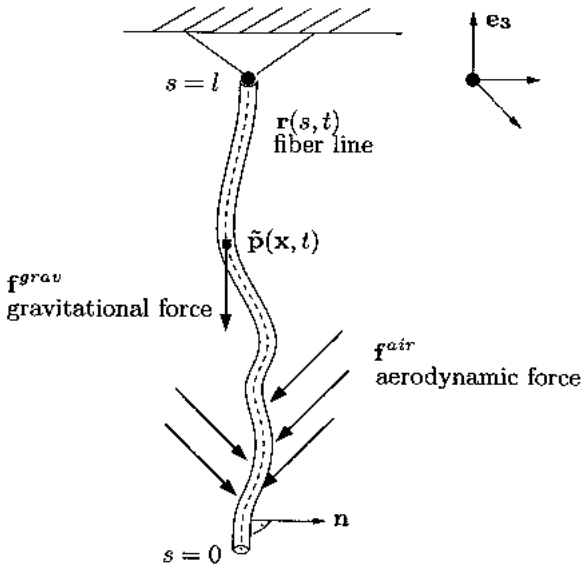

Figure 5.8: [53] Fiber dynamics caused by external forces.

Analogously to the random ODE model in the last section the random velocity field acts as input parameter for the given air drag model (5.1.1), which represents the aerodynamic force acting on the fiber. Assuming we want to observe the motion of a fiber in the time interval $[0, \mathrm{T}]$ for different realizations of our turbulent velocity field $\mathbf{U}'$, the random PDAE model is the following.

Model 5.6 (Random PDAE model)**.** *Let the random velocity field* $\mathbf{U}'$ *be defined*

on a probability space $(\Omega, \mathcal{A}, P)$*. The random PDAE system for the fiber position* $\mathbf{r} : [0, \ell(\mathrm{T})] \times [0, \mathrm{T}] \times \Omega \to \mathbb{R}^3$*, the fiber velocity* $\mathbf{v} : [0, \ell(\mathrm{T})] \times [0, \mathrm{T}] \times \Omega \to \mathbb{R}^3$*, and the tangential tension force* $\chi : [0, \ell(\mathrm{T})] \times [0, \mathrm{T}] \times \Omega \to \mathbb{R}$ *reads*

$$\begin{aligned} &\partial_{\mathrm{t}}\mathbf{r}(\mathrm{s},\mathrm{t}) = \mathbf{v}(\mathrm{s},\mathrm{t}) \\ &(\varrho \mathrm{A}_0)\partial_{\mathrm{t}}\mathbf{v}(\mathrm{s},\mathrm{t}) = \partial_{\mathrm{s}}\left(\chi(\mathrm{s},\mathrm{t})\partial_{\mathrm{s}}\mathbf{r}(\mathrm{s},\mathrm{t}) - \mathrm{b}\,\partial_{\mathrm{sss}}\mathbf{r}(\mathrm{s},\mathrm{t})\right) + (\varrho \mathrm{A}_0)\mathbf{g} + \mathbf{f}_{\mathbf{U}}(\mathrm{s},\mathrm{t}) \\ &|\partial_{\mathrm{s}}\mathbf{r}(\mathrm{s},\mathrm{t})| = 1 \end{aligned} \tag{5.2.1}$$

for $(\mathrm{s},\mathrm{t}) \in]0, \ell(\mathrm{T})[\times]0, \mathrm{T}]$ *with time-dependent boundary conditions*

$$\mathbf{r}(\ell(\mathrm{t}),\mathrm{t}) = \mathbf{r_0}, \quad \partial_{\mathrm{s}}\mathbf{r}(\ell(\mathrm{t}),\mathrm{t}) = \boldsymbol{\tau_0}, \quad \mathbf{v}(\ell(\mathrm{t}),\mathrm{t}) = \mathrm{v}_0\boldsymbol{\tau_0},$$

at the nozzle (nozzle position $\mathbf{r_0}$*, exit speed* $\mathrm{v}_0 > 0$*, fiber orientation* $\boldsymbol{\tau_0} \in S^2$*) as well as*

$$\partial_{\mathrm{ss}}\mathbf{r}(0,\mathrm{t}) = \mathbf{0}, \quad \partial_{\mathrm{sss}}\mathbf{r}(0,\mathrm{t}) = \mathbf{0}, \quad \chi(0,\mathrm{t}) = 0,$$

at the end of the fiber.

Let us now give a short description of the appearing terms. For more details we refer to [53]. The term

$$\partial_{\mathrm{s}}\left(\chi(\mathrm{s},\mathrm{t})\partial_{\mathrm{s}}\mathbf{r}(\mathrm{s},\mathrm{t}) - \mathrm{b}\,\partial_{\mathrm{sss}}\mathbf{r}(\mathrm{s},\mathrm{t})\right)$$

represents the inner stresses, which stem from traction and bending with bending stiffness

$$\mathrm{b} = \mathrm{E}\frac{\pi \mathrm{d}_0^4}{16} > 0,$$

where $\mathrm{E} > 0$ denotes Young's modulus and d_0 the diameter of the fiber. The bending stiffness describes the resistance of the fiber to deformation (bending) in response to applied forces. Neglecting torsion this term is essentially derived from Euler-Bernoulli beam theory. The function χ can be viewed as tractive force containing tension and curvature due to bending. The outer force densities

$$(\varrho \mathrm{A}_0)\mathbf{g} + \mathbf{f}_{\mathbf{U}}(\mathrm{s},\mathrm{t})$$

come from gravity ($\mathbf{g} = 9.81\,\boldsymbol{\tau_0}\,[\mathrm{m/s^2}]$, $\mathrm{A}_0 = \pi \mathrm{d}_0^2/4$) and the aerodynamic line force

$$\mathbf{f_U}(\mathrm{s},\mathrm{t}) = \frac{\rho\nu^2}{\mathrm{d}_0}\boldsymbol{f}\left(\frac{\partial_\mathrm{s}\mathbf{r}(\mathrm{s},\mathrm{t})}{|\partial_\mathrm{s}\mathbf{r}(\mathrm{s},\mathrm{t})|}, \frac{\mathrm{d}_0}{\nu}\left(\mathbf{U}(\mathbf{r}(\mathrm{s},\mathrm{t}),\mathrm{t}) - \mathbf{v}(\mathrm{s},\mathrm{t})\right)\right), \tag{5.2.2}$$

which crucially depends on the relative velocity between fiber and air flow, cf. (5.1.1). Hence, the turbulent velocity fluctuations $\mathbf{U}'$ act as input parameter for the deterministic force $\boldsymbol{f}$. Thus, for every realization of $\mathbf{U}'$ the system (5.2.1) is a deterministic PDAE system and thus can be simulated with help of numerical schemes for deterministic systems, cf. Remark 5.8.

Remark 5.7 (SPDAE Model)**.** In [53, 56] the authors have chosen a linearization approach

$$\boldsymbol{f}_a(\boldsymbol{\tau}, \boldsymbol{v} + \boldsymbol{U}'(\boldsymbol{r},t)) = \boldsymbol{m}(\boldsymbol{\tau},\boldsymbol{v},k) + \boldsymbol{L}(\boldsymbol{\tau},\boldsymbol{v},k)\,\boldsymbol{U}'(\boldsymbol{r},t) \tag{5.2.3}$$

for the approximation of the stochastic force

$$\boldsymbol{f}(\boldsymbol{\tau}, \boldsymbol{v} + \boldsymbol{U}'(\boldsymbol{r},t))$$

based on the local random velocity field $\boldsymbol{U}'$. Here,

$$\boldsymbol{v} = \overline{\boldsymbol{U}}(\boldsymbol{r},t) - \partial_t \boldsymbol{r}$$

denotes the mean relative velocity between air flow and fiber. The functions

$$\boldsymbol{m} : S^2 \times \mathbb{R}^3 \times \mathbb{R}_+ \to \mathbb{R}^3, \quad \boldsymbol{L} : S^2 \times \mathbb{R}^3 \times \mathbb{R}_+ \to \mathbb{R}^{3\times 3},$$

are determined as solution of the optimization problem

$$\min_{\boldsymbol{m},\boldsymbol{L}} \mathbb{E}\left(\left(\boldsymbol{f}(\partial_s\boldsymbol{r}, \boldsymbol{v} + \boldsymbol{U}'(\boldsymbol{r},t)) - \boldsymbol{f}_a(\partial_s\boldsymbol{r}, \boldsymbol{v} + \boldsymbol{U}'(\boldsymbol{r},t))\right)^2\right).$$

Particularly, we get

$$\boldsymbol{m}(\boldsymbol{\tau},\boldsymbol{v},k) = \frac{1}{(2\pi)^{3/2}}\int_{\mathbb{R}^3} \boldsymbol{f}\left(\boldsymbol{\tau}, \boldsymbol{v} + \sqrt{\frac{2k}{3}}\xi\right)\exp\left(-\frac{|\xi|^2}{2}\right)\,d\xi,$$

$$\boldsymbol{L}(\boldsymbol{\tau},\boldsymbol{v},k)=\frac{1}{(2\pi)^{3/2}}\sqrt{\frac{3}{2k}}\int_{\mathbb{R}^3}\boldsymbol{f}\left(\boldsymbol{\tau},\boldsymbol{v}+\sqrt{\frac{2k}{3}}\xi\right)\xi^T\exp\left(-\frac{|\xi|^2}{2}\right)\,d\xi,$$

see [56]. An approximation of $\boldsymbol{U}'$ in the linearization approach (5.2.3) by Gaussian white noise $(\boldsymbol{W}(s,t))_{(s,t)\in[0,\ell]\times\mathbb{R}_+}$ with $\mathbb{R}^{3\times3}$-valued, flow-dependant amplitude

$$\boldsymbol{D}(\boldsymbol{\tau},\boldsymbol{v},\zeta)=\sqrt{\int_{\mathbb{R}^2}\boldsymbol{\gamma}_\zeta(s\boldsymbol{\tau}-t\boldsymbol{v})\varphi(t)\;ds\;dt}$$

yields a further approximation

$$\boldsymbol{f}_a(\boldsymbol{\tau},\boldsymbol{v}+\boldsymbol{U}'(\boldsymbol{r},t))=\boldsymbol{m}(\boldsymbol{\tau},\boldsymbol{v},k)+\boldsymbol{L}(\boldsymbol{\tau},\boldsymbol{v},k)\boldsymbol{D}(\boldsymbol{\tau},\boldsymbol{v},\zeta)\boldsymbol{W}(s,t).$$

For details on this approximation approach we refer to [53]. The proposed approximation leads then to an SPDAE model (in short notation)

$$(\varrho\mathrm{A}_0)\partial_{\mathrm{tt}}\mathbf{r}\;\mathrm{ds}\;\mathrm{dt}=(\partial_{\mathrm{s}}(\chi\partial_{\mathrm{s}}\mathbf{r}-\mathrm{b}\partial_{\mathrm{sss}}\mathbf{r}))+(\varrho\mathrm{A}_0)\mathbf{g}+\mathbf{m})\;\mathrm{ds}\;\mathrm{dt}+\mathbf{LD}\;\mathrm{d}\boldsymbol{W}$$

with algebraic constraint of inextensibility

$$|\partial_{\mathrm{s}}\mathbf{r}|=1$$

as described in [56]. The numerics of these equations are already implemented in the fiber simulation software FIDYST that is developed at the Fraunhofer ITWM, Kaiserslautern.

Remark 5.8 (Numerical treatment)**.** For the following numerical investigations the k-ϵ simulations show snippets of a typical spunbond process of the industrial partner Oerlikon Neumag. The CFD data is provided by the Fraunhofer ITWM, Kaiserslautern. The system (5.2.1) is computed in MATLAB using a finite volume discretization in space on a staggered grid. The spatial derivatives are approximated by finite differences and the time integration is realized by an implicit Euler scheme. The resulting nonlinear system for each time step is solved with Newton's method and Armijo step size control.

5.2.1 Numerical Results

The numerical schemes for PDAE models have a significant higher computational effort than for example the scheme for the random ODE model from the last section. The computational speed of the considered numerical scheme (cf. Remark 5.8) is strongly affected by the grid size of the chosen discretization. Therefore, we address the question: what is a sufficient grid size (in both space and time) so that the simulated fibers are represented properly, i.e., are smooth enough. Let the random field $\mathbf{U}'$ be defined on a probability space $(\Omega, \mathcal{A}, P)$. To assess the smoothness of a fiber realization $\mathbf{r}(\cdot, \omega)$ in $[0, \mathrm{T}]$ corresponding to $\mathbf{U}'(\cdot, \omega)$ we introduce the quantity q_{min} in the following.

Let $\{\mathrm{t}_0, \ldots, \mathrm{t}_m\}$ be an equidistant discretization of $[0, \mathrm{T}]$ with $\mathrm{t}_0 = 0$, $\mathrm{t}_m = \mathrm{T}$, and grid size $\Delta_\mathrm{t} > 0$. Let $\{\mathrm{s}_0, \ldots, \mathrm{s}_{n(\mathrm{t}_j)}\}$ be an equidistant discretization of the interval $[0, \ell(\mathrm{t}_j)]$ with $\mathrm{s}_0 = 0$ and $\mathrm{s}_{n(\mathrm{t}_j)} = \ell(\mathrm{t}_j)$. Denoting the constant arclength grid size by $\Delta_\mathrm{s} > 0$ (i.e., we have the same grid size for every t_j) we define a function $\boldsymbol{\alpha}_{i,j} : \Omega \to \mathbb{R}^3$ by

$$\boldsymbol{\alpha}_{i,j}(\omega) = \frac{\mathbf{r}(\mathrm{s}_i, \mathrm{t}_j, \omega) - \mathbf{r}(\mathrm{s}_{i-1}, \mathrm{t}_j, \omega)}{\Delta_\mathrm{s}}$$

for $j \in \{0, \ldots, m\}$, $i \in \{1, \ldots, n(\mathrm{t}_j)\}$ and a function $\beta_{i,j} : \Omega \to [0, 1]$ by

$$\beta_{i,j}(\omega) = \frac{1}{2}\left(\frac{\langle \boldsymbol{\alpha}_{i,j}(\omega), \boldsymbol{\alpha}_{i-1,j}(\omega)\rangle}{|\boldsymbol{\alpha}_{i,j}(\omega)|\,|\boldsymbol{\alpha}_{i-1,j}(\omega)|} + 1\right),$$

for $j \in \{0, \ldots, m\}$, $i \in \{2, \ldots, n(\mathrm{t}_j)\}$. For a realization $\mathbf{r}(\cdot, \omega)$ the number $\beta_{i,j}(\omega)$ can be viewed as normalized measurement of the angle between $\boldsymbol{\alpha}_{i,j}(\omega)$ and $\boldsymbol{\alpha}_{i-1,j}(\omega)$ at time instance t_j. In more detail (geometrical interpretation)

$$\beta_{i,j}(\omega) = \begin{cases} 1 & \boldsymbol{\alpha}_{i,j}(\omega), \boldsymbol{\alpha}_{i-1,j}(\omega) \text{ have same orientation} \\ ]0.5, 1[& \text{obtuse angle between } \boldsymbol{\alpha}_{i,j}(\omega), \boldsymbol{\alpha}_{i-1,j}(\omega) \\ 0.5 & \boldsymbol{\alpha}_{i,j}(\omega), \boldsymbol{\alpha}_{i-1,j}(\omega) \text{ orthogonal} \\ ]0, 0.5[& \text{acute angle between } \boldsymbol{\alpha}_{i,j}(\omega), \boldsymbol{\alpha}_{i-1,j}(\omega) \\ 0 & \boldsymbol{\alpha}_{i,j}(\omega), \boldsymbol{\alpha}_{i-1,j}(\omega) \text{ have opposite orientation.} \end{cases}$$

In particular, $\beta_{i,j} = 1$ can be interpreted as maximal smoothness, whereas the smoothness decreases with decreasing values of $\beta_{i,j}$. We are interested at the

minimal $\beta_{i,j}$ among all time and all arclength points in the given discretization and therefore introduce the function $q_{min} : \Omega \to [0, 1]$,

$$q_{min}(\omega) = \min_{j\in\{0,\dots,m\}} \min_{i\in\{2,\dots,n(\mathrm{t}_j)\}} \beta_{i,j}(\omega).$$

Clearly, q_{min} depends on realizations of $\mathbf{U}'$ and thus can be estimated by Monte Carlo simulations as we will see in the following.

The flow situation for our forthcoming simulations is usual for spunbond and is similar to the melt-blowing case. Figure 5.9 shows the values of ζ in the respective flow domain.

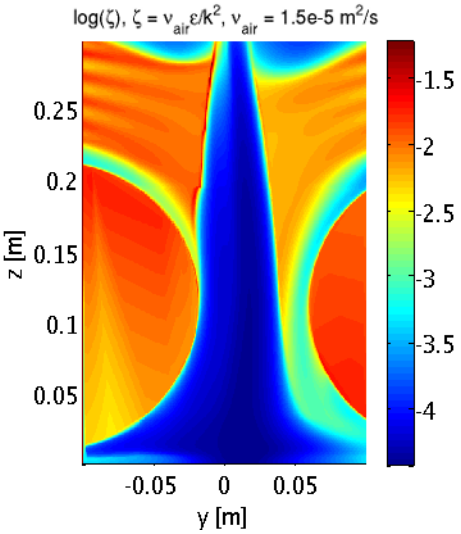

Figure 5.9: Ratio of fine and large scales $\zeta = \epsilon\nu/\mathrm{k}^2$ in logarithmic plot.

The immersed fiber is initialized at the nozzle with

$$\mathrm{v}_0 = 80\ [\mathrm{m/s}], \quad \mathrm{d}_0 = 1.2 \cdot 10^{-5}\ [\mathrm{m}], \quad \varrho = 0.9 \cdot 10^3\ [\mathrm{kg/m^3}],$$

and Young's modulus $\mathrm{E} = 4.5 \cdot 10^9\ [\mathrm{N/m^2}]$, i.e., the bending stiffness is

$$\mathrm{b} = 1.83 \cdot 10^{-11}\ [\mathrm{Nm^2}].$$

The simulation interval is $[0, \mathrm{T}]$ with $\mathrm{T} = 2{\cdot}10^{-3}$ [s]. For the estimation of q_{min} we use 10 independent realizations of the random field $\mathbf{U}'_N$ in (4.4.1) as well as of the construction (4.4.2) for $\zeta = 10^{-3}$ and $\zeta = 10^{-4}$. We use $N = 100$. The simulation

results for the different constructions and different grid sizes Δ_s, Δ_t, are listed in Table 5.1. Here, $\zeta(\mathbf{x}, \mathrm{t})$ stands for the construction (4.4.1) with non-constant ζ. The entries are formatted as

$$\overline{q_{min}},\ \sigma,\ \overline{t_{cpu}}$$

where $\overline{q_{min}}$ denotes the mean of all q_{min} among the 10 realizations of the turbulent velocity field, σ denotes the respective standard deviation, and $\overline{t_{cpu}}$ denotes the mean CPU-time in seconds for the 10 realizations and the respective parameters.

$\zeta \setminus \Delta_s, \Delta_t$	$5 \cdot 10^{-3},\ 5 \cdot 10^{-5}$	$10^{-3},\ 10^{-5}$
$\zeta(\mathbf{x}, \mathrm{t})$	0.1716, 0.1135, 50.68	0.45, 0.064, 216.6
10^{-3}	0.1975, 0.15, 9.23	0.4625, 0.08, 175.64
10^{-4}	0.1830, 0.12, 9.21	0.477, 0.12, 175.92
$\zeta \setminus \Delta_s, \Delta_t$	$5 \cdot 10^{-4},\ 5 \cdot 10^{-6}$	$2 \cdot 10^{-4},\ 2 \cdot 10^{-6}$
$\zeta(\mathbf{x}, \mathrm{t})$	0.8, 0.057, 807.73	0.9675, 0.01, $5 \cdot 10^3$
10^{-3}	0.8355, 0.022, 684.07	0.974, 0.003, $4.12 \cdot 10^3$
10^{-4}	0.8237, 0.028, 683.37	0.9682, 0.007, $4.11 \cdot 10^3$

Table 5.1: Numerical results for $\overline{q_{min}}$, standard deviation σ, and mean CPU-time $\overline{t_{cpu}}$.

As expected the results for $\overline{q_{min}}$ are mostly better in the case $\zeta = 10^{-3}$ than in the case $\zeta = 10^{-4}$, cf. Remark 4.3, Figures 4.4, 4.5, and the discussion there. The simulation results also show that a discretization with

$$\Delta_s = 2 \cdot 10^{-4}, \quad \Delta_t = 2 \cdot 10^{-6},$$

is sufficient regarding the introduced quantity q_{min}. Because we have approximately $\zeta = 10^{-4}$ in the whole free air stream (cf. Figure 5.9) and comparing the mean CPU-time for the different globalization strategies, it clearly makes sense to use the strategy with constant $\zeta = 10^{-4}$ in this case.

So far we have only considered what are appropriate spatial and temporal grid sizes regarding q_{min}. The question remains if the constructed random velocity field $\mathbf{U}'_N$ is either resolved properly. Figure 5.10 shows the turbulent large-scale length l_T and time t_T in a logarithmic plot. These are the minimum scales that have to be resolved. Near the nozzle they are very small increasing in z-direction.

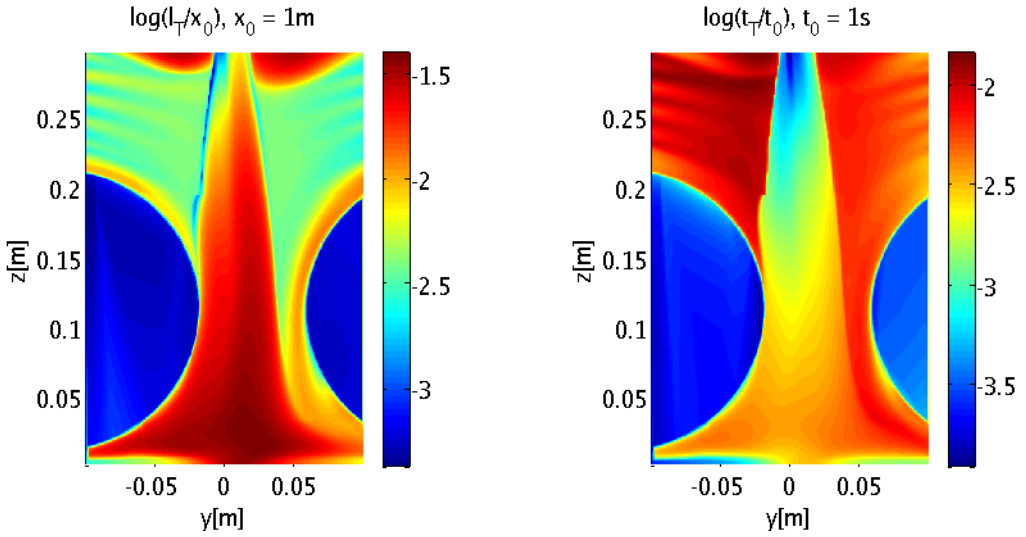

Figure 5.10: Turbulent large-scale length $l_T = k^{3/2}/\epsilon$ and time $t_T = k/\epsilon$ in logarithmic plots.

Thus, we would expect that the behaviour of a realization of $\mathbf{U}'_N$ is more 'irregular' near the nozzle. Figure 5.11 affirms this expectation. It shows a realization of one component of $\mathbf{U}'_N$ at a certain time with a spatial grid size of $\Delta_x = 10^{-3}$ in y and z-direction. As we can see the realization seems to be more irregular near the nozzle (marked red). Thus, one might think of an adaptive discretization for the numerics of the fiber dynamics that adapts to the underlying turbulent scales and makes sure that the random velocity is resolved properly. However, the development of adaptive numerical schemes is not straightforward. Another, yet heuristic and algorithmic, idea could be to think of a hybrid simulation method that uses the white-noise approach (cf. Remark 5.7) near the nozzle and switches to the numerics of the random PDAE model with the construction $\mathbf{U}'_N$ at some point.

Remark 5.9. The proposed random field constructions (4.4.1), (4.4.2) are currently implemented in the fiber simulation software FIDYST, which is written in the programming language `C++` and thus will permit faster simulations of the random velocity fields and the random PDAE system.

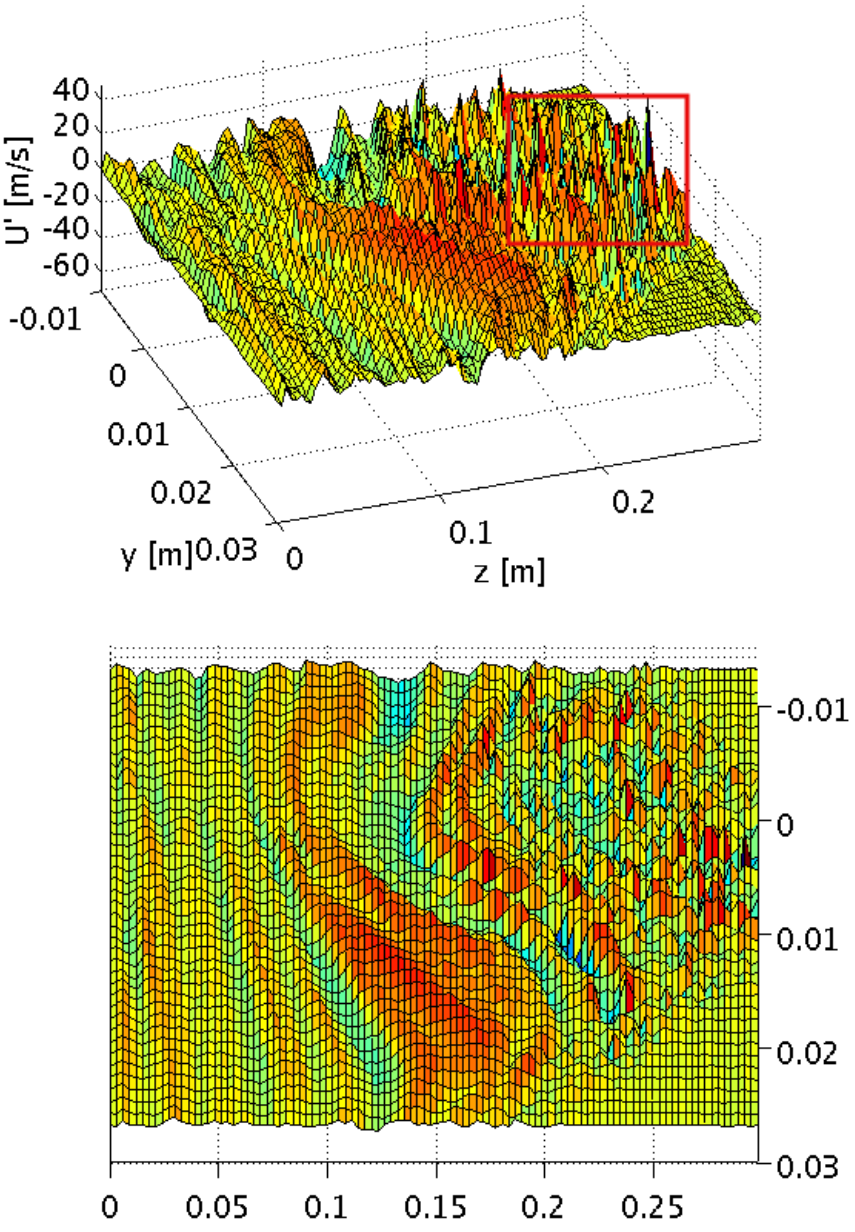

Figure 5.11: Realization of a component of $\mathbf{U}'_N$ with non-constant ζ, plotted over two-dimensional space at a certain time.

Bibliography

[1] R. Adler and J. Taylor. *Random Fields and Geometry.* Springer, 2007.

[2] S. Antman. *Nonlinear Problems of Elasticity.* Springer, 2006.

[3] W. Arne, N. Marheineke, A. Meister, and R. Wegener. Numerical analysis of Cosserat rod and string models for viscous jets in rotational spinning processes. *Math. Models Methods Appl. Sci.*, 20:1941–1965, 2010.

[4] W. Arne, N. Marheineke, J. Schnebele, and R. Wegener. Fluid-fiber-interactions in rotational spinning process of glass wool production. *J. Math. Ind.*, 1:2, 2011.

[5] W. Arne, N. Marheineke, and R. Wegener. Asymptotic transition of Cosserat rod to string models for curved viscous inertial jets. *Math. Models Methods Appl. Sci.*, 21(10):1987–2018, 2011.

[6] W. Arne, A. Meister, and R. Wegener. Finite volume approach for the instationary Cosserat rod model describing the spinning of viscous jets. *arXiv:1207.0731*, 2012.

[7] S. Asmussen and P. Glynn. *Stochastic Simulation: Algorithms and Analysis.* Springer, 2007.

[8] B. Audoly, N. Clauvelin, P. Brun, M. Bergou, E. Grinspun, and M. Wardetzky. A discrete geometric approach for simulating the dynamics of thin viscous threads. *J. Comput. Phys.*, 253:18–49, 2013.

[9] V. Bansal and R. Shambaugh. On-line Determination of Diameter and Temperature during Melt Blowing of Polypropylene. *Ind. Eng. Chem. Res.*, 37(5):1799–1806, 1998.

[10] G. Batchelor. *The Theory of Homogeneous Turbulence.* Cambridge University Press, 1959.

[11] S. Bochner. Monotone Funktionen, Stieltjes Integrale und harmonische Analyse. *Math. Ann.*, 108:378–410, 1933.

[12] N. Bouleau and D. Lépingle. *Numerical Methods for Stochastic Processes.* John Wiley and Sons, 1994.

[13] J. Boussinesq. Essai sur la théorie des eaux courantes. *Mémoires présentés par divers savants à l'Académie des Sciences*, 23(1):1–680, 1877.

[14] R. Bresee and W. Ko. Fiber Formation During Melt Blowing. *Int. Nonwovens J.*, 12:21–28, 2003.

[15] C. Cameron. Relative efficiency of Gaussian stochastic process sampling procedures. *J. Comput. Phys.*, 192:546–569, 2003.

[16] R. Chhabra and R. Shambaugh. Experimental Measurements of Fiber Threadline Vibrations in the Melt-Blowing Process. *Ind. Eng. Chem. Res.*, 35(11):4366–4374, 1996.

[17] H. Cramér. On the Theory of Stationary Random Processes. *Ann. Math.*, 41(1):215–230, 1940.

[18] R. Dalang, D. Khoshnevisan, C. Mueller, D. Nualart, and Y. Xiao. *A Minicourse on Stochastic Partial Differential Equations.* Springer, 2009.

[19] R. Dudley. *Real Analysis and Probability.* Cambridge University Press, 2004.

[20] F. Elliot and A. Majda. A New Algorithm with Plane Waves and Wavelets for Random Velocity Fields with Many Spatial Scales. *J. Comput. Phys.*, 117:146–162, 1995.

[21] F. Elliott, D. Horntrop, and A. Majda. A Fourier-wavelet Monte Carlo method for fractal random fields. *J. Comput. Phys.*, 132:384–408, 1997.

[22] V. Entov and A. Yarin. The dynamics of thin liquid jets in air. *J. Fluid Mech.*, 140:91–111, 1984.

[23] J. Ferziger and M. Peric. *Computational Methods for Fluid Dynamics*. Springer, 2002.

[24] C. Foias, O. Manley, R. Rosa, and R. Temam. *Navier-Stokes Equations and Turbulence*. Cambridge University Press, 2008.

[25] F. Frenkiel and P. Klebanoff. Higher-Order Correlations in a Turbulent Field. *Phys. Fluids A*, 10(3):507–520, 1967.

[26] U. Frisch. *Turbulence. The Legacy of A.N. Kolmogorov*. Cambridge University Press, 1995.

[27] L. Grafakos. *Classical Fourier Analysis*. Springer, 2008.

[28] M. Grothaus and N. Marheineke. On a nonlinear partial differential algebraic system arising in technical textile industry: Analysis and numerics. *arXiv:1203.3692*, 2012.

[29] D. Horntrop and A. Majda. An overview of Monte Carlo simulation techniques for the generation of random fields. In P. Muller and D. Henderson, editors, *Monte Carlo Simulations in Oceanography, Proceedings of the Ninth 'Aha Huliko' a Hawaiian Winter Workshop*, pages 67–79, 1997.

[30] F. Hübsch, N. Marheineke, K. Ritter, and R. Wegener. Random field sampling for a simplified model of melt-blowing considering turbulent velocity fluctuations. *J. Stat. Phys.*, 150(6):1115–1137, 2013.

[31] F. Hübsch, N. Marheineke, and R. Wegener. Efficient simulation of random fields for fiber-fluid interactions in isotropic turbulence. In M. Fontes, M. Günther, and N. Marheineke, editors, *Progress in Industrial Mathematics at ECMI 2012*, Mathematics in Industry, pages 119–126. Springer, 2014.

[32] W. Jones and B. Launder. The Prediction of Laminarization with a Two-Equation Model of Turbulence. *Int. J. Heat Mass Transfer*, 15:301–314, 1972.

[33] Y. Kaneda. Lagrangian and Eulerian time correlations in turbulence. *Phys. Fluids A*, 5:2835–2845, 1993.

[34] I. Karatzas and S. Shreve. *Brownian Motion and Stochastic Calculus.* Springer, 1998.

[35] S. Kase and T. Matsuo. Studies on melt spinning. 1. Fundamental equations on the dynamics of melt spinning. *J. Polym. Sci., Part A*, 3:2541–2554, 1965.

[36] A. Kolomogorov. The local structure of turbulence in incompressible viscous fluid for very large Reynolds numbers. *Dokl. Akad. Nauk SSSR*, 30:299–303, 1941.

[37] A. Kolomogorov. A refinement of previous hypotheses concerning the local structure of turbulence in a viscous incompressible fluid at high Reynolds numbers. *J. Fluid Mech.*, 13:82–85, 1962.

[38] P. Kramer. A review of some Monte Carlo simulation methods for turbulent systems. *Monte Carlo Methods Appl.*, 7:229–244, 2001.

[39] P. Kramer, O. Kurbanmuradov, and K. Sabelfeld. Comparative analysis of multiscale Gaussian random field simulation algorithms. *J. Comput. Phys.*, 226:897–924, 2007.

[40] S. Kruse. *A generalized parametrix method, smoothness of random fields and applications to parabolic stochastic partial differential equations.* Logos Verlag, 2001.

[41] O. Kurbanmuradov and K. Sabelfeld. Stochastic spectral and Fourier-wavelet methods for vector Gaussian random fields. *Monte Carlo Methods Appl.*, 12:395–445, 2006.

[42] O. Kurbanmuradov and K. Sabelfeld. Convergence of Fourier-Wavelet Models for Gaussian Random Processes. *SIAM J. Numer. Anal.*, 46(6):3084–3112, 2008.

[43] B. Launder and B. Sharma. Application of the energy dissipation model of turbulence to the calculation of flow near a spinning disc. *Letters in Heat and Mass Transfer*, 1(2):131–138, 1974.

[44] M. Ledoux and M. Talagrand. *Probability in Banach Spaces.* Springer, 2010.

[45] Y. Lee and L. Wadsworth. Effects of melt-blowing process conditions on morphological and mechanical properties of polypropylene webs. *Polymer*, 33:1200–1209, 1992.

[46] P. Lemarie-Rieusset. *Recent Developments in the Navier-Stokes Problem.* Chapman and Hall/CRC, 2002.

[47] M. Lifshits. *Gaussian Random Functions.* Kluwer Academic Publishers, 1995.

[48] Q. Lu. An approach to modeling particle motion in turbulent flows. *I. Homogeneous isotropic turbulence Atmos. Environ.*, 29:423–436, 1995.

[49] A. Majda. Random shearing direction models for isotropic turbulent diffusion. *J. Stat. Phys.*, 75:1153–1165, 1994.

[50] A. Majda and P. Kramer. Simplified models for turbulent diffusion: theory, numerical modelling and physical phenomena. *Phys. Rep.*, 314:237–574, 1999.

[51] S. Malkan. An overview of spunbonding and meltblowing technologies. *Tappi J.*, 78(185-190), 1995.

[52] N. Marheineke. *Turbulent Fibers - On the Motion of Long, Flexible Fibers in Turbulent Flows.* PhD thesis, Technische Universität Kaiserslautern, 2005.

[53] N. Marheineke and R. Wegener. Fiber Dynamics in Turbulent Flows: General Modeling Framework. *SIAM J. Appl. Math.*, 66(5):1703–1726, 2006.

[54] N. Marheineke and R. Wegener. Fiber Dynamics in Turbulent Flows: Specific Taylor Drag. *SIAM J. Appl. Math.*, 68(1):1–23, 2007.

[55] N. Marheineke and R. Wegener. Asymptotic model for the dynamics of curved viscous fibers with surface tension. *J. Fluid Mech.*, 622:345–369, 2009.

[56] N. Marheineke and R. Wegener. Modeling and application of a stochastic drag for fiber dynamics in turbulent flows. *Int. J. Multiph. Flow*, 37:136–148, 2011.

[57] V. Marla and R. Shambaugh. Three-dimensional model of the melt-blowing process. *Ind. Eng. Chem. Res.*, 42:6993–7005, 2003.

[58] M. Matovich and J. Pearson. Spinning a molten threadline. Steady-state isothermal viscous flows. *Ind. Eng. Chem. Res. Fundam.*, 8:512–520, 1969.

[59] A. Monin and A. Yaglom. *Statistical Fluid Mechanics: Mechanics of Turbulence, Volume I.* Dover Publications, INC., 2007.

[60] A. Monin and A. Yaglom. *Statistical Fluid Mechanics: Mechanics of Turbulence, Volume II.* Dover Publications, INC., 2007.

[61] T. Müller-Gronbach, E. Novak, and K. Ritter. *Monte Carlo-Algorithmen.* Springer, 2012.

[62] S. Orszag. Numerical Methods for the Simulation of Turbulence. *Phys. Fluids Supp. II*, 12:250–257, 1969.

[63] R. L. Panton. *Incompressible Flow.* John Wiley and Sons, 2005.

[64] A. Papoulis and S. U. Pillai. *Probability, Random Variables, and Stochastic Processes.* McGraw-Hill, 2002.

[65] L. Pinchuk, V. Goldade, A. Makarevich, and V. Kestelman. *Melt Blowing: Equipment, Technology and Polymer Fibrous Materials.* Springer Series in Materials Processing. Springer, 2002.

[66] L. Pismen and A. Nir. On the motion of suspended particles in stationary homogeneous turbulence. *J. Fluid Mech.*, 84:193–206, 1978.

[67] S. Pope. *Turbulent Flows.* Cambridge University Press, 2000.

[68] R. Rao and R. Shambaugh. Vibration and stability in the melt blowing process. *Ind. Eng. Chem. Res.*, 32, 1993.

[69] O. Reynolds. On the Dynamical Theory of Incompressible Viscous Fluids and the Determination of the Criterion. *Philosophical Transactions of the Royal Society of London*, 186:123–164, 1895.

[70] N. Ribe. Coiling of viscous jets. *Proc. R. Soc. Lond. A*, 2051:3223–3239, 2004.

[71] N. Ribe, H. Huppert, M. Hallworth, M. Habibi, and D. Bonn. Multiple coexisting states of liquid rope coiling. *J. Fluid Mech.*, 555:275–297, 2006.

[72] J. Royston. An extension of Shapiro and Wilk's W test for normality of large samples. *Appl. Stat.*, 31:115–124, 1982.

[73] J. Royston. Some techniques for assessing multivariate normality based on the Shapiro-Wilk W. *Appl. Stat.*, 32:121–133, 1983.

[74] Y. Z. S. Xie. Turbulent air flow field and fiber whipping motion in the melt blowing process: experimental study. *Ind. Eng. Chem. Res.*, 51:5346–5352, 2012.

[75] S. Sinha-Ray and A. Yarin. Meltblowing: I-basic physical mechanism and threadline model. *J. Appl. Phys.*, 108, 2010.

[76] M. L. Stein. *Interpolation of Spatial Data.* Springer, 1999.

[77] Y. Sun and Y. Zeng. Three-dimensional model of whipping motion in the processing of microfibers. *Ind. Eng. Chem. Res.*, 50:1099–1109, 2011.

[78] G. Taylor. The spectrum of turbulence. *Proc. R. Soc. Lond. A*, 164:476–490, 1938.

[79] A. Trujillo-Ortiz, R. Hernandez-Walls, K. Barba-Rojo, and L. Cupul-Magana. Roystest: Royston's multivariate normality test. A MATLAB file. http://www.mathworks.com/matlabcentral/fileexchange/loadFile.do?objectId=17811, 2007.

[80] M. Uyttendaele and R. Shambaugh. Melt blowing: general equation development and experimental verification. *AIChE J.*, 36:175–186, 1990.

[81] H. Versteeg and W. Malalasekera. *An Introduction to Computational Fluid Dynamics.* Prentice Hall, 2007.

[82] J. von Neumann. Various techniques used in connection with random digits. *J. Res. Nat. Bur. Stand.*, 12:36–38, 1951.

[83] V. Wente. Manufacture of superfine organic fibers. Report PB111437 NRL-4364, US Department of Commerce, Office of Technical Services, Washington DC, 1954.

[84] D. Wilcox. *Turbulence Modeling for CFD.* DCW Industries, 1994.

[85] T. Wu and R. Shambaugh. Characterization of the melt blowing process with laser Doppler velocimetry. *Ind. Eng. Chem. Res.*, 31:379–389, 1992.

[86] A. Yarin. *Free Liquid Jets and Films.* Longman, 1993.

[87] A. Yarin, S. Sinha-Ray, and B. Pourdeyhimi. Meltblowing: II-linear and nonlinear waves on viscoelastic polymer jets. *J. Appl. Phys.*, 108, 2010.

[88] H. Yin, Z. Yan, and R. Bresee. Experimental study of the melt blowing process. *Int. Nonwovens J.*, 8:60–65, 1999.

[89] Y. Zeng, Y. Sun, and X. Wang. Numerical approach to modeling fiber motion during melt blowing. *J. Appl. Polym. Sci.*, 119:2112–2123, 2011.

[90] A. Ziabicki and H. Kawai. *High Speed Melt Spinning.* Wiley, 1985.

Scientific Career

June 2005	Abitur at the Albert-Schweitzer-Gymnasium Neckarsulm
October 2006	Beginning of studies in Computer Science at the University of Karlsruhe
October 2007	Change of major to Mathematics with minor Computer Science
March 2009	Vordiplom in Mathematics at the University of Karlsruhe
April 2009	Continuation of studies at the FU Hagen
October 2009	Continuation of studies at the TU Darmstadt
March 2011	Diploma in Mathematics at the TU Darmstadt. Diploma Thesis: "The first jump approximation of Lévy processes"
April 2011 - April 2014	Member of Computational Stochastics Group, TU Kaiserslautern Member of Transport Processes Department, Fraunhofer ITWM, Kaiserslautern Ph.D. Scholarship by the Fraunhofer Innovationszentrum Applied System Modeling, Kaiserslautern

Wissenschaftlicher Werdegang

Juni 2005	Abitur am Albert-Schweitzer-Gymnasium in Neckarsulm
Oktober 2006	Beginn des Informatikstudiums an der Universität Karlsruhe
Oktober 2007	Studienfachwechsel zur Mathematik mit Nebenfach Informatik an der Universität Karlsruhe
März 2009	Vordiplom in Mathematik an der Universität Karlsruhe
April 2009	Weiterführung des Mathematikstudiums an der FU Hagen
Oktober 2009	Weiterführung des Mathematikstudiums an der TU Darmstadt
März 2011	Diplom in Mathematik an der TU Darmstadt. Diplom-arbeit: "Die First-Jump-Approximation von Lévy-Prozessen"
April 2011 - April 2014	Mitglied der AG Computational Stochastics, TU Kaiserslautern Mitglied der Abteilung Transportvorgänge, Fraunhofer ITWM, Kaiserslautern Promotionsstipendium des Fraunhofer Innovationszentrums Applied System Modeling, Kaiserslautern